THE DEVELOPMENT OF AN OPTICAL IMMUNOSENSOR BASED ON ION-EXCHANGED WAVEGUIDES IN GLASS AND EVANESCENT EXCITATION OF FLUORESCENCE

A Thesis

Submitted to the Faculty of Engineering

of the University of Glasgow

for the Degree of

Doctor of Philosophy

by

Yan Zhou, B.Sc., M.Sc.

April 1992

DECLARATION

The author declares that the work of this thesis has not been previously submitted for any degree or award

Date 15 June 1992

SUMMARY

Although there are a number of optical techniques which can be used for immunosensing, optical evanescent wave immunosensors are considered to be promising because they can eliminate the washing step usually associated with conventional immunoassays. The low cost of fabrication of ion–exchanged waveguides favours the concept of a single use disposable immunosensor which will probably dominate the huge immunotesting market in the future. Consequently, the ion–exchange technique is employed to fabricate waveguides suitable for immunosensing purposes.

As a result of the research, a novel disposable wash–free optical immunosensor based on potassium ion–exchanged patterned waveguides in glass has been demonstrated. The immunosensor has shown very good performance when it is applied to multichannel (or multi–analyte) and differential immunoassays.

Potassium ion–exchanged surface planar waveguides have been successfully buried using a thermal sodium ion–exchange process. The idea of fabricating patterned waveguides and using them as the sensing element has been put forward and successfully implemented for the first time (to the author's knowledge). The wells etched in the superstrate of a completely buried waveguide make it possible to immobilise different antigens as well as control proteins in different individual wells. As a result, multichannel (or multi–analyte) immunoassays and differential immunoassays have been successfully conducted.

Experimental results have shown that the evanescent wave immunosensor has a sensitivity (or detection limit) of about 0.3μg/ml for FITC (fluorescein isothiocyanate) labelled antibodies and this is roughly equal to that of a corresponding conventional solid phase fluorescence immunoassay. Although the sensitivity is limited by background noise and is not high enough for diagnostic testing, it is very likely that the sensitivity can be increased substantially if the method of time–resolved fluorescence immunoassay is adopted.

ACKNOWLEDGEMENTS

First of all, I would like to thank the late head of the department, Prof. J. Lamb and Dept. of Electronics and Electrical Engineering, University of Glasgow for accepting me as a PhD student and supplying me with all the necessary equipment for me to carry out the research.

My sincere thanks go to my supervisors Prof. P.J.R. Laybourn and Dr. J.V. Magill. Without their consistent and close supervision, it would be impossible for me to make so much progress in the research. I greatly appreciate their patient reading of my thesis.

My special thanks are due to Prof. R.M. De La Rue for his consistent interest in the project, his great encouragement and very helpful suggestions and discussions. Also I would like to thank Dr. W. Cushley in the Department of Biochemistry for his very helpful assistance and discussions.

I am very indebted to the people in the Bioelectronics group of this department for their very helpful and practical assistance. They include Dr. P. Connolly, Ms. M. Robertson, Mr. W. Monaghan, Dr. R. Lind, Dr. S. Britland, Dr. M. Baker and Dr. J. Shen.

Helpful discussions and assistance from Prof. C.D.W. Wilkinson in this Department and from Prof. A.S.G. Curtis, Dr. G.R. Moores and Dr. P. Clark in the Department of Cell Biology are much appreciated.

I would also like to say that I have gained from occasional discussions with my colleagues Mr. G. Barbarossa, Mr. P.S. Jiang, Mr. J. Bebbington, Dr. J. Bell, Dr. F. Zhou and Mr. T. Krauss.

I gratefully acknowledge the financial support for my studentship from the Sir Y K Pao Foundation, the Chinese People, the Overseas Development Administration of Britain and the British Council; and the financial support for the project from the SERC and Unilever plc under grant GR/E 18704.

TABLE OF CONTENTS

KEY TO ABBREVIATIONS

Ab: antibody

Ag: antigen

Ar^+: argon ion

APTS: γ-aminopropyltriethoxy silane

ATR: attenuated total reflection

BSA: bovine serum albumin

CEA: carcinoembryonic antigen

Con A: concanavalin A

DIG: diffusion-in-gel

DNP: dinitrophenol

d_p: depth of penetration

Fab: fragments antigen-binding

Fc: fragment crystallizable

FCFD: the fluorescence capillary fill device

FITC: fluorescein isothiocyanate

hCG: human chorionic gonadotrophin

H: heavy

He-Ne: henium-neon

HF: hydrofloric acid

HSA: human serum albumin

IEA: immuno-electroadsorption

IgG: γ-immunoglobulin

IR: infrared

IRE: internal reflection element

IRS: internal reflection spectroscopy

K^+: potassium ion

K_a: association constant

K_d: dissociation constant

L: light

λ_{cut-on}: cut-on wavelength for a longpass optical filter

λ_e: the excitation wavelength

λ_f: the fluorescence emission wavelength

LCD: liquid crystal display

MTX: methotrexate

Na^+: sodium ion

n_c:	the refractive index of the cover sample
n_{eff}:	the effective refractive index
PCS:	photon correlation spectroscopy
RO:	reverse osmosis
SiO_2:	silica or silicon dioxide
SPR:	surface plasmon resonance
TE:	transverse electric
TM:	transverse magnetic
TIRF:	total internal reflection fluorescence
UV:	ultra-violet
Vis:	visible
v/v:	volume/volume
WKB:	Wentzel-Kramers-Brillouin

CHAPTER 1, INTRODUCTION

1.1 Optical biosensing

The conversion of biological binding (or recognition) events to quantitative analytical results has long been the goal of biologists and biochemists. Although traditional immunoassay is a well-established clinical measurement technique with high sensitivity and accuracy, it usually requires a relatively lengthy analytical procedure involving sample and reagent incubation and washing stages, and considerable participation and skill on the part of the operator. To simplify the procedure, a variety of electronic, piezoelectronic and optical methods have been proposed and deployed in which antibodies (or antigens) are immobilised on the solid surface of a transducer and the subsequent binding of antigens (or antibodies) to the transducer surface is sensed.

Optical biosensors are attractive because they offer a number of potential advantages over conventional biosensing schemes. These include low cost of fabrication of the sensor, electrical isolation, rapidity of the sensing process, safety and simplicity of operation, and ruggedness and miniaturisation of the device. An optical chemical sensor can be regarded as an analytical device which converts a chemical parameter of a molecular species into an optical signal that can be processed. When the sensor has a biomolecular transducing element which provides the specificity or selectivity required to recognise the analyte of interest, the sensor is termed a biosensor. The recognition molecules can be enzymes, antibodies, hormone and neuro-transmitter receptors, etc. If antibodies are used to recognise their appropriate antigens, the term immunosensor is then used.

Optical immunoassay can be highly sensitive and selective (or specific). The high sensitivity results from the optical techniques employed for immunosensing. The high selectivity is attributable to the extremely high equilibrium association (or affinity) constants of antibodies with their antigens. This high affinity makes it possible for low concentrations of analytes in complex matrices to be discriminated.

1.2 Evanescent wave immunosensing

Although there are a number of optical techniques which can be used for

immunosensing with high sensitivity, those involving the interaction of surface bound molecules with an electromagnetic evanescent wave which decays exponentially from an optical interface are particularly promising. Fig.1.2.1 shows both the conventional solid phase fluorescence immunoassay and the evanescent fluorescence immunoassay. In the conventional immunoassay, there are usually four stages. The washing stage is troublesome as it prevents the assay from being conducted outside a centralised lab. In the evanescent fluorescence immunoassay, the washing stage can be avoided because the dimension of the penetration depth of an optical evanescent wave (typically about 100nm) is approximately of the same order as that of the antibody– antigen complex (about ten to several tens of nanometers) and as a result, the interaction of light with the molecules in the cover medium is mainly restricted to those which are bound close to the surface of the optical transducer. Consequently, after the sensing element has been immobilised with appropriate antibodies or antigens, a wash– free one step operation of the sensor can be achieved.

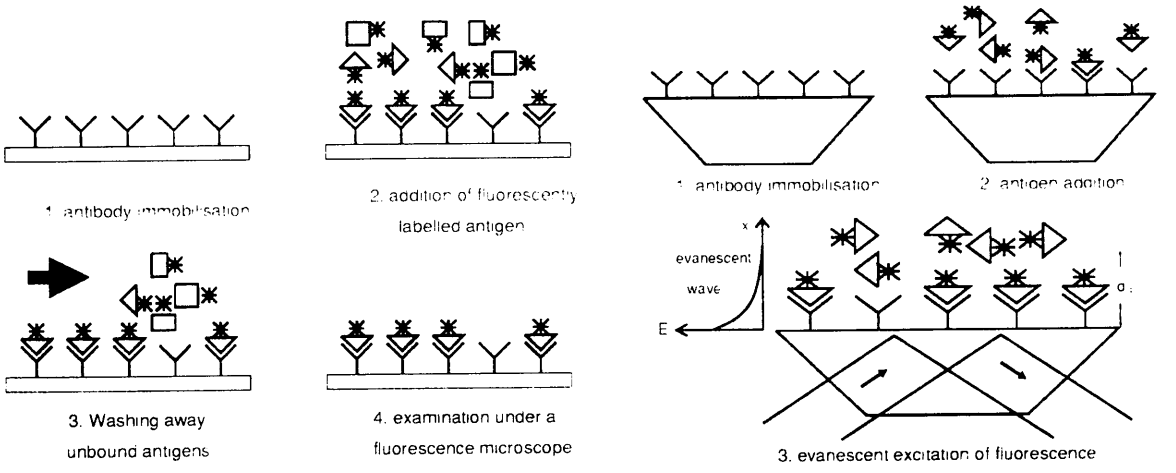

Fig.1.2.1 (a) conventional fluorescence immunoassay
and (b) evanescent fluorescence immunoassay

One of the most commonly used ways to generate an evanescent wave on a solid support is total internal reflection. This is achieved by directing a beam of light onto an optical interface from the optically denser medium at an incident angle greater than the critical angle (Fig.1.2.1b). Since light guided by an integrated optical waveguide or an optical fibre undergoes such total internal reflections, it is obvious that these waveguides can be used as sensing elements. In fact, their small

dimensions lead to an increase in the number of internal reflections over a reasonable length and this is advantageous because it allows more molecules bound to the optical interface to be probed.

1.3 Motivation and major achievements

Evanescent wave immunosensors have a potential in dominating the huge immunotesting market in the future (Bluestein et al. 1990) and are therefore worthy of research and development. The high affinity of antibodies for their respective antigens generally results in the formation of relatively stable antibody–antigen complexes and limits the reversibility of optical immunosensors. To solve the problem, the idea of a disposable sensor can be considered. The fabrication cost of the sensing element thus needs to be very low if the sensor is to be used for routine medical diagnostics outside a centralised lab. Although optical fibres are good candidates as the sensing element and have a number of advantages in term of *in vivo* applications, they are perhaps not as cheap as ion–exchanged glass waveguides to suit the idea of a single use disposable sensor.

The two most promising techniques for the fabrication of cheap planar optical waveguides as disposable transducing elements are, as suggested by Flanagan et al. (1988), the ion–exchange technique and the deposition of silica or silica/titania layers by the film sol/gel technique. The ion–exchange process is a simple, low cost, flexible and well characterised process for the fabrication of waveguides in glass. The expertise of the ion–exchange technique developed in this department thus provides the possibility to fabricate appropriate single mode or low–mode number planar waveguides suitable for evanescent wave immunosensing and is therefore the motivation of this research project.

In this research, the technology for fabricating ion–exchanged patterned waveguides suitable for evanescent fluorescence immunoassays has been successfully developed (Zhou et al 1990, 1991a/b/c/d and 1992). A patterned waveguide is a buried planar waveguide with well patterns etched in the superstrate as shown in Fig.1.3.1. Application of these waveguides to wash–free evanescent fluorescence immunosensing has resulted in very good performance. In addition, by immobilising different antigens and a control protein in each individual well respectively, both the idea of differential immunoassay which allows one to discriminate specific binding from non–specific binding and the idea of multi–analyte immunoassay using a single

sensing element have been successfully implemented.

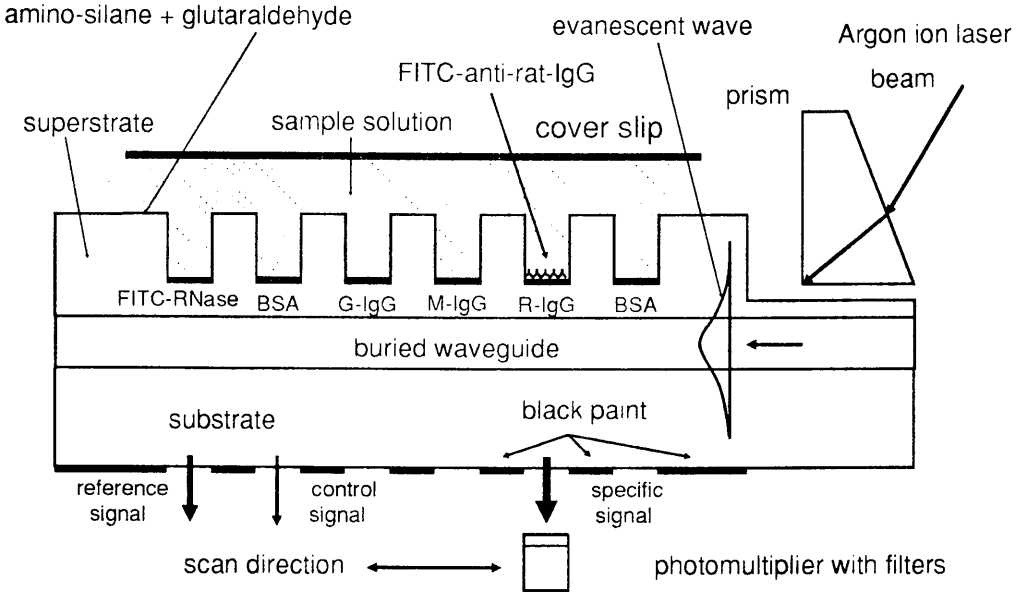

Fig.1.3.1 A patterned waveguide

1.4 Thesis outline

Following this introduction, optical techniques which have been developed for biosensing are reviewed (chapter 2). The ideas and methods which constitute the principle of operation of these sensing technique are described. Meanwhile, problems associated with these methods and their sensitivity are also discussed.

Considering that optical immunosensing is of a multidisciplinary nature, chapter 3 is devoted to the fundamental theories of ion–exchange in glass and optical waveguides. These include the ion–exchange mechanism and the diffusion equation, the electromagnetic field distribution of both three layer planar waveguides and graded–index planar waveguides, and the inverse WKB method for the determination of the refractive index profile of an experimental planar waveguide.

Chapter 4 describes the fabrication process and the characterisation of potassium ion–exchanged planar waveguides. It is shown with experiments that the fabricated waveguides do have the characteristics which are desired for them to act as the sensing element.

In chapter 5, fluorescence and its excitation by an evanescent wave are discussed. The possibility of enhancing the evanescently excited fluorescence through index–matching is explored. In addition, the evanescently excited fluorescence in the case of an immunoassays on a patterned waveguide is investigated.

Chapter 6 deals with the biological aspects of solid phase fluoroimmunoassays. Basic concepts and principles concerning antibody–antigen reaction and solid phase immunoassay are introduced. Protein immobilisation on glass surfaces and the efficient blocking of non–specific binding are then investigated. Finally, the experimental results of conventional fluorescence immunoassays on glass slides are discussed.

In chapter 7, the performance of patterned waveguides when they are applied to wash–free differential and multichannel (or multi–analyte) immunoassays is discussed. The experimental procedures for the preparation of the assay and the experimental set–up for the measurement of the evanescent fluorescence are also described. Suggestions for future research are put forward. A final conclusion of the whole research is provided at the end.

CHAPTER 2, REVIEW OF OPTICAL TECHNIQUES FOR IMMUNOASSAYS

2.1 Introduction

In chapter 1, it has been mentioned that an optical evanescent wave immunosensor based on ion–exchanged waveguides is what should be sought after if the idea of a wash–free and disposable single use sensor is to be accepted. However, this opinion will be not so convincing unless the performance as well as the principle of operation of previous optical biosensing techniques are well understood.

There are a number of optical biosensing techniques which are directly related to the study of immunological reactions at a continuous solid surface. They include internal reflection spectroscopy (IRS), ellipsometry, surface plasmon resonance (SPR), light coupling into and out of a planar waveguide with a grating, the fluorescence capillary fill device (FCFD) and light scattering techniques. Generally speaking, these techniques are based on the detection of a change in optical properties of light as a result of biological binding events. Absorbance, refractive index, molecular layer thickness, intrinsic or extrinsic fluorescence and scattered light intensities are the major parameters measured by these techniques.

The principle of operation of each technique will now be described and typical examples given of the application of the technique to biosensing, especially immunosensing. The advantages and drawbacks of each technique are also discussed.

2.2 Internal Reflection Spectroscopy (IRS), Attenuated Total Reflection (ATR) and Total Internal Reflection Fluorescence (TIRF)

2.2.1 Principle of IRS

Internal reflection spectroscopy (IRS) is the technique of recording the evanescent optical spectrum of a sample material that is in contact with an optically denser but transparent medium. It monitors reactions within the order of a wavelength of light at a continuous surface.

The idea of using an evanescent wave to study chemical reactions at a surface was put forward more than two decades ago (Harrick 1967). Of most importance is the fact that Kronick and Little (1973,1975) first demonstrated that a wash-free immunoassay at a solid surface could be performed using the excitation of fluorescence by an evanescent wave generated by total internal reflection.

When an absorbing material is placed in contact with the reflecting surface of an internal reflection element (IRE), the resultant internally reflected light is attenuated. The degree of this wavelength dependent attenuation is a measure of the chemical interaction at, or near, the surface. Two techniques fall into IRS. They are attenuated total reflection (ATR) and total internal reflection fluorescence (TIRF).

Attenuated total reflection is defined as 'reflection which occurs when an absorbing coupling mechanism acts in the process of total internal reflection to make the reflectance less than unity' (Harrick 1967). In this case, what is measured is the attenuated intensity of the internally reflected light as a function of the incident wavelength. In addition to ATR, the evanescent wave can also be used to excite fluorescence, if fluorescent materials are present. Instead of measuring attenuation, the evanescently excited fluorescence intensity is measured in TIRF. The difference between ATR and TIRF is that in TIRF, the absorption of the evanescent wave by fluorescent molecules is the first of a two-step process, where in the second process, fluorescence at a longer wavelength than the exciting light is re-emitted.

Prisms are frequently used in IRS for the generation of an evanescent wave (Fig.2.2.1). Assuming that the refractive index of the prism is greater than that of the sample solution above the base of the prism, if a monochromatic light beam is directed to strike the base of the prism at an incident angle greater than the critical angle, an evanescent wave is generated in the sample solution above the reflection area and it decays exponentially from the prism base into the sample solution.

A method to enhance the sensitivity is to use multiple reflection (Fig.2.2.1b). This is achieved by using an elongated prism or a glass side. Using ray optics, it is easy to see that the number of reflections (M) at one surface is related to the length (L), thickness (T) of the waveguide and the angle of incidence (θ) as:

$$M = L/[2T \cdot \tan\theta] \qquad (2.1)$$

The longer and thinner the waveguide, the larger is M and the more frequently the evanescent wave interacts with the surface chemical species.

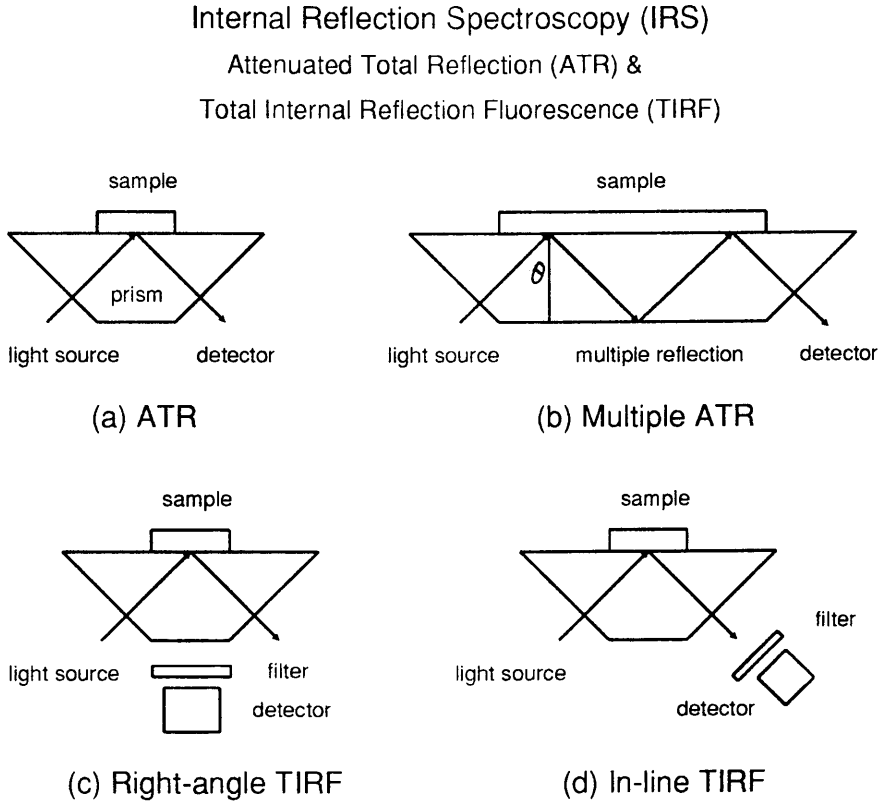

Fig.2.2.1 Total Reflection Spectroscopy

In the case of ATR (Harrick 1967), the reflectivity (R) for one reflection can be written as

$$R = 1 - \alpha \cdot d_e \qquad (2.2)$$

where α is the absorption coefficient of the sample in close contact with the transducing surface and d_e is the effective thickness of the absorbing layer. If the number of reflections at the upper surface is M, the sensitivity of the device can be increased by a factor of M, since after M reflections, the total reflectivity is expressed as

$$R^M \approx 1 - M \cdot \alpha \cdot d_e, \quad \text{when } \alpha \cdot d_e \ll 1 \qquad (2.3)$$

TIRF involves absorption and re-emission. Therefore, the sensitivity enhancement through multiple reflections applies to TIRF as well.

In TIRF, the emitted fluorescence can be detected in either the right-angle direction (Fig.2.2.1c) where the filter and the detector are placed below the prism/waveguide or in the in-line direction where the fluorescence propagating with the same angle as the exciting beam (i.e. in-line with the exciting beam) is detected (Fig.2.2.1d). The latter is performed because both theory and experiments have proved that its fluorescence intensity is substantially higher than that emitted at right angle (Lee et al. 1979), although fluorescence within a wider solid angle may be probed in the right-angle geometry.

2.2.2 Application of ATR to the study of biological reactions

Macromolecules usually have a number of characteristic absorbance maxima over a broad spectral range. Accordingly, ATR has been applied to monitoring immunoassays in the infrared (IR), visible (Vis) and ultra-violet (UV) regions of the spectrum. Fahrenfort proposed and demonstrated the principle of ATR and suggested its application in both identification and quantification of absorbing substances. In the IR region, he successfully used the technique to measure the reflection (or absorption) spectra of several organic compounds (Fahrenfort, 1961). Later, also in the visible region, Gendreau and coworkers (Gendreau et al. 1981, 1982) combined ATR with Fourier transform spectroscopy and monitored the exchange of albumin and fibrinogen at a germanium waveguide surface.

To observe antibody-antigen interactions, Ockman (1978) conducted experiments using polarised infrared ATR spectroscopy. His experiments showed that the specific binding of an antibody with its appropriate antigens could be observed. In his study, various serum albumins were adsorbed to the surface of a germanium crystal. Polarised ATR spectra of the initially adsorbed protein layer were recorded. The germanium crystal plate was then immersed in diluted antiserum solution and the ATR spectra of the additional adsorption were obtained. The increase in absorbance in the amide I band (1650 cm^{-1}) indicated an increase in the number of proteins at the surface and was interpreted as antibody binding.

Although successful, Ockman's approach did not make full use of the potential of IRS methods which should allow the continuous monitoring of the immunological

binding events without a separation step. In addition, no experimental data on the limits of detection sensitivity were published although the differentiation of specific binding from non-specific binding was pointed out to be a problem.

Sutherland and co-workers (1984a, 1987) applied ATR to the continuous monitoring of immunological reactions in both the visible and the UV regions. In the visible region, they covalently immobilised rabbit anti-haemoglobulin antibodies to the surface of a quartz microscope slide. The immobilised antibodies were then reacted with different concentrations of haemoglobulin. The absorption maximum of haemoglobulin is at 410nm and the attenuation of the reflected light at this wavelength was monitored.

Their experimental results showed a three-phase response curve (Sutherland 1987). On introduction of the antigen solution, there was an immediate fall in transmission at 410nm due to the presence of haemoglobulins. This was followed, before the reflected light intensity reached a plateau, by a relatively rapid attenuation in transmission as the haemoglobulin molecules were bound close to the surface by the immobilised antibodies. To make sure that this rapid attenuation was indeed an indication of antibody-antigen reaction, they used a second quartz slide on which bovine serum albumin (BSA) molecules were initially covalently immobilised. Subsequent introduction of haemoglobulin indicated that while the immediate fall in transmission was noted, a reduction in the following attenuation was also observed. This indicated that specific binding did occur on the first quartz slide.

Similarly, in the ultra-violet (UV) region, Sutherland et al. (1984a) used the reaction between the chemotherapeutic agent methotrexate (MTX) and anti-MTX as a model. Again, the antibody was immobilised to a UV transmitting fused-quartz slide. As MTX was immunologically sequestered at the interface, the reaction was monitored at 310nm by attenuation in reflected light. With this approach, a detection limit of 0.3μmol/litre was estimated.

Later, Sutherland and Dahne (1987) proposed a design for immunosensing using a multiple-internal reflection plate. The use of the two variable angle prisms made it possible to change the angle of incidence so that the penetration depth could be adjusted.

2.2.3 Application of TIRF to the study of biological reactions

Most early TIRF experiments were done with non-specific interactions of proteins with surfaces in different states of hydrophobicity and composition. Hirschfeld (1965) first described TIRF (then called total reflection fluorescence). He pointed out the advantages of the small penetration depth of the evanescent field for turbid or optically highly absorbing solutions, the efficient excitation of thin films by multiple reflections, and how variation of the penetration depth could be readily achieved simply by varying the incident angle.

Harrick and Loeb (1973) applied TIRF to the study of adsorbed films of a dansyl conjugate of the protein plasma albumin. A quartz slide was used as the internal reflection element (IRE). After a fixed incubation time and washing, the fluorescence spectrum of the dried surface was measured. It was found that increasing fluorescence was obtained with longer incubation time and that the final fluorescence signal was as strong with wet or with dried slides.

Kronick and Little (1973, 1975) first demonstrated that a wash-free immunoassay at a solid surface could be performed using TIRF. In their method, antigens (i.e. hapten-protein conjugates) were first immobilised on a quartz slide by physical adsorption, FITC (fluorescein isothiocyanate)-labelled antibody solution was introduced into a cell on the antigen attached surface and evanescently excited fluorescence was detected. After a certain incubation time, the system came to equilibrium with equal numbers of antibodies leaving from, and arriving at the surface. When free haptens were present in the solution, some of the antibodies would bind to these haptens, lowering the concentration of antibody free to bind to the surface. As a result, a concentration dependent reduction of the binding of FITC-labelled antibodies to the immobilised haptens was reflected by the reduction in the intensity of the fluorescence detected. They reported a minimum detection limit of 0.2μmol/l of morphine, using right-angle detection.

Following the demonstration of a continuous monitoring of chemical reactions at a solid surface using TIRF, a number of different TIRF systems with flow cells were advocated. Watkins and Robertson (1977) continuously measured FITC-labelled bovine-γ-globulin binding to silicone rubber.

Van Wagenen et al. (1980, 1982) used the intrinsic fluorescence of the amino

acid tryptophan, which is a constituent of most proteins, to generate a signal following the adsorption of BSA or bovine-γ-globulin onto a quartz surface (the excitation wavelength λ_e= 284nm, and the fluorescence emission wavelength λ_f= 335nm). In addition to the continuous monitoring of the adsorption process, they indentified two major components of the signal as being due both to the molecules adsorbed on the surface and proteins free in solution but within the penetration depth of the evanescent wave. Following this work, Andrade and Van Wagenen (1983) suggested that the intrinsic tryptophan fluorescence could be used to monitor TIRF immunoassays at interfaces.

Rockhold et al. (1983) studied the adsorption of γ-globulin (IgG) using both intrinsic tryptophan fluorescence and extrinsic fluorescence from fluorescein-labeled IgG.

Lok et al. (1983a, 1983b) investigated quantitatively the adsorption of FITC-BSA and FITC-bovine fibrinogen on crosslinked polydimethylsiloxane (silicone rubber) from flowing solutions. Their experimental results showed that there were three components of the fluorescence signal; FITC-BSA bound to the surface, FITC-BSA free but within the penetration depth of the evanescent wave, and FITC-BSA free in solution but subject to fluorescence excitation by light scattered at the interface. They concluded that at high solution concentrations (>100μg/ml), fluorescence from solution protein both within the evanescent field and excited by scattered light could contribute a significant fraction of the total fluorescence signal.

In an attempt to examine the kinetic behaviour of immunological reactions, Sutherland et al. (1984a) investigated the binding between human-IgG and anti-human-IgG using flow cell systems. Antibodies (anti-human-IgG) were covalently immobilised onto the surface of either a planar (microscope slide) or cylindrical (fibre optic) waveguide made of fused quartz. The binding reaction of antigen (human-IgG) with the immobilised antibody was monitored by directly applying FITC-labelled human-IgG.

Alternatively, a sandwich fluorescence immunoassay (i.e. two-site immunofluorometric assay) was conducted. Human-IgG was first reacted with the immobilised anti-human-IgG. After 10 minutes of incubation, FITC-labelled anti-human-IgG solution was injected into the cell. Their experimental results with both slides and optical fibres showed three major components of the binding curve.

These were 1) an initial increase in signal which is attributable to free molecules fluorescing within the penetration depth of the evanescent wave; 2) a rapid increase in the signal, characteristic of the immunological binding reaction and 3) a signal plateau. With the two-site immunofluorometric assay for human-IgG, it was estimated that the detection limit was 30nmol/L.

In addition to the direct fluorescence method, two other TIRF techniques, photobleaching recovery and fluorescence correlation spectroscopy, were proposed and developed (Burghardt & Axelrod 1981, Thompson et al. 1981). The dynamics of the adsorption and desorption of tetramethylrhodamine-labelled bovine serum albumin to a quartz slide was studied. The technique combined total internal reflection fluorescence with either fluorescence photobleaching recovery or fluorescence correlation spectroscopy. In fluorescence photobleaching recovery, a laser beam was focused to the liquid/solid interface to evanescently excite the fluorescence of adsorbed proteins. The beam was flashed with high intensity in a single short pulse when a shutter was activated, thus photobleaching the fluorescence of surface bound solute molecules within the evanescent region. The same laser beam was then much attenuated by the shutter so that it was non-bleaching and the evanescently excited fluorescence was monitored. A subsequent recovery of fluorescence was observed as unbleached molecules from the solution or surrounding nonilluminated regions of the surface replaced bleached ones in the illuminated area because of adsorption/desorption and/or surface diffusion. The investigation proved successful in examining the kinetic behaviour of rhodamine-labelled BSA adsorbed to quartz slide. It also demonstrated the feasibility of the technique for measuring molecular dynamics on a solid surface.

In fluorescence correlation spectroscopy, the laser beam was not focused and a non-bleaching laser pulse was used. The spontaneous fluctuations of fluorescence due to individual molecules entering and leaving a portion of the evanescent field (defined by an aperture in the image plane of the fluorescence detection optical system) was observed. The average rate of decay of these fluctuations depended on the rates of surface adsorption and desorption and surface diffusion, and was measured by autocorrelating the fluctuations from the equilibrium value of fluorescence.

Following the application of the technique to the interaction of rhodamine-labelled IgG and insulin with BSA-coated quartz slides, Thompson et al. (1983) used it to monitor the immunological binding of rhodamine-labelled antibodies

to dinitrophenol (DNP) attached to the quartz slide via adsorbed albumin. He showed that the specific binding of anti-DNP to DNP-coated surfaces was accompanied by a large amount of non-specific binding. In one series of experiments, it was found that nearly 60% of the bound signal was due to non-specific binding. One conclusion by Thompson was that the high level of non-specific binding prevented continuous measurement of the kinetics of binding.

To solve the problem of non-specific binding, Sutherland et al. (1984c) used the reaction between human-IgG and two antisera to investigate some of the critical factors which might overcome the non-specific binding in a TIRF system. By including an excess (200-fold relative to the antibody) of appropriate non-immune animal serum in the assay buffer, they reduced non-specific binding by more than 150 times. Application of this technique to a two-site immunofluorometric assay for IgG indicated a detection limit of approximately 5μg/ml of IgG in right-angle detection. In in-line geometry, detection limits of 3.0 and 1.5μg/ml of IgG for glass slides and optical fibres respectively were reported (Sutherland et al. 1984a, Dahne et al. 1984).

Since integrated optical waveguides provide small guiding layer dimensions for the enhancement of sensitivity, investigations on the fabrication of cheap optical planar waveguides for TIRF biosensors were made (Flanagan et al. 1988, Sloper and Flanagan 1988). These metal phosphate glassy monomode waveguides were later applied to a sandwich immunoassay for human chorionic gonadotrophin (hCG) in serum and it was found that an eight-fold increase in sensitivity was obtained on using a thin film waveguide as opposed to multiple internal reflections in a microscope slide (Sloper et al. 1990).

2.3 Ellipsometry

Ellipsometry is a technique concerned with the measurement of changes in the state of polarization of a monochromatic light upon reflection from a surface. When a beam of light is reflected from a surface, in addition to a change in the amplitude of the two perpendicularly polarised light components, a phase change different for each component occurs as well. The state of polarization of the reflected light is determined by the relative phase and the amplitude ratio of the two components. It is very sensitive to the refractive index of the optical medium and the thickness of the film (if there is one) on the surface. As a result, ellipsometry is one of the

most commonly used techniques for the measurement of either the optical constants of the reflecting surface or the thicknesses and refractive indices of very thin films on the surface.

The application of ellipsometry to molecular sensing is based on the fact that the formation of molecular layers on a solid surface leads to changes in both the refractive index and the thickness of the adsorbed film.

When ellipsometry was initially used to study immunological binding events, the binding of antibodies to immobilised antigens was recorded as an increase in film thickness after washing and drying of the surface. For instance, Rothen (1947a,b,) coated a chromium－plated glass slide with a film of antigen polysaccharide from Types III or VIII pneumococcus. After drying it, the thickness of the layer was measured to be 5Å. Following the immersion of the slide in antibody solution, the thickness of the layer on the slide was found to be 500Å. The increase in the thickness was interpreted as binding of antibody to the immobilised antigen.

In order to continuously monitor the binding, Trurnit (1953) first introduced an incubation cell and succeeded in recording the generation of biological films by ellipsometry. Using similar approaches, Moss (Poste and Moss 1972) differentiated between specific and non－specific binding by examining the difference of the increase in film thickness.

However, experiments conducted by a number of people using ellipsometry and incubation cells showed large variations in the measured film thickness both before and after the binding of anti－BSA to adsorbed BSA (Poste and Moss 1972, Giaever 1974, Azzam et al. 1977 and Cuypers et al. 1978). Reported film thickness of initially adsorbed BSA ranged from 7Å to 30Å and the increase in film thickness due to the binding of anti－BSA to the immobilised BSA ranged from 6Å to 270Å. These results showed the problem with ellipsometry when the interpretation was based solely on the change in film thickness.

Based on the straightforward ellipsometric analysis, two improved techniques were developed. One was the immuno－electroadsorption (IEA) method (Rothen 1974). In this method, a weak current (300μA) was employed for 1－2 minutes during both the initial adsorption of antigens from dilute antigen solutions ($<1\,\mu$g/ml) and the subsequent reaction of antibodies with adsorbed antigens. The metallised slide

acted as one electrode and a thin platinum wire (1.9mm in diameter) placed a short distance from the slide surface acted as the other electrode. Reported benefits included increased adsorption of available antigens, enhanced kinetics of immunological reaction, and enhancement in sensitivity by 6 orders of magnitude over non-IEA ellipsometry (Mathot and Rothen 1965, Mathot et al. 1967, Rothen et al. 1969 and Rothen 1974). With this method, a minimum detection limit of 0.2ng/ml for human growth hormone was claimed. However, the usefulness of the method was later questioned as problems concerning its reproducibility, stability and differentiation of specific binding from non-specific binding were discovered (Williams et al. 1969, Poste and Moss 1972).

The second technique was the diffusion-in-gel (DIG) technique (Elwing & Stenberg 1981). Either antibody or antigen was allowed to diffuse in a gel over a surface coated with the other binding component. In practice, antigen was first adsorbed on a hydrophobic surface and a film (2mm thick) of gel was formed on the surface. A trough (2mm wide) was then cut in the gel and antibody applied to the trough to diffuse through the gel. After the removal of the gel from the surface, the thickness profile and the bound layers were measured by conventional ellipsometry. An interesting feature of the method was that only one prepared plate was required for several assays. A by-product of this technique was that reduction in non-specific binding by the gel was observed. Moreover, the fact that more concentrated antibody solution led to further diffusion of antibody from the trough gave a basis for relating the antibody concentration to the distance from the trough.

More recently, a technique to amplify the sensitivity of ellipsometry for biospecific interactions was put forward with success (Mandenius and Mosbach 1988). In the technique, an amplifier conjugate was formed by binding the affinity ligand to a 12-nm silica particle which could be readily detected by the ellipsometer. Two biosystems were tested with the technique. They were immunoglobulin G (IgG) with anti-IgG and lectin concanavalin A (Con A) with yeast cells. Amplifications of 5 to 7 times and a detection limit of 20pg/mm^2 were reported.

All the above ellipsometric measurements were based on external, not internal, techniques. Carter et al. (1982) suggested that these measurements could be carried out using either single or multiple-internal reflection waveguide systems. Nevertheless, published information on this internal technique was very limited.

Although ellipsometric measurements may reveal dielectric changes and film thicknesses with high sensitivity and can thus be used as sensitive molecular sensors, the fact that their use for biosensing at a reasonable range of sensitivity requires large, complex and expensive instrumentation prevents them from being acceptable as practical diagnostic biosensors.

2.4 Surface Plasmon Resonance (SPR)

A surface plasmon is a special kind of electromagnetic wave mode which propagates along the surface of a metal. A surface plasmon can be excited by an optical evanescent wave resulting from total internal reflection or with a metal grating. In the former case, prisms are usually used to generate the evanescent wave. There are three kinds of geometry for the excitation of SPR (Fig.2.4.1). It has been claimed that the middle geometry can enhance the SPR field by as much as an order of magnitude with respect to the other two (Sarid et al. 1982)

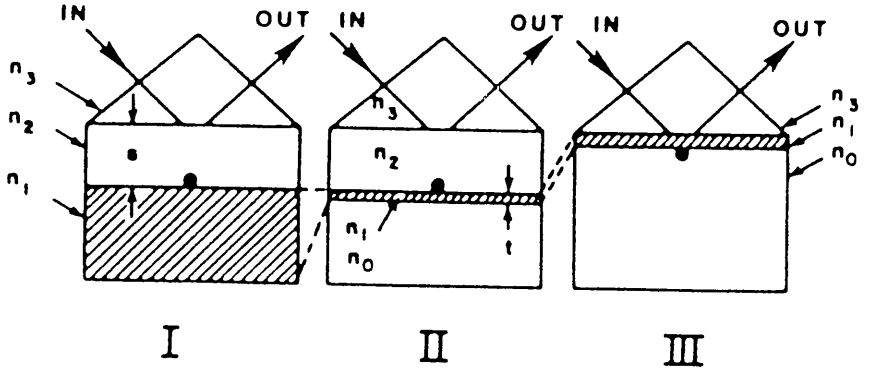

Fig.2.4.1 Prism geometries for the excitation of SPR

SPR excitation may be used for two methods of molecular sensing, namely, the angular selectivity of SPR excitation and the electric field enhancement for the evanescent excitation of fluorescent light.

2.4.1 Angular Selectivity With a Prism

In the angular selectivity method, when the metal and its thickness are properly chosen, strong absorption of p−polarised exciting monochromatic light by SPR can occur at a certain incident angle. This angle is very sharp and is strongly dependent on the refractive index of the medium close to the metal surface (within a few

hundred nm). As a result, adsorption of proteins onto the metal surface can lead to a substantial shift of the resonance angle (Fig.2.4.2).

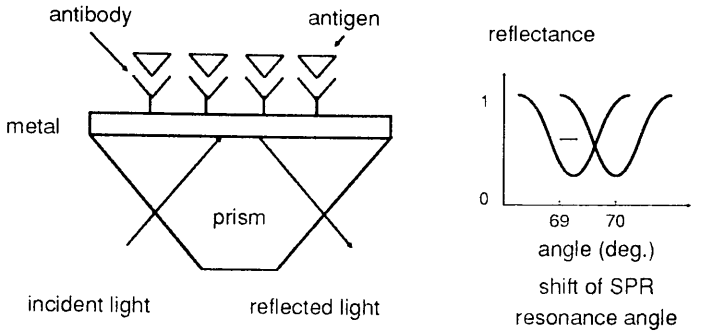

Fig.2.4.2 Shift of SPR resonance angle

The third prism geometry of Fig.2.4.1 (i.e. Kretschmann configuration) has always been used for molecular sensing purposes. The most common method is to measure the attenuated reflection as a function of the incident angle at a fixed wavelength or alternatively, as a function of wavelength for a fixed angle. SPR has been used for the analysis of chemical adsorptions and thin organic films on a metal surface by a number of people (Pockrand et al. 1977, Eagen and Weber 1979). As far as immunosensing is concerned, Liedberg et al. (1983) first demonstrated the principle on the model system IgG/anti−IgG and showed how less than 2μg/ml could be readily detected within a few seconds. In the experiment, they selected an angle of incidence which was half−way down the reflectance profile and measured the change in the reflected light intensity. With this approach, changes in the refractive index of the order of 10^{-5} were detected. The same system was also used for gas detection and sensitivities down to a few ppm of gas exposure were reported (Nylander 1982/83).

Flanagan and Pantell (1984) did some theoretical analysis of SPR in which the dependence of the reflected power on the surface roughness of adsorbed biomolecular layers was studied. In addition, they used a similar arrangement as described above to investigate the binding between human serum albumin (HSA) and anti−HSA. Their experiments showed the shift of the resonance angle when HSA and anti−HSA were sequentially applied to the metal surface.

More recently, Daniels et al. (1988) applied a similar geometry to study the binding of avidin with biotin and the binding of α−feto protein with an antibody to

α− feto protein. By using a measurement of initial rate of change, they claimed that concentrations in the nanomolar range could be determined within a few minutes. Meanwhile, they pointed out that the intrinsic sensitivity of SPR, the maximum rate of the primary antibody− antigen combination and the constraints of non− specific adsorption would likely restrict the detection limit of this method to nanomolar range.

2.4.2 Field Enhancement

In field enhancement, the evanescent emission of a fluorescently labelled immuno− complex immobilised at the metal surface from the sample solution may be enhanced via SPR compared with TIRF. This enhancement is achieved through the high electric field at the metal surface due to the electromagnetic energy stored in the resonance of SPR. It has been shown that with Krestchmann's geometry, the enhancement of the surface field intensity could be as large as 60 (Weber and Ford 1981). With the middle prism geometry of Fig.2.4.1, Sarid et al. (1982) showed theoretically that a total enhancement of about 600 for the intensity might be attainable compared with that associated with TIRF. Furthermore, the emitted fluorescence couples back into the substrate over a narrow range of angles via a surface plasmon (Benner et al. 1979). More recently, Attridge et al. (1990) pointed out that unlike conventional total internal reflection techniques, the optimum enhancement of the evanescent field occurred away from the critical angle where the evanescent field penetration depth was much reduced. This could give good discrimination of surface bound fluorophores from free ones. Consequently, the technique might offer the possibility of increasing the sensitivity of evanescent fluorescence immunosensors by both increasing the detected signal and reducing background noises. Unfortunately, up till now, no report seems to have been published on the application of this enhancement effect to immunosensing.

2.4.3 Metal Grating Coupling

As mentioned earlier, metal gratings can also be employed to excite SPR. Cullen et al. (1988) reported the use of diffraction gratings as an alternative to prisms in SPR devices. They used a gold− coated diffraction grating to excite surface plasmons. The binding of antigen to immobilised antibody was followed by monitoring the change in the resonance angle. Similar sensitivities to those in prism based SPR devices were reached. As mass production of high− quality diffraction gratings has been addressed by manufacturers of compact audio discs, this investigation implied the

possibility of cheap diffraction grating SPR immunosensing devices.

The main limitation of the SPR angular selectivity technique is that the sensitivity depends on the molecular weight or, more accurately, the optical thickness of the adsorbed layer and, consequently, small molecules such as haptens are unlikely to be measurable in low concentrations. In addition, compared with IRS and ellipsometry, the SPR technique is particularly sensitive to non-specific binding. In an attempt to overcome this problem, refractive index labelling has been suggested (Drake et al. 1988). However, no publications on the application of this idea to molecular sensing have appeared. For the prism system, its performance is heavily dependent on the deposition of very thin (about 30nm) and highly reproducible metal layers, whereas, for the diffraction grating system, restrictions on the optical properties of sample solutions are imposed by the need for the incident light beam to pass through the sample solution.

2.5 Light Coupling Into and Out of Planar Waveguides With a Grating

The coupling of light into or out of a planar waveguide using a prism or a grating is a well established method in integrated optics. However, the application of such a technique to molecular sensing is comparatively new.

The fact that the coupling of light into and out of a planar waveguide can be used for molecular sensing can be explained as follows. The effective refractive index of a planar waveguide is governed by a resonance condition required by electromagnetic theory. It depends on the refractive indices of the three optical media, the thickness of the guiding layer and the wavelength of the light used. In the case of light coupling with a grating of definite period, this effective refractive index determines the input or output coupling angle of the light beam. Formation of biomolecular layers on the surface of the waveguide changes the resonance condition and consequently changes the light coupling angle. Like IRS and SPR, the light wave interacting with the cover sample is evanescent. As a result, only those molecules within the penetration depth play a significant role in the change of the coupling angle.

The reason for this technique not having been adopted for molecular sensing previously is that waveguides normally used for integrated optical components compatible with monomode optical fibre technology have large thickness and small

index difference. As a result, the sensitivity (Lukosz and Tiefenthaler 1988) is low. Here, the sensitivity is defined as the differential of the effective refractive index (n_{eff}) with respect to the refractive index of the cover sample (n_c), i.e. $\partial n_{eff}/\partial n_c$. Tiefenthaler and Lukosz (1989) investigated the sensitivity theoretically and experimentally. By using a SiO_2-TiO_2 film as the guiding layer so that the index difference was high ($\geq$0.3) and the thickness of the guiding layer was small (80−180nm), they obtained an increase of several orders of magnitude in the sensitivity. They concluded that changes in thickness $\geq$0.01nm of an adsorbed or bound protein layer on a waveguide surface and changes in refractive index $\geq 2\times10^{-5}$ could be measured.

It was reported that the incoupled light intensity of an input grating coupler fabricated on a high refractive index planar waveguide responded extremely sensitively to the adsorption or desorption of molecules on the waveguide (Lukosz and Tiefenthaler 1983, Tiefenthaler and Lukosz 1984a). Such a grating coupler was proved to be able to act as humidity and gas sensor with submonolayer sensitivity (Tiefenthaler and Lukosz 1984b, 1985).

The possibility of using the sensor for biological sensing was investigated by Seifert et al. (1986). By attaching a flow cell onto the grating coupler, these authors showed that the refractive index change of the sample solution caused by an enzymatic reaction could be sensed with a resolution as low as $n_c = 5\times10^{-5}$.

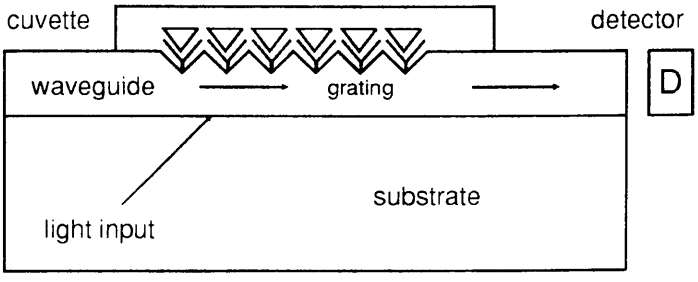

Input grating biosensor

Fig.2.5.1 Schematic diagram of input grating biosensor

Lukosz and Tiefenthaler (1988) theoretically analysed the sensitivity of input and output grating couplers and proposed an application in immunosensing through the addition of a chemoresponsive coating. This idea was put into practice by Nellen et al. (1988) who studied the specific immunoreaction between anti−human−IgG and human−IgG adsorbed (but not covalently linked) to the waveguide surface. By

measuring the effective refractive index shifts $\Delta n_{eff}(TE_0)$ and $\Delta n_{eff}(TM_0)$ through the input coupling angles of the guided TE_0 and TM_0 modes, the adsorption of human–IgG out of aqueous solutions on the waveguide surface as well as the slow and partial desorption of these proteins from the surface were noticed (Fig.2.5.1). More importantly, the specific binding of anti–human–IgG to the immobilised human–IgG was observed and a detection limit of 6μg/ml was reported.

The instrumentation of this device was later improved and with the same antibody–antigen pair, a detection limit of 0.16μg/ml (about 1nM) for anti–h–IgG was reported (Nellen and Lukosz 1990). Meanwhile the idea of using output grating couplers as sensors was implemented (Lukosz et al. 1990a) and an antibody detection limit of 4μg/ml was reported (Lukosz et al 1990b).

Although the feasibility of grating coupler sensors as immunosensors has been demonstrated, like SPR, grating coupling senses changes in the refractive index and therefore has similar problems to SPR. The device is sensitive to any factor which might influence the refractive index of the sample solution or the thickness of the adsorbed molecular layer (e.g. non–specific binding). By investigating the influence of salt concentration and pH value to the sensor, Nellen and Lukosz (1990) pointed out that in immunosensing with such a device, the pH value and salt concentrations of the aqueous solutions have to be controlled.

2.6 The Fluorescence Capillary Fill Device (FCFD)

The fluorescence capillary fill device (FCFD) (Badley et al. 1987) is an immunosensor which combines such techniques as fluorescence, waveguiding, the competitive binding of proteins and the mass production technology of liquid crystal display (LCD) cells. Because of the adherence throughout the development programme to the concept of an inexpensive, disposable and manufacturable product, this device is considered to be more important in the sense of commercial significance than in the sense of scientific techniques.

The FCFD is composed of two glass plates separated by a narrow (typically 100μm) gap (Fig.2.6.1). Antibodies are immobilised on the surface of the lower plate and this whole glass plate is used as a multimode waveguide. The upper plate is coated with dissolvable fluorophor labelled antigens (or haptens). Due to the capillary effect, when a sample solution with unlabelled antigens is dropped on to one end of

the gap, a fixed volume of the solution is drawn into the gap. The dissolved labelled antigen from the upper plate competes with the unlabelled antigen in the solution for the limited number of antibody binding sites on the lower plate. In the end, the lower plate is coated with an amount of the labelled antigen which is inversely proportional to the concentration of the unlabelled antigen.

When excited by a light source of suitable wavelength from either above or below the plate, all the fluorophors emit fluorescent light in all directions. Since the labelled antigens bound to the waveguide are close enough to the surface for evanescent coupling, the fluorescent light emitted by these antigens is much more likely to enter the waveguide at smaller angles measured with respect to the waveguide surface, and hence to emerge at smaller angles to the end of the waveguide. As a result, by comparing the intensity of the fluorescent light emerging at smaller angles to the axis of the waveguide with that at larger angles, a discrimination is reached between the fluorescent emission of the fluorophors bound to the waveguide surface and that of the ones in the bulk solution (Fig.2.6.1). As evanescent coupling is involved, the need for a separation step is avoided and no accurate measurement of the volume of the sample or any additional reagents is required.

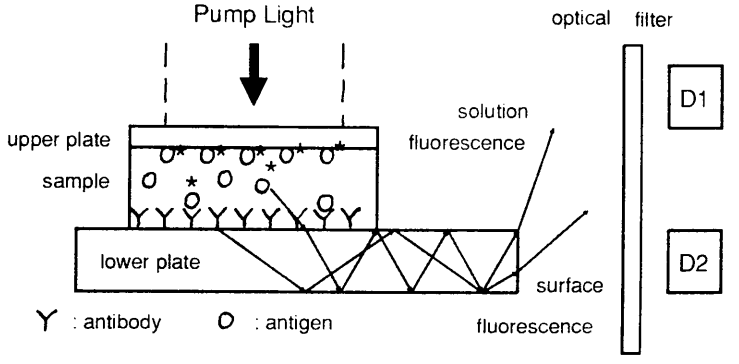

Fig.2.6.1 Schematic diagram showing ray paths of emitted fluorescent light in the FCFD

In the first phase of the FCFD development program, a competitive immunoassay for human− IgG was performed. Polyclonal anti− human− IgG was covalently immobilised on the lower plate and FITC− h− IgG solution was introduced into the cell. It was reported that h− IgG could be detected in the range of 100 to 660 nM in a 20 minute assay (Badley et al. 1987).

The FCFD was later applied to the detection of Rubella antibody in serum, plasma and whole blood (Parry et al. 1990). The assay time was reduced to less than 19 minutes. More recently, application of the FCFD to the assay for human chorionic gonadotrophin was reported (Deacon et al. 1990).

Although the FCFD has been successfully applied to a number of immunoassays, it suffers from some inherent problems. Firstly, as the excitation light is incoherent, the fluorophors are not efficiently excited. Secondly, owing to the nature of incoherent light which prevents the exciting light from being efficiently coupled into the waveguide, instead of evanescent excitation, the excitation of fluorescence is achieved through the illumination from either above or below the glass plate. As a result, all the fluorophors are excited and this may contribute to the background noise. The discrimination against fluorescence from within the bulk solution is disrupted to some extent by the appearance of some bulk fluorescence in the smaller angle zone. In addition, the device must be emptied and rinsed before measurement can be made, in order to lower background noise.

2.7 Light Scattering Techniques

Light scattering has long been a method of deriving information as to the size, shape and composition of particles. There are several analytical methods based on light scattering (Carr et al. 1987 and Price et al. 1983). Here only a few of them concerning immunoassays are briefly reviewed.

It was claimed (Robinson 1990) that Giaever's description on the visual observation of the antibody–antigen reaction introduced the first true optical immunosensor (Giaever 1973, 1974). This sensor is special in that antibody–antigen reaction can be observed with unaided eyes and the instrumentation for the assay is very simple. The technique is based on the fact that when electromagnetic radiation is scattered from conducting metallic spheres, the scattering is larger if the dimensions of the spheres is of the order of the wavelength of light. In addition, the scattering can be strongly influenced by coating the spheres with a thin dielectric layer.

In Giaever's experiments, indium was first evaporated on to glass coverslips or glass microscope slides, producing particles a few hundred nanometers in size on the

surface. After this, the coverslip or slide was covered with antigen (BSA, in Giaever's case) and with antibody specific to the covered antigen (rat anti– BSA in this case), by exposing it to appropriate solutions. As more light was scattered with the binding of proteins on the surface step by step, the increase in the darkness of the coverslip when illuminated from behind could be observed with naked eyes.

Giaever (1976a,b) successfully applied the technique to the detection of carcinoembryonic antigen (CEA) and its appropriate antibody (anti– CEA) at clinically interesting concentrations. In brief, for anti– CEA detection, CEAs were physically adsorbed onto indium treated slides as spots and the slides were immersed in different concentrations of anti– CEA solutions. In order to achieve high sensitivity, a long incubation time (about 15 hours) for the primary antibody– antigen reaction was adopted and a double sandwich immunoassay technique was subsequently performed. Experimental results showed that a very high detection sensitivity of 1ng/ml for the anti– CEA could be achieved. In the detection of CEA, a surface– inhibition test was also used. Here, an equal volume of different concentrations of CEA solutions was mixed with a same volume of a constant concentration of anti– CEA solution in a vial. A CEA spotted slide was then put into each vial and incubated in the same manner as for anti– CEA detection. Visual examination of the slides revealed a detection limit of 20ng/ml for CEA.

By performing a development step (i.e. a sandwich step) and using a densitometer to measure the light transmitted, Giaever et al. (1984) applied this technique to the detection of rheumatoid factors in controls and patients with arthritis.

A somewhat different method was advocated for surface immunoassay measurements by Sutherland et al.(1984b). Instead of shining light from above or below the slide, light of appropriate wavelength (410nm) was guided within the slide. Binding of antibody to antigen adsorbed on the slide was detected as an increase in the intensity of scattered light perpendicular to the surface. Sufficient sensitivity to differentiate 20μg/ml IgG from background was claimed.

In addition to the solid phase light scattering immunoassay technique, most light scattering immunoassays are performed employing the immunoprecipitation phenomenon within a solution. These immunoassays are not done at a continuous surface and consequently have little relevance to optical waveguide immunosensors.

Therefore, they are only briefly mentioned here. The immunoprecipitation following antibody–antigen binding is attributable to the fact that a protein usually possesses many antigenic determinants and as a result, will react with its respective antibodies to yield a precipitated immuno–complex. The amount of the immunoprecipitate is dependent upon the ratio of antibody to antigen concentration and can be monitored by the scattered light.

The scattered light can be measured by several techniques. The two most commonly used are turbidimetry and nephelometry. In turbidimetry, the decrease in light intensity of the incident beam as it passes through the sample is measured. The loss of light is caused by scattering as well as absorption and reflection. Usually a spectrophotometer or a colorimeter is used for the purpose. In nephelometry, the increase in light intensity is measured at some angle θ when the incident beam is passed through the sample. The angle θ is usually 90^0 (with respect to the light beam direction) or a forward angle.

As far as the performance of these techniques are concerned, turbidimetric assays have, in general, detection limits of 50–100ng antigen per cuvette (cuvette volume$\approx$200μl) while 90^0 nephelometry may offer a slight improvement in sensitivity compared with turbidimetry (Price et al 1983).

Of the dynamic light scattering methods used for the analysis of immunoassay reaction, photon correlation spectroscopy (PCS) has shown promise by offering a 100–fold increase in sensitivity compared to conventional assays. Being as sensitive as radioimmunoassay, the PCS method does not use radiochemicals, can be performed rapidly with no prior separation of bound and unbound antigen and can work with sample volumes as low as 1μl (Cohen and Benedek 1975; von Schulthess et al. 1976a,b).

A major problem associated with light scattering techniques is that the sensitivity can be seriously reduced by the presence of significant amounts of scattering background material as is often found in serum sample. To overcome the problem, attachment of optical markers to the reactants has been tested (Price et al. 1983). However, there are still such disadvantages as high cost and large size of the instrumentation, the requirement for frequent and careful calibration (except PCS), a high level of operator expertise and more often, a considerable amount of sample preparation and manipulation.

2.8 Summary and Discussion

Optical techniques for immunoassays include internal reflection spectroscopy (IRS), ellipsometry, surface plasmon resonance (SPR), grating coupling, fluorescence capillary fill device (FCFD) and light scattering. In terms of a wash-free immunosensor, IRS, SPR, grating coupling and the FCFD are promising because they all involve the interaction of an evanescent wave with analytes bound to an optical interface.

Ellipsometry and light scattering techniques are less likely to be employed for the development of a portable immunosensor, because their performance usually involves a number of steps, requiring a trained operator. Giaever's experiments concerning the visual observation of antibody-antigen reaction use very simple instrumentations and therefore may have a high commercial value, although the washing steps involved are still troublesome.

As far as meeting the market needs is concerned, in addition to the requirement of selectivity and sensitivity, an immunosensor should also be rapid, simple in operation and small in size. Furthermore, the sensor must be capable of handling such complex samples as whole blood, serum, plasma and urine, and be reagentless.

As will be shown later, the penetration depth of an optical evanescent wave is generally only a fraction of the wavelength (typically 100nm). The dimension of an antibody-antigen complex is about several tens of nanometers. Consequently, when an optical evanescent wave is used, it will interact mainly with those molecules which are bound to the surface. Using the optical interface as the solid phase of the immunoassay, the washing step for the separation of bound molecules from unbound ones can thus be easily avoided.

Although there are investigations using TIRF, SPR, grating coupling and the FCFD for the development of a wash-free solid phase immunosensor, a number of problems need to be solved. Generally speaking, a solution to the sensitivity of these techniques (especially the direct ones including SPR and grating coupling) to non-specific interactions has to be found. Most experimental results only show a sensitivity at nanomolar range, while a sensitivity better than picomolar range is

desirable for clinical applications (Miller 1990, Bluestein et al. 1990, Soini and Lövgren 1988). The cost of fabrication of the transducing element needs to be further reduced (Flanagan et al. 1988 and Sloper et al. 1990).

Among the evanescent wave immunosensors, indirect fluorescent label based sensors are more likely to offer a much higher sensitivity than direct refractive index based sensors. This is because it has been demonstrated that time–resolved fluorescence immunoassays could provide a very high sensitivity which is comparable with or even better than that of radio immunoassays (Soini and Lövgren 1988). On the other hand, the best sensitivity demonstrated with direct refractive index based immunosensors is at nanomolar range as reviewed in this chapter.

It is therefore reasonable to predict that, in the long run, devices based on evanescent fluorescence are more attractive than devices based on refractive index sensing techniques. Taking into consideration that multiple reflection can increase the sensitivity considerably, low mode–order or singlemode integrated optical waveguides and optical fibres are probably the best candidates for future internal reflection elements.

In biological aspects, investigations on the optimisation of the existing techniques for protein immobilisation onto solid surfaces and the efficient blocking of non–specific binding should be carried out. The immobilisation procedure should produce a uniform reproducible monolayer of protein on the surface without impairing the biological function of the protein.

Having all these techniques in mind, the author has attempted to develop a sensor which is based on the excitation of fluorescence by an optical evanescent wave generated on an ion–exchanged patterned waveguide in an ordinary microscope glass slide. The following chapters describe how such a sensor is developed and how some of the problems cited here are solved.

CHAPTER 3 THEORY OF ION-EXCHANGE AND PLANAR OPTICAL WAVEGUIDES

3.1 Introduction

Optical biosensors can be classified as reversible and irreversible. Reversible sensors are capable of following changes in analyte concentration continuously over a suitable period. Irreversible sensors are only capable of one measurement or assay and must then be discarded or regenerated. Since the extremely high equilibrium association constant of antibody-antigen reaction greatly favours the formation of antibody-antigen complexes, it would limit the reversibility of an immunosensor based on solid phase immunoassays. As an alternative, the idea of a single use disposable sensor is thus accepted. It is immediately obvious that the fabrication cost of the transducing element of such a sensor must be low to be of any commercial value. To address this problem, a method of preparing inexpensive thin glassy films of metal phosphates that form planar waveguides for evanescent biosensors has been devised (Sloper et al. 1988). While this is one way to tackle the problem, an alternative way is to use the ion-exchange technique to fabricate low loss optical planar waveguides in ordinary glass. This is because the fabrication cost of an ion-exchanged waveguide is extremely low. The task of fabricating a suitable ion-exchanged waveguide for evanescent fluorescence immunosensing thus comprises a major part of the author's research project.

In this chapter, an introductory discussion is given to the mechanisms of ion-exchange for the formation of waveguides in glass, the ion-exchange diffusion equation and its solution, the eigenvalue equation of planar optical waveguides, the electromagnetic field distribution of both step index and graded index planar waveguide, and the inverse WKB (Wentzel-Kramers-Brillouin) method for the determination of refractive index profiles.

3.2 Ion-exchange In Glass

The formation of waveguides in glass by the ion-exchange process is due to the increase of the refractive index of the glass caused by the process. Three major effects are responsible for the change in the refractive index. The first is the change in the size of the exchanging ions in glass, the second relates to the electronic

polarizability of the exchanging ions and the third comes from the stress induced by the substitution of ions (Ramaswamy and Srivastava 1988).

The refractive index change is proportional to the concentration of the indiffusing ions in the glass. In other words, the index profile in an ion–exchanged waveguide is a replica of the diffusion (concentration) profile. The index profile of ion–exchanged waveguides can therefore be predicted by solving the ion–exchange diffusion equation (Stewart 1979).

3.2.1 Glass composition and ion–exchange property

Soda lime glass is a mixture of inorganic oxides. Its essential component is silica (SiO_2) which is called the network former. The silicon ion is associated with four neighbouring oxygen ions to form a tetrahedral structural unit and these tetrahedra are randomly arranged in space (Stewart 1979). Glass constituents also include network modifiers. These are additional oxides (Na_2O, K_2O, CaO and MgO, etc.) which disrupt the continuity of the network and give monovalent or divalent ions.

The network modifying cations (especially the alkali metal ions such as Na^+ and K^+) have higher mobilities than those of the silicon and oxygen ions. These cations in glass are believed to diffuse readily through the essentially immobile silicate structure and can exchange with ions diffusing into the glass from such molten solutions as potassium nitrate and sodium nitrate (Stewart 1979).

3.2.2 The ion–exchange diffusion equation

In a binary one dimensional ion–exchange process, if no external electric field is applied, the ion–exchange process can be described by the following nonlinear diffusion equation (Stewart 1979).

$$\frac{\partial c}{\partial t} = \frac{\partial}{\partial x}\left[\frac{D_1}{(1-\alpha c)}\cdot\frac{\partial c}{\partial x}\right] \qquad (3.2.1)$$

where,

$$c=c_1/c_0, \quad \alpha=1-(D_1/D_0) \qquad (3.2.2)$$

and t is the diffusion time, x is the coordinate of depth measured from the surface of the glass into the substrate, c_1 is the concentration of incoming ions in the glass and c_0 is the total concentration of diffusing ions in the glass (i.e. incoming plus

outgoing), D_1 is the self-diffusion coefficient of the incoming ions and D_0 is the self-diffusion coefficient of the outgoing ions. Electrical neutrality requires that c_0 is a constant. The value of the self-diffusion coefficient D_i ($i=0,1$) depends on temperature and glass composition (Ramaswamy and Srivastava 1988).

In Equ. (3.2.1), the free parameters are α and D_1. The shape of the diffusion profile depends strongly on the value of α as pointed out by Walker et al (1983). It varies from an error function complement for $\alpha=0$ to a rectangular function for $\alpha=1$. Other profiles for $0<\alpha<1$ include a second-order polynomial profile (Stewart et al. 1977) and a Guassian profile (Albert and Yip 1985).

3.2.3 General solution of the diffusion equation

The solution of the non-linear differential equation (3.2.1) can be obtained by the finite difference method (Stewart 1979). Consider a plane glass slide of thickness $2l$ as shown in Fig.3.2.1. If it is assumed that the non-dimensional variables, $X=x/l$, $T=D_1t/l^2$ are used, the initial and boundary conditions of ion-exchange for the slide are

$$c = c_i(X), \qquad 0 < X < 1, \; T = 0 \qquad (3.2.3)$$

$$c = H, \qquad X = 1, \; T > 0 \qquad (3.2.4)$$

$$\partial c/\partial X = 0, \qquad X = 0, \; T > 0 \qquad (3.2.5)$$

where $c_i(X)$ is the initial concentration distribution in the glass slide, and H is the normalised surface concentration during ion-exchanging ($0 \leqslant H \leqslant 1$).

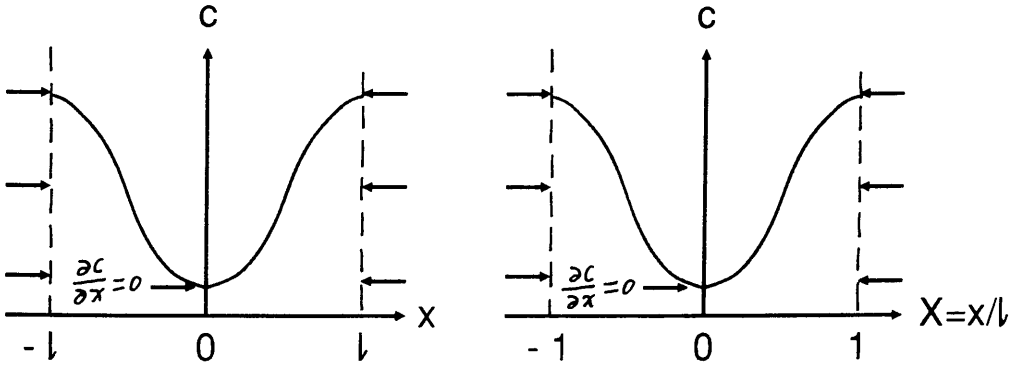

Fig.3.2.1 Coordinate systems for the thin plane sheet (after G. Stewart 1979)

If it is defined that

$$s = -[\ln(1-\alpha c)]/\beta \qquad (3.2.6)$$

where

$$\beta = -\ln(1-\alpha) \qquad (3.2.7)$$

the diffusion equation (3.2.1) becomes

$$\frac{\partial s}{\partial T} - e^{\beta s} \cdot \frac{\partial^2 s}{\partial X^2} = 0 \qquad (3.2.8)$$

In terms of s, the initial and boundary conditions of ion-exchange for the slide can now be re-expressed as

$$s(1,T) = (-1/\beta) \cdot \ln(1-\alpha \cdot H) \qquad (3.2.9)$$

$$s(0,T) = s(\delta X, T) \qquad (3.2.10)$$

$$s(X,0) = (-1/\beta) \cdot \ln[1-\alpha \cdot c_i(X)] \qquad (3.2.11)$$

Detailed description of the solution of the above partial differential equation with appropriate initial and boundary conditions using the finite difference method has been given by Stewart (1979). Using Stewart's (1979) flow chart, a computer program has been written which gives the general solution of the diffusion equation.

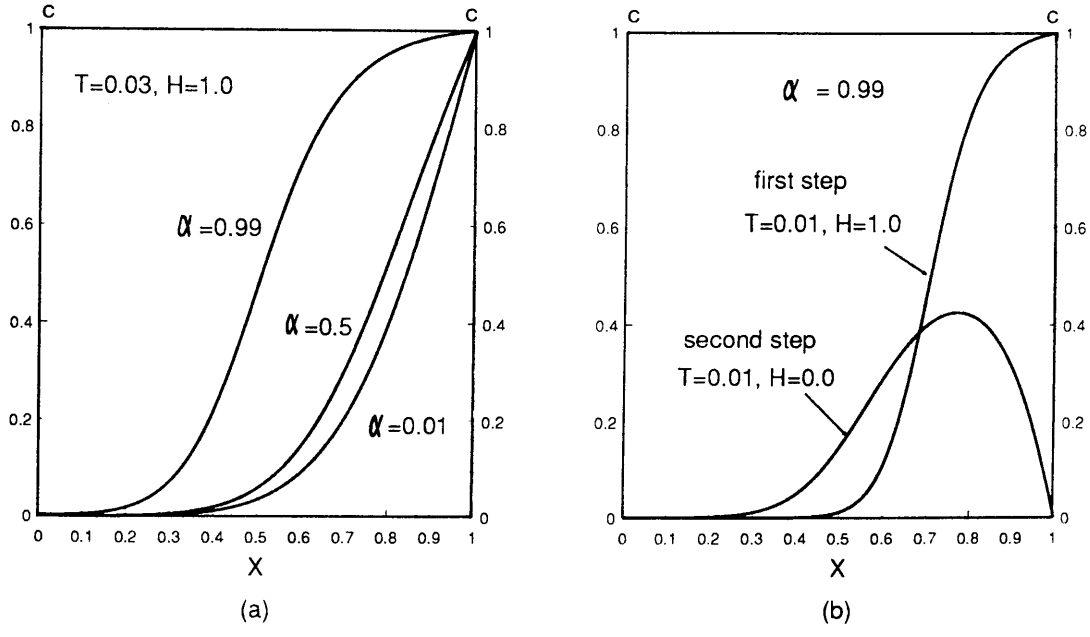

Fig.3.2.2 Diffusion profiles of silver ion-exchange

The solutions of the diffusion equation for a one step ion-exchange with

$c_i(X)=0$, H = 1 (corresponding to the silver ion−exchange case) and α = 0.01, 0.5, 0.99 are shown in Fig.3.2.2a.

Since buried waveguides are fabricated by a second step sodium ion−exchange (i.e., H= 0), the diffusion profile of the first step ion−exchange can be viewed as the initial concentration distribution of the second step sodium ion−exchange (i.e., $c_i(X)= c_1(X)\,|_{T=T_1}$, where 1 stands for the first step and T_1 is the normalised diffusion time of the first step silver ion−exchange). Fig.3.2.2b shows the diffusion profile of a buried silver ion−exchanged waveguide.

In the case of potassium ion−exchange, the maximum concentration of exchanged ions is only a fraction of the total concentration c_0 (i.e. H= 0.9) (Albert and Yip 1985, Cullen et al. 1986). Solutions of the diffusion equation for H= 0.9 in the case of both surface and buried waveguides are shown in Fig.3.2.3 (a) and (b) respectively.

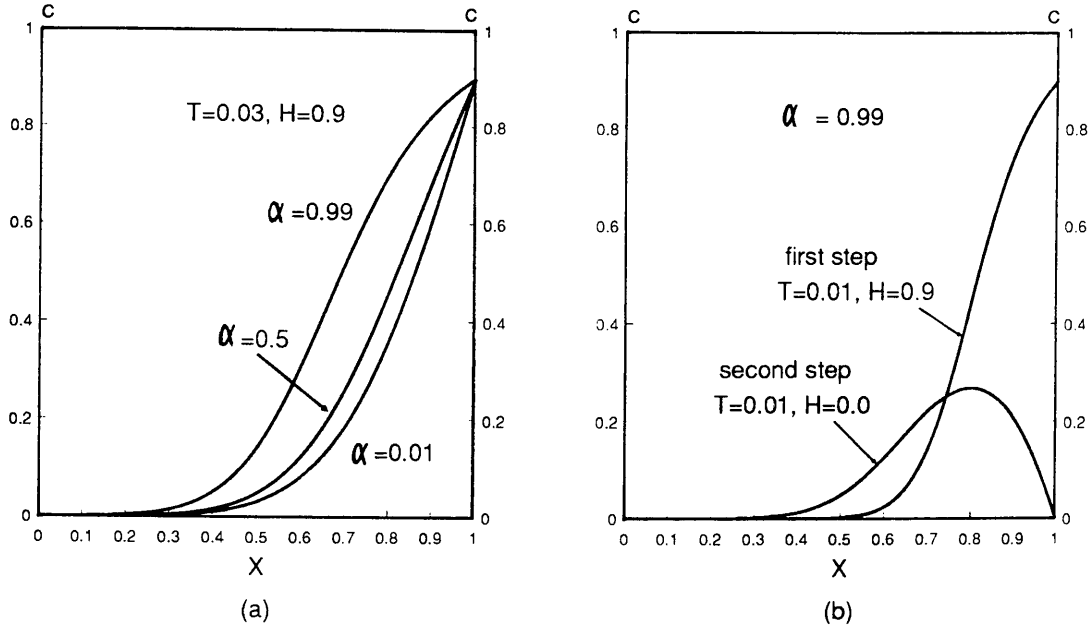

Fig.3.2.3 The diffusion profiles of potassium ion−exchanged waveguides

3.3 Theory of planar optical waveguides

Given the refractive index profile of a planar optical waveguide, the electromagnetic field distribution of such a waveguide can be determined using Maxwell's equations. Since the immunosensor under development is an evanescent

wave device, it is important to show that an evanescent wave can be generated on the surface of a planar waveguide.

3.3.1 Three-layer dielectric planar waveguides

Consider first the simplest case of a three-layer dielectric planar waveguide. Such a waveguide consists of a high refractive index layer of thickness d and index n_1, sandwiched between two layers of low refractive indices media (n_2 and n_3, with $n_2 < n_1 > n_3$, Fig.3.3.1).

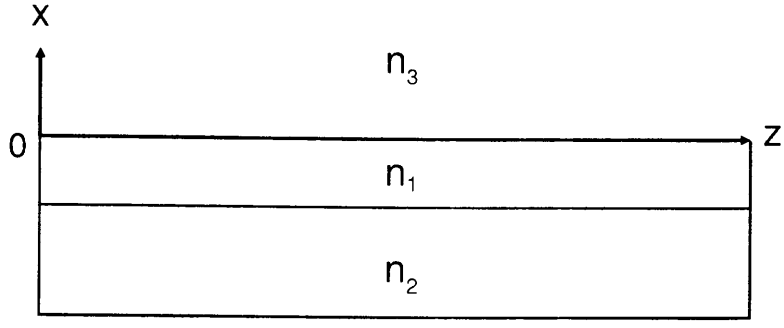

Fig.3.3.1 Three layer dielectric planar waveguide

In the ray optics approach, the reason why such a structure can guide light is explained by total internal reflections. If the angle of incidence (θ_i) of the light ray at both the upper and lower interfaces exceeds the appropriate critical angles, i.e. $n_2/n_1 < \sin\theta_i > n_3/n_1$, the light ray will bounce up and down in a zig-zag way. However, not all the rays satisfying this incident angle condition will propagate in the waveguide because the light rays will interfere with each other and only those which interfere constructively will survive.

The electric field distribution in such a waveguide can be obtained by solving Maxwell's equations. For TE modes (i.e., the electric vector normal to the plane of incidence), the electric field is given by the following expression (Marcuse 1974)

$$E_y = A\cdot\exp(-\delta\cdot x), \qquad x \geq 0 \qquad (3.3.1)$$

$$= A\cdot[\cos(\kappa x) - (\delta/\kappa)\cdot\sin(\kappa x)], \qquad 0 \geq x \geq -d \qquad (3.3.2)$$

$$= A\cdot[\cos(\kappa d) + (\delta/\kappa)\cdot\sin(\kappa d)]\cdot\exp(\gamma(x+d)), \qquad x \leq -d \qquad (3.3.3)$$

where A is the amplitude of the electric field at the interface x= 0,

$$\kappa = (n_1^2 k^2 - \beta^2)^{\frac{1}{2}} \qquad (3.3.4)$$

$$\gamma = (\beta^2 - n_2^2 k^2)^{\frac{1}{2}} \qquad (3.3.5)$$

$$\delta = (\beta^2 - n_3^2 k^2)^{\frac{1}{2}} \qquad (3.3.6)$$

and the longitudinal propagation constant β is given by

$$\beta = k \cdot n_{eff} = k \cdot n_1 \cdot \sin\theta_i \qquad (3.3.7)$$

with n_{eff} being the effective refractive index of the waveguide.

The longitudinal propagation constant β can only have discrete values corresponding to different modes. These values are determined by the following eigenvalue equation.

$$\tan(\kappa d) = [(\delta/\kappa) + (\gamma/\kappa)]/[1 - (\delta/\kappa)(\gamma/\kappa)] \qquad (3.3.8)$$

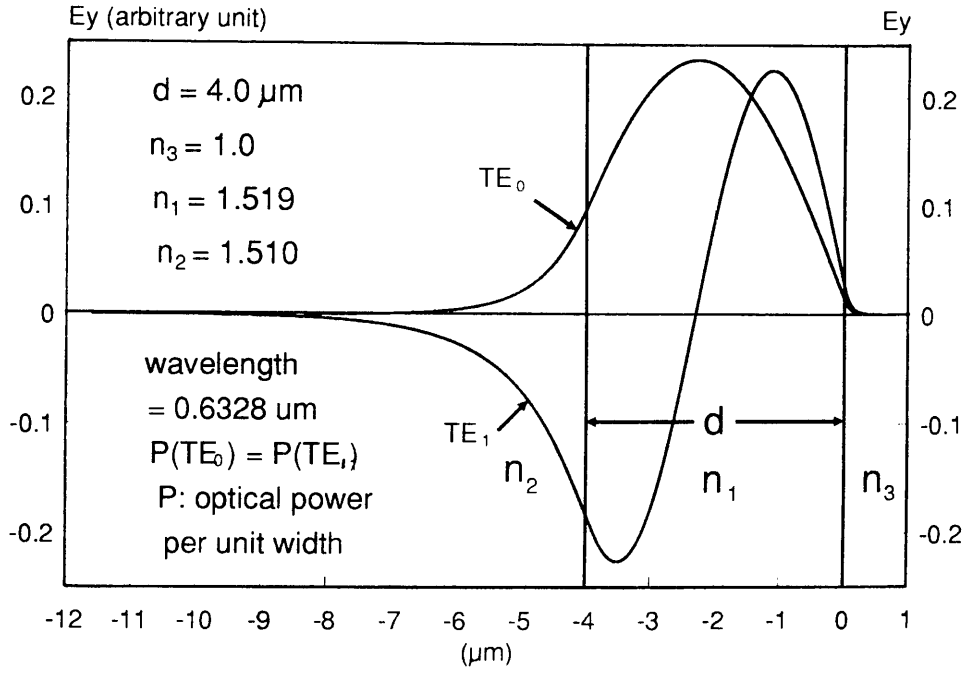

Fig.3.3.2 Electric field distribution of a three layer planar waveguide

In the case of TM modes, the electromagnetic wave is characterised by the magnetic field normal to the plane of incidence. Its distribution and the corresponding eigenvalue equation are given by (Marcuse 1974)

$$H_y = -(n_3^2\kappa/n_1^2\delta)B\cdot\exp(-\delta\cdot x), \qquad x \geq 0 \quad (3.3.9)$$

$$= B[-(n_3^2\kappa/n_1^2\delta)\cos(\kappa x)+\sin(\kappa x)], \qquad -d \leq x \leq 0 \quad (3.3.10)$$

$$= -B[(n_3^2\kappa/n_1^2\delta)\cos(\kappa d)+\sin(\kappa d)]\cdot\exp(\gamma(x+d)), \quad x \leq -d \quad (3.3.11)$$

with

$$E_x = (\beta/n^2\omega\varepsilon_0)H_y \quad (3.3.12)$$

$$E_z = (-i/n^2\omega\varepsilon_0)\partial H_y/\partial x \quad (3.3.13)$$

and

$$\tan(\kappa d) = \frac{[(n_1^2\delta/n_3^2\kappa) + (n_1^2\gamma/n_2^2\kappa)]}{[1-(n_1^2\delta/n_3^2\kappa)\cdot(n_1^2\gamma/n_2^2\kappa)]} \quad (3.3.14)$$

Examination of equations (3.3.1)–(3.3.3) and (3.3.9)–(3.3.11) indicates that the electromagnetic field has an oscillatory behaviour in the guiding region and an exponential decay behaviour within the two optically rarer medium. This means that an evanescent wave can be generated on the surface of such a planar waveguide. Fig.3.3.2 shows the normalised field distribution in the waveguide.

3.3.2 Planar waveguides with a graded–index profile

The homogeneous three layer dielectric waveguide is just a simple example of planar waveguides. In practical situations, a large number of waveguides are fabricated by diffusion techniques which result in an inhomogeneous refractive index distribution. These waveguides are called graded–index waveguides.

In the ray optics approach, the propagation of rays in a graded index structure is explained by ray bending (and total internal reflection, if the diffused waveguide is not a buried one). For a particular ray (i.e. mode), the longitudinal propagation constant β is fixed. Keeping this fact in mind, it can be seen from (3.3.7) that if n_1 is replaced by n(x), a decrease in the value of n(x) is accompanied by an increase in θ_i (the direction of the ray) and vice versa. In addition, in order for the direction of the ray, i.e. θ_i, to have a real meaning, the ray should be within a region $x_{c1} \leq x \leq x_{c2}$ so that $k\cdot n(x) \geq \beta$ (where $n(x_{c1}) = n(x_{c2}) = \beta$ when n(x) is continuous, and x_{c1} and x_{c2} are called the turning points or caustics). The ray trajectories for the case of buried and surface ion–exchanged planar waveguides are shown in Fig.3.3.3.

To get the electromagnetic distribution of such a waveguide, there are a

number of methods for the solution of Maxwell's equations. A relatively simple and widely applied method is the WKB (Wentzel– Kramers– Brillouin) approximation method. This method gives a good approximation as long as the variation of the refractive index n(x) is small over distances of the order of the wavelength (Adams 1981).

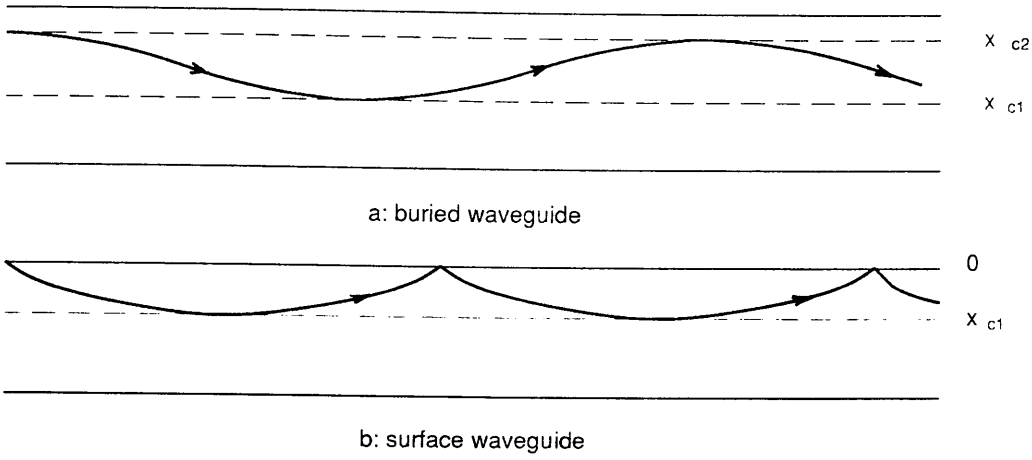

Fig.3.3.3 Ray trajectories in graded– index planar waveguides
a) buried waveguide; b) surface waveguide

In the case of a surface planar waveguide or patterned waveguide where internal reflection occurs at the upper interface of the index discontinuity (Fig.3.3.3b), the solution of the Maxwell's equations for TE modes using this method is (Adams 1981)

$$E_y \propto \frac{1}{2P^{1/2}} \exp\left(-\int_0^x P\,dx\right), \qquad x>0, \quad (3.3.15)$$

$$E_y \propto \frac{1}{Q^{1/2}} \cos\left(\int_{x_{c1}}^x Q\,dx - \frac{\pi}{4}\right), \qquad x_{c1}<x<0, \quad (3.3.16)$$

$$E_y \propto \frac{1}{2P^{1/2}} \exp\left(-\int_x^{x_{c1}} P\,dx\right), \qquad x<x_{c1}, \quad (3.3.17)$$

where

$$Q^2 = -P^2 = k^2n^2(x)-\beta^2 \qquad (3.3.18)$$

and x_{c1} is the caustic or turning point, i.e. $k^2n^2(x_{c1})=\beta^2$,

It should be noted that the above approximate solutions can not be applied to the vicinity of the caustic or turning point, x_{c1}, as there is a pole. The solution in the vicinity of x_{c1} has been discussed by Stewart (1979) and Adams (1981) and will not be given here as it is not important for an evanescent wave biosensor.

Again, the propagation constant β can only have discrete values corresponding to different modes and these values are determined by the following eigenvalue equation

$$\int_{x_{c1}}^{0} (k^2 \cdot n^2(x)-\beta^2)^{1/2} dx = m\pi + \frac{\pi}{4} + \tan^{-1}\left[\frac{((\beta^2-k^2n_3^2)^{1/2}}{(k^2n_s^2-\beta^2)^{1/2}}\right] \qquad (3.3.19)$$

where $m = 0, 1, 2,\cdots$ is the mode order, n_s is the surface refractive index of the waveguide and n_3 is the refractive index of the cover medium.

The treatment for TM modes is little different from that for TE modes and details of this treatment can be found in Adams (1981). It will therefore not be discussed here.

The expressions for the electric field distribution show that within the region $x_{c1} < x < 0$, the electromagnetic field has an oscillatory behaviour, whereas outside this region it has an exponential decay behaviour. In the case of an evanescent wave biosensor, the cover medium is usually a homogeneous medium (such as an aqueous solution) and the optical interface acts as an internal reflection interface. Suppose that n_3 is the refractive index of the cover medium. Since n_3 is a constant and the propagation constant β is also a constant for a specific mode, in the region above the interface,

$$P = [\beta^2-k^2n_3^2]^{1/2} = \delta \qquad (3.3.20)$$

Completion of the integration in Eq.(3.3.15) results in the electric field distribution in the cover medium as

$$E_y \propto \frac{1}{2\cdot\delta^{1/2}} \cdot \exp[-\delta\cdot x], \qquad x>0, \qquad (3.3.21)$$

It can be seen from this equation that a graded-index planar waveguide gives

the same exponential decay behaviour as in the case of a three layer homogeneous planar waveguide (i.e. Eq.(3.3.1)).

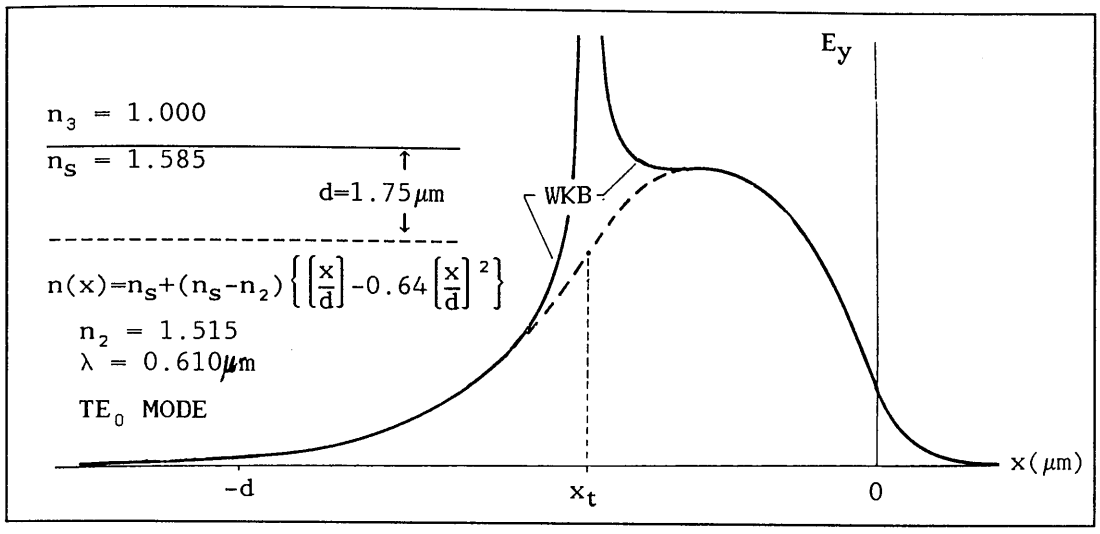

Fig.3.3.4 The electric field distribution of a Ag^+ – exchanged graded– index planar waveguide (After Yan 1978)

Fig.3.3.4 shows the electric field distribution of a graded– index Ag^+ – exchanged planar waveguide (after Yan 1978). The refractive index profile is of a second order polynomial function as reported by Stewart et al. (1977). Only the electric field distribution of the TE_0 mode is given. As has been pointed out previously, the WKB approximate solution can not be applied to the region near the turning point x_t as it breaks down there. The value of E_y in this region is thus determined graphically as shown by the dashed line.

A comparison of Fig.3.3.2 and Fig.3.3.4 shows that the electric field distribution of a step– index waveguide is similar in shape to that of a graded index waveguide. For the purpose of evanescent wave immunosensing, what is important is the evanescent field beyond the upper interface of the waveguide. The theoretical results show that such a field does exist although it is only a small fraction of the maximum electric field within the guiding layer.

3.3.3 The inverse WKB method for the determination of the modal turning points

The WKB approximation method is very useful because once given n(x), the effective refractive index and the field distribution can be calculated with good

accuracy (Gedeon 1974). More interestingly, the WKB method can be used inversely, i.e. given the measured effective refractive indices, an approximate index profile n(x) of a surface planar waveguide can be obtained with the aid of the eigenvalue equations (White and Heidrich 1976).

Re-examine the eigenvalue equation (3.3.19). Let $u = x/\lambda$, where λ is the wavelength, and let $u_m = x^m{}_{c_1}/\lambda$, where m stands for the mode order. The eigenvalue equation can be rearranged to give an approximate expression for u_m in terms of u_i (i= m−1, m−2, ..., 1, 0,−1) and n_i (i= m, m−1, ..., 1, 0, −1), where n_m is the effective refractive index of the mth mode, $u_{-1} = 0$ and $n_{-1} = n_s$ (the surface refractive index) (White and Heidrich 1976) i.e.

$$u_m = u_{m-1} - \left(\frac{3}{2}\right)\left[\frac{n_{m-1}+3n_m}{2}\right]^{-1/2} \cdot (n_{m-1}-n_m)^{-1/2} \cdot \left[\frac{4m+3}{8} - A\right] \qquad (3.3.22)$$

where

$$A = \frac{2}{3} \cdot \sum_{j=0}^{m-1}\left[\frac{n_{j-1}-n_j}{2} + n_m\right]^{1/2} \cdot \left[\frac{u_{j-1}-u_j}{n_{j-1}-n_j}\right] \cdot \left[(n_{j-1}-n_m)^{3/2} - (n_j-n_m)^{3/2}\right]$$

For the case when m= 0,

$$u_0 = -\frac{9}{16}\left[\frac{n_s+3n_0}{2}\right]^{-1/2} \cdot (n_s-n_0)^{-1/2} \qquad (3.3.23)$$

A computer program can be written to calculate u_m using (3.3.22) and (3.3.23). However, in general, only the effective refractive indices can be easily measured and the surface index n_s is unknown. To solve this problem, a number of guessed values of n_s ($>n_0$) can be used for the calculation and the n_s which gives the smoothest profile is selected.

Having calculated u_m for each n_m, the refractive index profile can then be obtained. In section 3.2, it has been mentioned that the diffusion profile of an ion-exchanged waveguide is a replica of the refractive index profile. Here, it has been shown that using the inverse WKB method, the refractive index profile can be reconstructed from measured mode effective indices. It is therefore possible to predict the index profile of an ion-exchanged planar waveguide for an arbitrary diffusion time at a given temperature. To achieve this, a multimode surface waveguides can be fabricated and its index profile obtained with the aid of the inverse WKB method. The non-linear diffusion equation can be solved by adjusting the diffusion parameters

α and D_1 so that the theoretical dispersion curves best match the experimental ones. The diffusion parameters determined can then be used to give the diffusion profile for any given time at the used temperature.

3.4 Summary and Discussions

A disposable evanescent wave immunosensor requires that the fabrication cost of the sensing element is low. The ion–exchange technique is a well established method for the fabrication of cheap optical waveguides in glass. It is therefore quite suitable for the purpose.

The refractive index change in glass caused by the ion–exchange process is proportional to the concentration of the indiffused ions. It is possible to predict the refractive index profile by solving the non–linear diffusion equation.

In either a three layer homogeneous planar waveguide or a diffused inhomogenous planar waveguide, the solution of Maxwell's equations shows that internal reflections at the upper optical interface of these waveguides result in an exponential decay of the electromagnetic field from the interface. It is therefore possible to use a planar waveguide as the internal reflection element of an evanescent wave immunosensor.

The inverse WKB method is a very useful method for the characterisation of a planar waveguide because once the effective refractive indices of a multimode planar waveguide are obtained experimentally, the refractive index profile of the waveguide can be determined approximately. The diffusion equation can be combined with the inverse WKB method to get the diffusion parameters and these diffusion parameters can, in turn, be used to predict the refractive index profile of an ion–exchanged planar waveguide. In the next chapter, it will be shown how the theory developed here can be used for the characterisation of experimental waveguides.

CHAPTER 4 FABRICATION AND CHARACTERISATION OF POTASSIUM ION-EXCHANGED WAVEGUIDES

4.1 Introduction

The theoretical analysis in the last chapter indicates that ion-exchanged planar waveguides can be used as the internal reflection element (IRE) of optical immunosensors. The most important task is, therefore, to develop the technology for the fabrication of the IRE which is suitable for evanescent wave immunosensing. A patterned waveguide is preferred because it has a number of advantages when it is used as the IRE. The author has succeeded in fabricating such a waveguide (Zhou et al. 1990, 1991a/b/c/d, 1992) and the fabrication procedures of surface, buried and patterned waveguides will now be described. Results obtained from the characterisation of experimental waveguides will also be given.

It should be noted that although K^+-exchange has been widely used to fabricate surface waveguides (Yip and Finak 1984, Chiang 1985, Gortych and Hall 1986), few reports has been made on the fabrication of buried and patterned waveguides using this technique (Ramaswamy and Iraj Najafi 1986, Miliou et al. 1989). It was once reported that the K^+ would not diffuse out during the second thermal Na^+-exchange process (McCourt et al. 1987). Only recently has Miliou et al. (1989) reported the successful burial of K^+-exchanged waveguides using electric field assistance during the second step Na^+-exchange process.

This investigation has been successful in burying K^+-exchanged surface planar waveguides completely, using only a second-step thermal Na^+-exchange process without electric field assitance (Zhou et al 1992). Appropriate ion-exchange temperatures and time durations have been experimentally determined which overcome the problems of incomplete burial and microcracking of the guiding layer normally associated with burying K^+-exchanged surface waveguides.

In characterising the waveguide, the refractive index profiles of both surface and buried K^+-exchanged waveguides have been directly observed for the first time (to the author's knowledge) using a Mach-Zehnder transmitted-light interference microscope (Leitz Wetzlar, Germany) (Zhou et al. 1992). Although, the refractive index profiles of Ag^+-exchanged waveguides have been observed using the

interference fringe method (Stewart 1979, Izawa and Nakogome 1972), the same technique does not seem to have been successfully applied to K^+ – exchanged waveguides.

Throughout the work, potassium instead of silver ion– exchange has been consistently used. This is attributable to the following facts. 1) Silver nitrate is more expensive than potassium nitrate; 2) Ag^+ – exchanged waveguides are more lossy than K^+ – exchanged ones (for pure silver nitrate exchanged waveguides the loss can be in the range of 2dB/cm while in the case of pure potassium nitrate the loss is of the order of 0.2dB/cm (Findakly 1985)); 3) Ag^+ – exchanged waveguides are more strongly fluorescent than K^+ – exchanged ones when excited by the 488nm laser light; and 4) Ag^+ – exchanged waveguides are not stable, namely, they are prone to deterioration in their optical transmission. This deterioration is exemplified by the silver staining effect due to the reduction of silver ions in glass (Stewart 1979). Other metal nitrates suitable for ion– exchange for waveguide fabrication are relatively expensive (some of them are even toxic) and are therefore not selected.

4.2 Waveguide Fabrication

4.2.1 The ion– exchange facilities

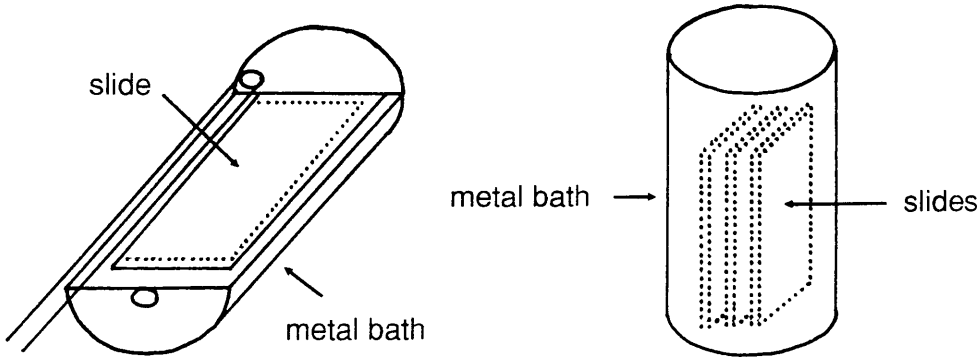

Fig.4.2.1 The old and new ion– exchange arrangement

Since much work concerning ion– exchanged waveguides has been done previously in this department, all facilities required for ion– exchange are in place. However, with the old arrangement as shown in Fig.3.4.1 (a), only one slide can be ion– exchanged each time. To improve the efficiency, the whole arrangement is improved as shown in Fig.3.4.1 (b). With this set– up, a number of waveguides can

be fabricated in a batch mode. In addition, by removing slides during processing, ion–exchanged waveguides fabricated at the same temperature but for different time durations can be readily obtained.

4.2.2 The glass cleaning procedures

Soda lime glass microscope slides (75.5mm×26mm×1mm) from BDH Ltd (U.K.) are cleaned before ion–exchange. The standard cleaning is carried out by soaking the slides successively in each of the following solutions in an ultrasonic bath for 5 minutes; a) trichloroethylene; b) methanol; c) acetone. These slides are rinsed with RO (reverse osmosis) water, blown dry with compressed filtered nitrogen gas and placed over a hot plate (90°C) for about 10 minutes.

When particularly thorough cleaning is required as in the case of protein immobilisation, the slides are acid–cleaned and/or scrubbed before the rinsing step in the standard cleaning procedure. Acid cleaning is achieved by gently pouring 30% hydrogen peroxide into concentrated sulphuric acid, agitating the mixture mildly until the temperature reaches 80°C, and soaking the slide in the mixture for 10–15 minutes. Still further cleaning can be performed by immersing the slide in a Petrie dish filled with acetone and scrubbing the surface with cotton buds.

4.2.3 Fabrication of surface planar waveguides

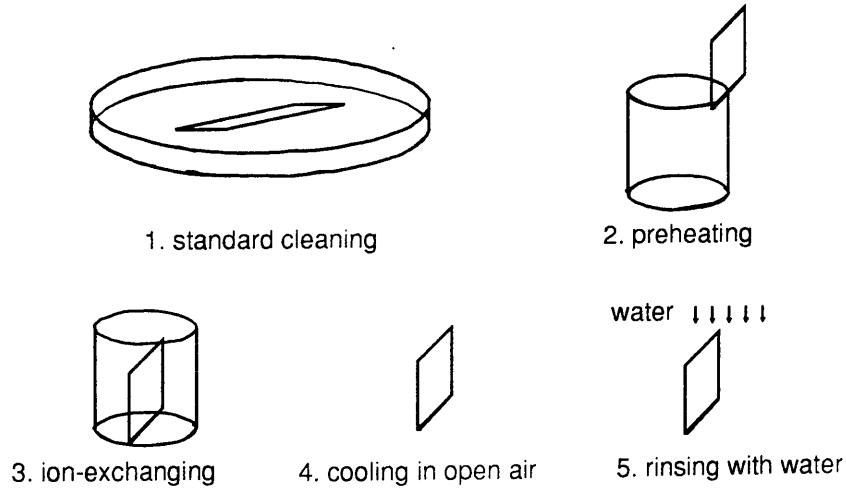

Fig.4.2.2 The ion–exchange procedures

The ion–exchange is conducted in a small tube furnace at temperatures of

340 °C to 500 °C. A metal bath inside the furnace is filled with either potassium nitrate or sodium nitrate. To fabricate surface planar waveguides, potassium nitrate is used. An ion–exchange temperature is first set and a thermocouple is inserted into the metal bath to monitor the temperature. After the temperature has reached the required value and has stabilised (±2 °C), the cleaned glass slides are lowered into the tube furnace and set on the edge of the metal bath for 5 minutes before being immersed into the molten nitrate. This preheating stage prevents cracking of the slides induced by abrupt increase in temperature. After immersion in the melt for a specified time which is anything between 20 minutes to 24 hours, the slides are taken out of the bath, cooled down to room temperature in open air and rinsed with hot water. The rinsing dissolves away the excess potassium nitrate which adheres and recrystalises onto the slide. Fig.4.2.2 illustrates the major steps of the ion–exchange process.

4.2.4 Fabrication of buried planar waveguides

To bury K^+ – exchanged surface planar waveguides completely with a thermal sodium ion–exchange process, the ion–exchange time and temperature for the two processes must be properly chosen. Otherwise, the waveguide will be either only partially buried or damaged as a result of microcracking. The author has found that good buried waveguides can be fabricated if the ion–exchange time and temperature for both steps are $t \approx 30$ minutes and $T \approx 490$ °C. In practice, the second step Na^+ – exchange process is virtually the same as the first step K^+ – exchange process except that, instead of potassium nitrate, sodium nitrate is used.

4.2.5 Patterning of buried waveguides

To pattern a completely buried planar waveguide, standard wet etching technique is used. The slides are first cleaned as described above and dried over a hot plate (90 °C). The slide is placed on the chuck of a spinner and filtered photo–resist 1450–31 (from Shipley) is applied to the surface of the slide with a syringe. After spinning at 4000 rpm for 30 sec, the photo–resist film is cured at 90 °C for half an hour. Rectangular patterns are then exposed with UV light on the resist coating using a predesigned mask. The exposed slide is developed for 90 sec in a mixture of 1:1 RO water with 1450–31 developer (from Shipley). The developed slide is then rinsed with RO water and dried. The patterns are etched into the glass slide by immersing the slide in SiO_2 etchant (4:1 HF) with mild agitation for 2 to 3 minutes, rinsing it

with RO water and blowing it dry with compressed nitrogen gas. Finally, the unexposed photo– resist is removed in acetone. Fig.4.2.3 shows the major stages involved in patterning a completely buried planar waveguide.

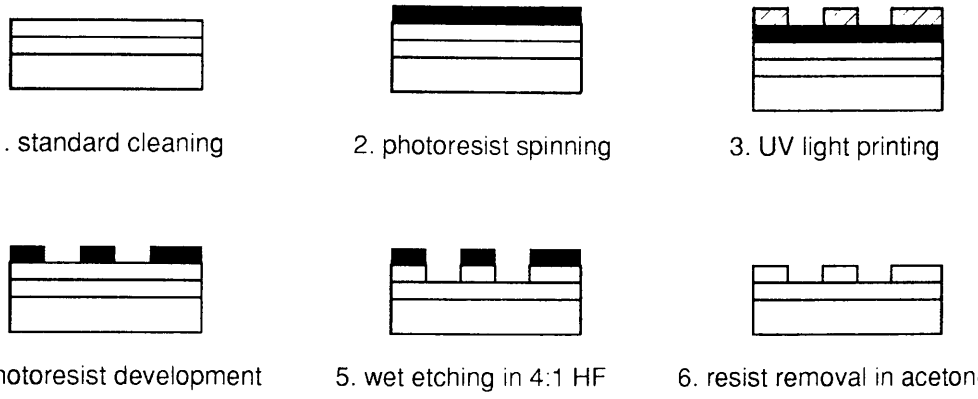

Fig.4.2.3 Waveguide patterning procedures

To facilitate the coupling of light into the waveguide with prism coupling, one end of the slide (about 10mm) is also etched by immersing just this part in the SiO_2 etchant (4:1 HF) for 4 minutes, resulting in an etching depth of about 8μm.

4.3 Characterisation of Fabricated Waveguides

4.3.1 The experimental set– up

Fig.4.3.1 shows the experimental set– up for prism coupling of light into a planar waveguide. The waveguide slide is mounted under an input coupling prism which is fixed on a rotation table. Laser beams from either a He– Ne laser (λ= 632.8nm) or from an Ar^+ laser (λ= 488nm) are directed to a beam splitter where they superimpose and propagate in the same direction. A chopper and a polariser are placed behind the beam splitter. The laser beam of either 488nm or 630nm is reflected by a mirror and directed to the input coupling prism. The rotation table is turned until strong coupling of light into the planar waveguide takes place. The reason for keeping the slide in an approximately level position is to facilitate the retaining of aqueous solutions on the slide when immunosensing of aqueous solutions is intended. The plane of polarisation of the He– Ne laser is at a 45^0 azimuthal angle and the selection of either TE or TM mode is achieved by the rotation of the polariser. Because of its size and integral cool system, the Ar^+ laser is always vertically polarised (i.e. TM mode).

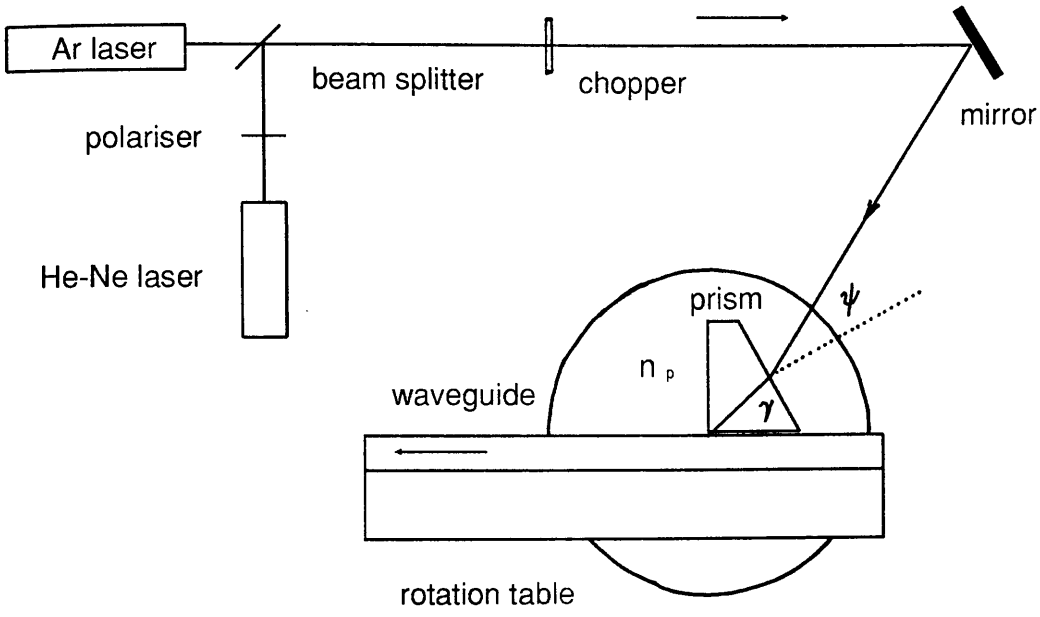

Fig.4.3.1 Experimental set– up for light input coupling and waveguide characterisation

4.3.2 Observation of waveguide guided modes

Guided modes in a planar waveguide can usually be observed by putting an output coupling prism on the waveguide surface and watching the discrete mode lines from the output coupling prism on a screen. It is necessary, in this case, to discriminate between waveguide guided mode lines and substrate guided mode lines which also appear as discrete bright lines. Although this method is good for surface planar waveguides, it can not be applied to completely buried planar waveguide since waveguide guided modes can not be coupled out due to the presence of a thick superstrate layer. The observation of a streak of light appearing along the surface of the slide can indicate the guiding of light by the waveguide, but in the case of completely buried planar waveguides, the scattering of guided light is low. The author has found that an alternative way to observe and differentiate waveguide guided modes from substrate guided mode is to examine the light field pattern emerging from the front end of the slide. A particular feature of the field pattern relating to the waveguide guided mode is that the pattern shows a large number of vertical straight bright lines whereas substrate guided light does not. Fig.4.3.2a) shows the typical light field pattern of waveguide guided modes and Fig.4.3.2b) shows the case of substrate guided modes.

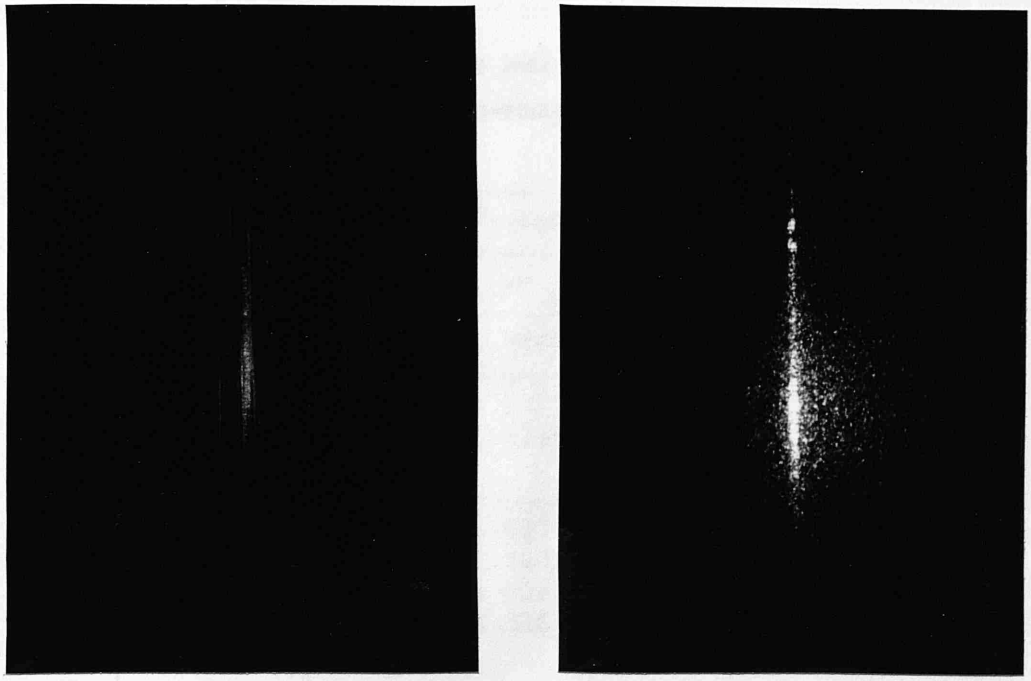

(a) (b)

Fig.4.3.2 Typical light field pattern of a): waveguide guided modes and b): substrate guided modes

4.3.3 Measurement of effective refractive indices of surface planar waveguides

One of the parameters which can be obtained experimentally from an optical waveguide is the mode effective refractive index. It is usually obtained for each mode by measuring the synchronous input coupling angle using the prism coupling method. The mechanism of prism light coupling is that the evanescent field associated with the total internal reflection of light at the prism base—air gap interface allows the tunnelling the light into the waveguide. However, the coupling of light to the guided mode occurs only when the evanescent field in the gap region travels at the same phase velocity as the guided modes. With the parameters defined as in Fig.4.3.1, the effective refractive index is related to the synchronous coupling angle ψ by

$$n_{eff} = n_p \cdot \sin[\gamma + \sin^{-1}(\sin\psi/n_p)] \qquad (4.3.1)$$

where n_p is the refractive index of the right—angled prism,

γ is the angle between the base and the hypotenuse of the prism,

ψ is the angle between the direction of the incident beam and the normal to the hypotenuse of the prism.

Table 4.3.1 The effective refractive index vs the K^+ – exchange condition (TM mode, the two wavelengths are λ= 488nm and λ= 632.8nm)

n_{eff} (λ=488nm) $\pm 1.5\times10^{-4}$ (TM mode)		K^+-exchange Time (minutes)				
		20	40	60	80	100
temperature	350 (C^0)	—	1.5168	1.5180	1.5189	1.5195
	400 (C^0)	1.5195	1.5211 1.5166	1.5220 1.5177	1.5226 1.5185	1.5229 1.5190 1.5160
	450 (C^0)	1.5225 1.5187	1.5233 1.5205 1.5181 1.5167	1.5236 1.5212 1.5191 1.5174	1.5239 1.5217 1.5198 1.5182 1.5170	1.5239 1.5218 1.5201 1.5186 1.5174
	500 (C^0)	1.5222 1.5203 1.5187 1.5172	1.5222 1.5208 1.5196 1.5185 1.5168	**	**	**

n_{eff} (λ=632.8nm) $\pm 1.5\times10^{-4}$ (TM mode)		K^+-exchange Time (minutes)				
		20	40	60	80	100
temperature	350 (C^0)	—	—	1.5096	1.5101	1.5107
	400 (C^0)	1.5106	1.5123	1.5134 1.5088	1.5140 1.5094	1.5143 1.5099
	450 (C^0)	1.5137 1.5095	1.5144 1.5110 1.5087	1.5148 1.5119 1.5097	1.5149 1.5123 1.5102 1.5088	1.5152 1.5129 1.5110 1.5094
	500 (C^0)	1.5137 1.5115 1.5096	1.5140 1.5126 1.5112 1.5099	**	**	**

where — means that no waveguide is formed.

** means that some of the modes can no longer be distinguished.

Most reported K^+ – exchanges have been done at temperatures between 340 °C and 440 °C. Within this temperature range, the sodium ions in glass near the surface exchange readily with potassium ions in the molten nitrate and the waveguide is quite reproducible. One particular feature of the present technique for the fabrication of buried K^+ – exchanged waveguide is the use of relatively high ion–exchange temperatures (around 500 °C) which has been found to play a significant role in whether a K^+ – exchanged surface waveguide can be completely buried or not.

Table 4.3.1 shows the measured effective refractive indices of surface planar waveguides ion–exchanged at different temperatures for different time durations. The wavelengths used for the measurement are $\lambda = 488$nm and $\lambda = 632.8$nm and only TM mode values are shown here for comparison between the two wavelengths. As the synchronous input coupling angle can only be measured to an accuracy of 0.02 °, the corresponding inaccuracy of effective refractive index n_{eff} is about 3×10^{-4}. Although the number of modes guided by the surface planar waveguide increases with the ion–exchange time and temperature, the characterisation of high mode–number planar waveguides is difficult because the separation of the guided modes of these waveguides can not be clearly distinguished by the prism coupling method. Therefore, Table 4.3.1 only shows the distinguishable values.

4.3.4 The refractive index profiles

Determination of the surface refractive index and the turning points

To find the refractive index profile of a surface waveguide, the inverse WKB method described in the last chapter is used. The surface refractive index as well as the depths corresponding to the turning point of each modal effective index are first determined using a FORTRAN computer program written by the author and run in a IBM computer.

Referring to section 3.3.3, equations (3.3.22) and (3.3.23) indicate that the turning point u_m can be determined in terms of lower order turning points u_i ($i = m-1, m-2, \ldots, 0, -1$, where $u_{-1} = 0$) and the effective refractive indices n_i ($i = m, m-1, \ldots, 0, -1$, where $n_{-1} = n_s$). Since the surface refractive index n_s is unknown, a guessed value of n_s within a reasonable range (n_{smin}, n_{smax}) is substituted into (3.3.22) and (3.3.23). The range (n_{smin}, n_{smax}) is equally divided into N parts where N is determined by the accuracy of the calculation for n_s. The

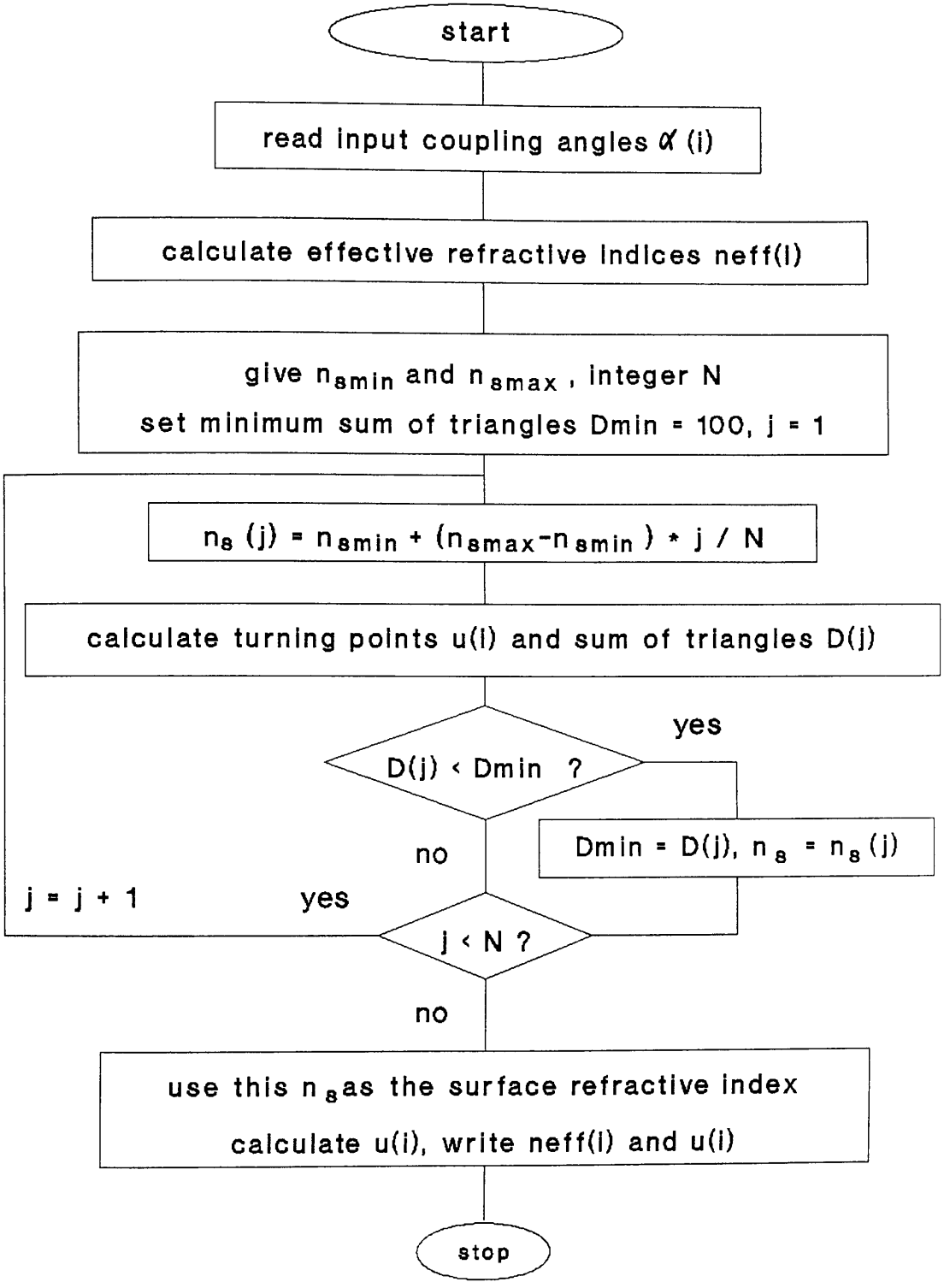

Fig.4.3.3 Flow diagram of the program for the calculation of the surface refractive index n_S and turning points u(i)

sum of the areas of triangles, D, formed by points (u_i,n_i), (u_{i-1},n_{i-1}) and (u_{i-2},n_{i-2}) $(i=M,M-1,...1$, where M is the total number of TE (or TM) modes), representing the smoothness of the refractive index profile, is obtained. The n_s which gives the smallest sum, D_{min}, is chosen as the surface index. Using this n_s, the corresponding turning points, u_i $(i=M,M-1,...,0)$, are obtained. Fig.4.3.3 shows the flow diagram of the computer program for the calculation. The x or u coordinate is inverted in the calculation, i.e. $u_i > u_{i-1} \geq 0$.

The small squares in Fig.4.3.4 show the depth of the turning points of an experimental surface waveguide calculated using the above computer program. The ion−exchange temperature is T= 490 °C and the ion−exchange time duration is t= 30min. The modal effective indices are measured at the wavelength of 632.8nm.

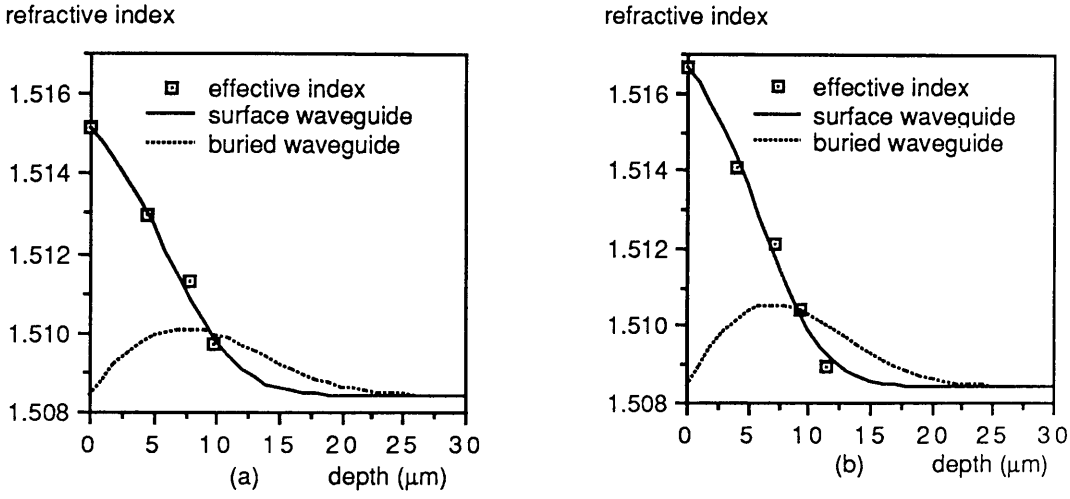

Fig.4.3.4 Turning points and refractive index profiles of K^+ − exchanged surface planar waveguide and Na^+ − exchanged buried planar waveguide (K^+ and Na^+ − exchange: T= 490 °C and t= 30min; λ= 632.8nm), (a) TE mode; (b) TM mode

Determination of the refractive index profile of a surface waveguide

It has been mentioned in the last chapter that the refractive index profile is a replica of the diffusion profile. It is therefore possible to obtain the theoretical refractive index profile by solving the one dimensional diffusion equation (3.2.1). A number of methods have been described for the solution of the diffusion equation (Stewart 1979). Since the finite difference method is claimed to be the best, it is used here for the solution of the diffusion equation. A computer program has been written for this purpose (Stewart 1979).

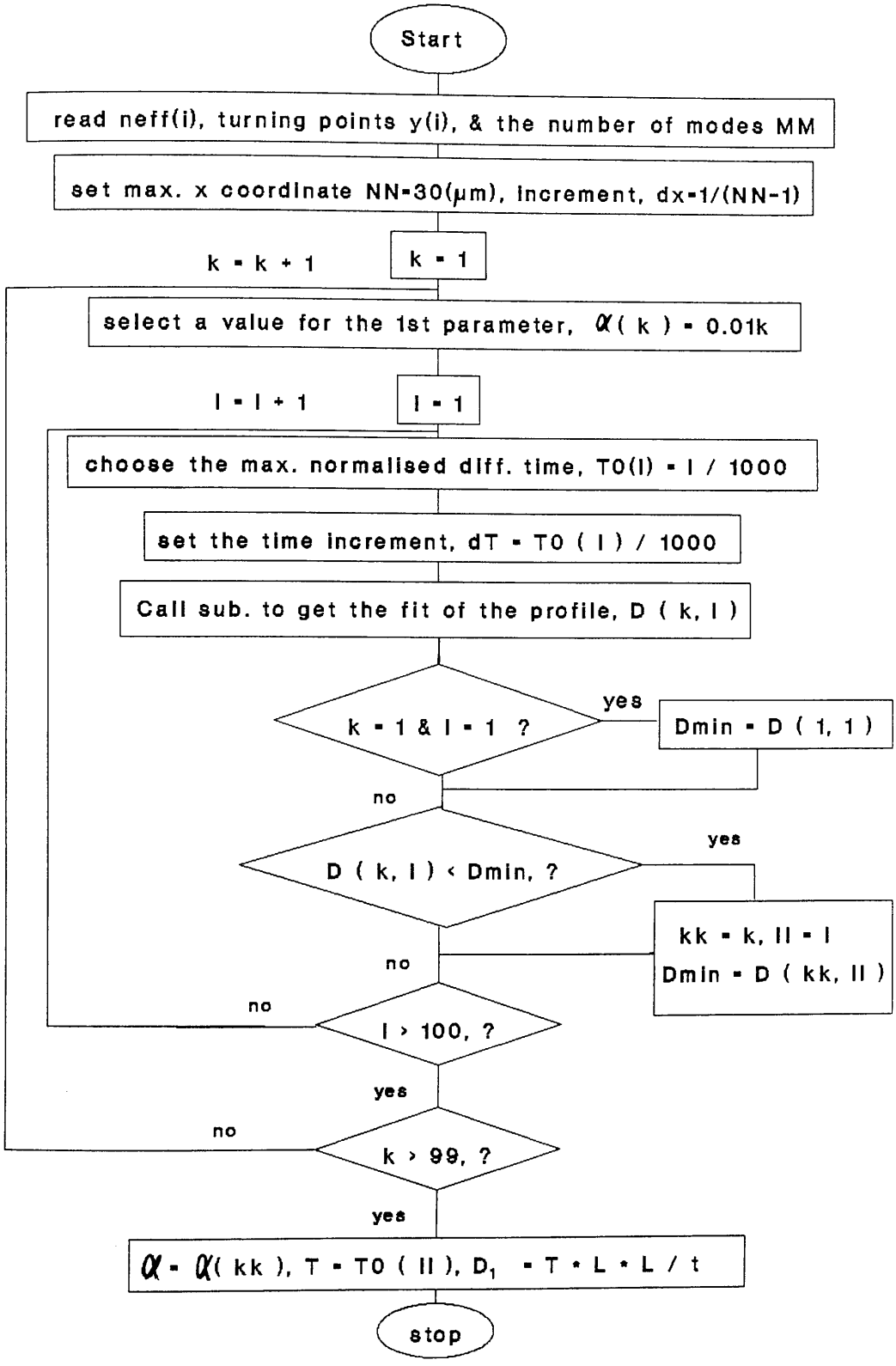
Start
read neff(i), turning points y(i), & the number of modes MM
set max. x coordinate NN=30(μm), increment, dx=1/(NN-1)
k = k + 1
k = 1
select a value for the 1st parameter, α(k) = 0.01k
l = l + 1
l = 1
choose the max. normalised diff. time, T0(l) = l / 1000
set the time increment, dT = T0 (l) / 1000
Call sub. to get the fit of the profile, D (k, l)
k = 1 & l = 1 ?
yes
Dmin = D (1, 1)
no
D (k, l) < Dmin, ?
yes
kk = k, ll = l
Dmin = D (kk, ll)
no
no
l > 100, ?
yes
no
k > 99, ?
yes
α = α(kk), T = T0 (ll), D1 = T * L * L / t
stop

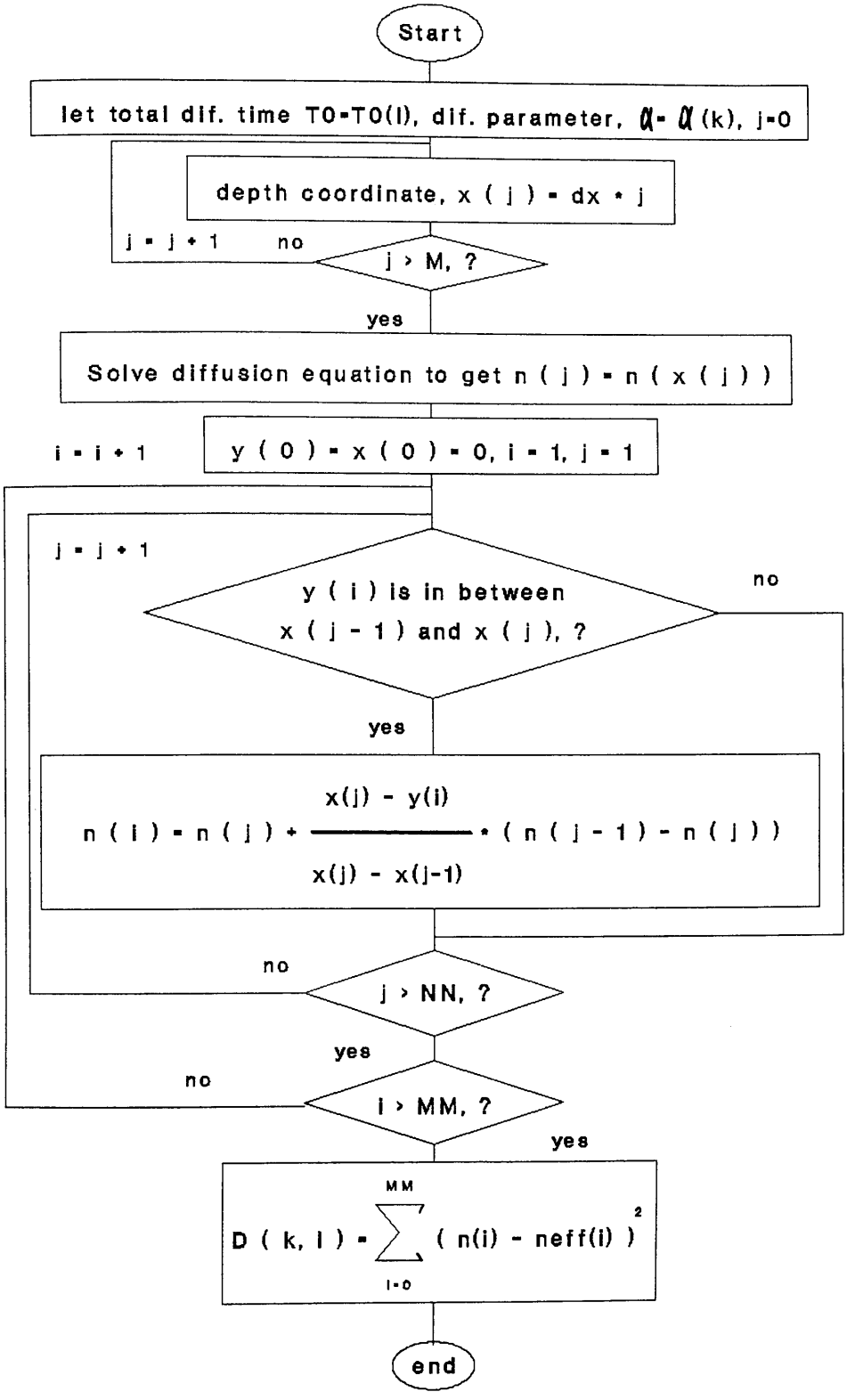

Fig.4.3.5 Flow diagram of the computer program for the determination of the diffusion parameters α and D_1, (a) main program; (b) subroutine for the calculation of profile fit parameter D

There are two free parameters, α and D_1, in the diffusion equation. If a diffusion profile is to be predicted, the important thing is to determine the two parameters. Cullen (1986) pointed out that the determination can be achieved by adjusting α and D_1 so that the diffusion profile gives the best least-squares fit to the experimental effective refractive indices and their corresponding turning points obtained using the inverse WKB method. Using this method, a FORTRAN computer program has been written for the determination of α and D_1. Fig.4.3.5 shows the flow diagram of the program.

Table 4.3.2 gives the values of α and D_1 calculated by the program for the BDH soda-lime glass at the ion-exchange temperature of 490°C. It should be pointed out that the diffusion parameters are in principle independent of the polarisation of light. The slight discrepancy of the diffusion parameters between the TE and the TM modes is possibly attributable to the fact that the inverse WKB method does not take into account the difference between TE and TM modes, so it is inherently an approximate method, and the fact that there is a limit in the accuracy of the measurement of input coupling angles. Given the two parameters α and D_1, the refractive index profile can then be obtained by solving the diffusion equation. The solid curves in Fig.4.3.4 show the theoretical index profile determined from the calculated diffusion parameters.

Table 4.3.2, α and D_1 for BDH glass at T=490°C

	TE mode	TM mode
α	0.84	0.87
D_1	0.53(μm^2/min)	0.48 (μm^2/min)

Determination of the refractive index profile of a buried waveguide

Given α and D_1, the refractive index profile of a K^+-exchanged surface planar waveguide for any ion-exchange time is then predictable by solving the diffusion equation, providing that the glass type and ion-exchange temperature are not changed.

The effective refractive indices of a completely buried planar waveguide cannot be easily determined experimentally because the superstrate prevents light from being coupled significantly into the waveguide using the prism coupling method. Accordingly,

the inverse WKB method for the case of a buried waveguide developed by White and Heidrich (1976) could not be directly used.

To predict the index profile of a buried waveguide, the diffusion parameters α and D_1 obtained with the surface planar waveguide are used and the diffusion equation is solved for the second step sodium ion−exchange. In this case, the diffusion profile of the surface planar waveguide serves as the initial potassium ion concentration profile and the boundary conditions are changed accordingly. The dotted lines in Fig.4.3.4 show the refractive index profile of a buried planar waveguide determined with this method. The second step ion−exchange temperature is $T=490^{0}C$ and the ion−exchange time duration is $t=30min$. The wavelength is $0.6328\mu m$.

4.3.5 Direct observation of the refractive index profiles

The refractive index profiles of silver ion−exchanged waveguide have been observed using the interference fringe method on finite thickness waveguiding cross−sections (Stewart 1979, Izawa and Nakagome 1972). But the same technique does not seem to have been successfully applied to potassium ion−exchanged waveguides. The reason for this is attributable to the fact that the refractive index change in potassium ion−exchanged waveguides is substantially smaller than that in silver ion−exchanged waveguides.

Using a Mach−Zehnder transmitted−light interference microscope, the author has successfully observed the refractive index profile of both K^{+}−exchanged surface and buried waveguides. Compared with laser based interference systems (Stewart 1979), a particular advantage of the Mach−Zehnder interference microscope system is that it uses an incoherent light source, which eliminates many irrelevant interference fringe patterns. The waveguide glass slide and a plain slide are first sliced and polished to an appropriate thickness. The plain slide piece is put in the reference arm and the waveguide slide piece is properly positioned in the sample arm. Fig.4.3.6(a) shows the ray path of the interference microscope. To get a good interference fringe pattern, the position of the illumination white light source is properly adjusted and the objectives for both arms are well focused.

Fig.4.3.6 (b) and (c) shows the interference fringe patterns of both surface and buried planar waveguides at the wavelength of $0.546\mu m$. Fig.4.3.7 shows a comparison

between the refractive index profile determined from the interference fringe patterns and that predicted by the diffusion theory. Since distinction between TE and TM modes can not be easily made in the interference fringe observation, the diffusion profiles of TE and TM modes are averaged and a mean diffusion profile is obtained for the comparison. The interference refractive index profiles are obtained by measuring the fringe shift at different depths and performing appropriate calculations according to the thickness of the sliced piece and the wavelength used ($\lambda = 0.546\mu m$). In the case of the surface waveguide, the thickness of the sliced piece is $l \approx 170\mu m$. Since the maximum fringe shift $\triangle N_{max} \approx 2.5$, the maximum index increase is therefore calculated to be $\triangle n_{max} = (\triangle N_{max} \cdot \lambda)/l = (2.5 \times 0.546)/170 \approx 0.008$. This agrees well with previously reported values (Chiang 1985, Gortych and Hall 1986, Yip and Albert 1985).

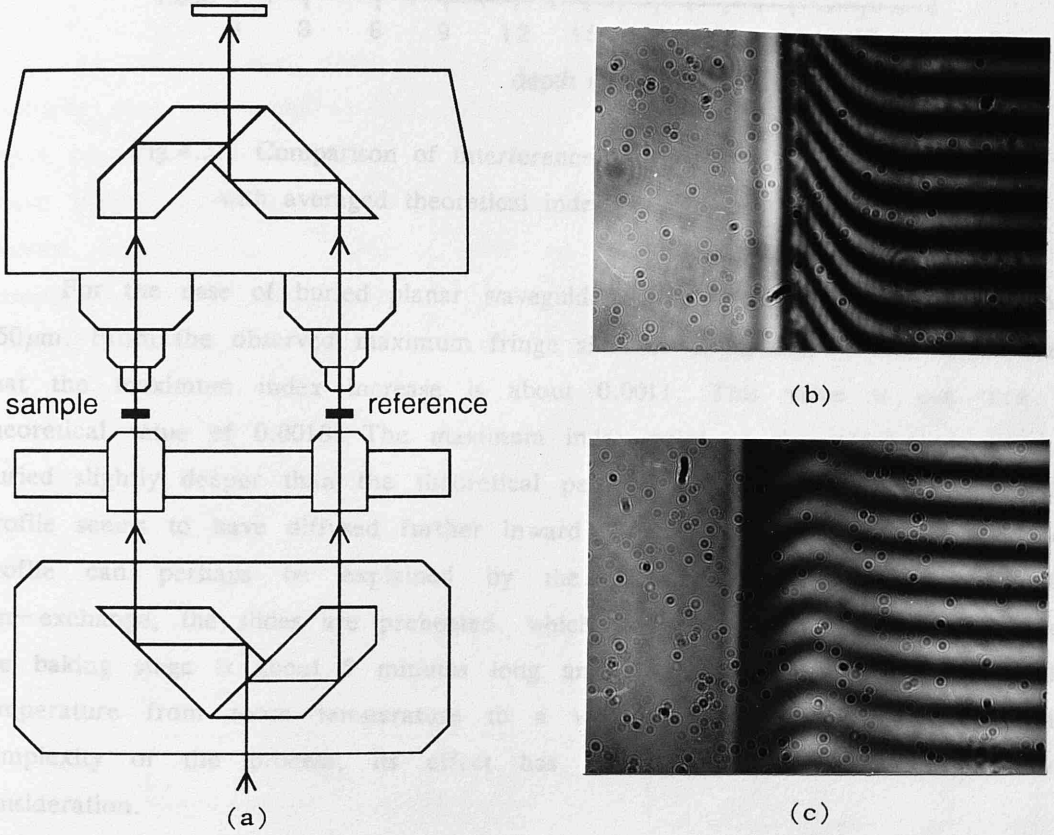

Fig.4.3.6 Ray path of the transmitted-light interference microscope (a) and photographs of the interference fringe patterns of surface waveguides (b) and buried waveguides (c)

As can be seen from the Fig.4.3.7, in the case of the surface waveguide, the shapes of the refractive index profiles match quite well, although the theoretical curve is slightly lower than the observed one.

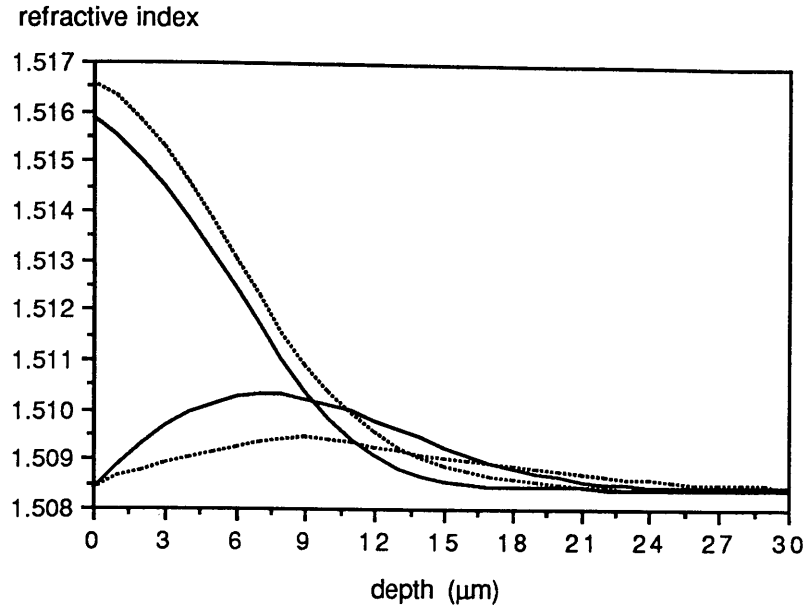

Fig.4.3.7 Comparison of interference index profiles (dotted lines) with averaged theoretical index profiles (solid lines)

For the case of buried planar waveguides, the thickness of the slice is about 450μm. From the observed maximum fringe shift of about 0.9, it can be calculated that the maximum index increase is about 0.0011. This value is less than the theoretical value of 0.0018. The maximum index point of the interference curve is buried slightly deeper than the theoretical peak. The fact that the observed index profile seems to have diffused further inward from the surface than the theoretical profile can perhaps be explained by the fact that before the second step ion–exchange, the slides are preheated, which acts as a baking stage. In practice, the baking stage is about 5 minutes long and involves an increase in the baking temperature from room temperature to a value close to 490 ^{0}C. Owing to the complexity of the process, its effect has not been taken into the theoretical consideration.

4.3.6 Confirmation of complete burial using the etching technique

To confirm that the waveguide is indeed completely buried, a measurement of the output coupling efficiency of a buried waveguide as a function of the etching depth from the original surface has been carried out with the experimental set–up shown in Fig.4.3.8a. In order to couple light into the buried planar waveguide using

the prism coupling method, one end of the slide is first etched about 8μm deep as described in Section 4.2.5. The other end of the slide is then etched step by step and an output coupling prism is placed on this etched area after each etching step. The etching depth is measured with a TALYSTEP machine (Rank Taylor Hopson) after each etching step. The output coupling efficiency, $\eta = I_{out}/(I_{out}+I_{emit})$, is measured as a function of the etching depth, where I_{out} is the light intensity coupled out by the output coupling prism and I_{emit} is the light intensity emitted from the front end of the waveguide. Fig.4.3.8b shows a typical result. Although the measured values are not very accurate because the contact between the prism and the waveguide surface can not be made the same each time, they are still representative of the situation. The ion–exchange conditions for both processes are again T= 490 °C and t= 30min.

As can be seen, when there is no etching, the output coupling efficiency is virtually zero. This implies that there is hardly any penetration of the evanescent wave beyond the surface. This is advantageous for a patterned waveguide evanescent wave immunosensor since any penetration of the guided light beyond the original surface would act as a source of noise. As the etching depth increases, the output coupling efficiency also increases. Maximum efficiency is reached at 6 to 7μm. Further etching reduces the thickness of the guiding layer which finally disappears.

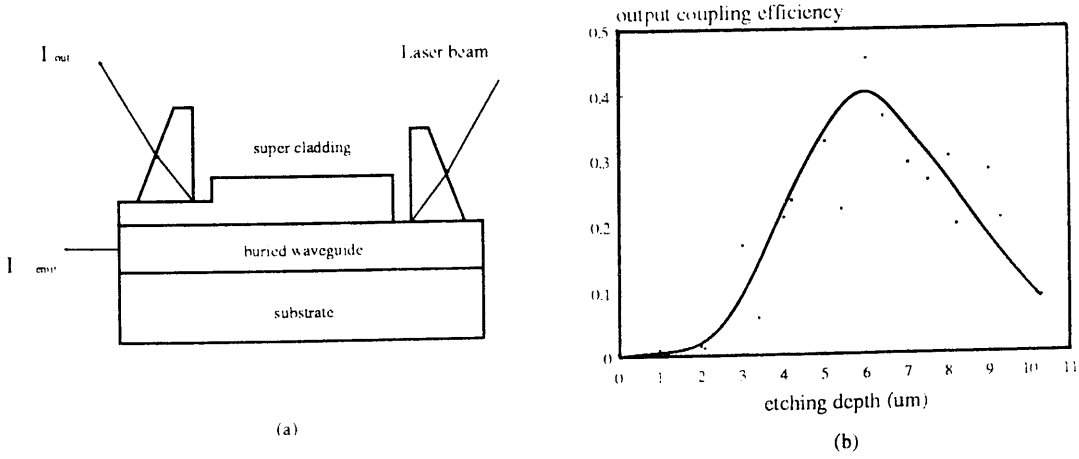

Fig.4.3.8 a) Experimental design for the measurement of the output coupling efficiency of a buried planar waveguide as a function of the etching depth and b) typical values. K^+– and Na^+–exchange: T= 490 °C, t= 30m.

4.3.7 Partial burial and microcracking

There are two major problems associated with burying K^+ – exchanged waveguides. The first is incomplete or partial burial of the waveguide and the second is the appearance of microcracking on the surface of a slide. It has been found that the ion– exchange temperature plays a very important role in whether a waveguide can be completely buried or not and that for different types of soda lime glass, different ion– exchange temperatures are required.

Microcracking has been investigated by Brandenburg (1986) and Albert and Yip (1987) and it has been shown that such microcracking is caused by the stress induced during the ion– exchange process. One of the purposes of burying a waveguiding layer is to reduce scattering loss. If a second ion– exchange process step induces too much microcracking, even though the waveguide is buried, the value of burying the waveguide is lost.

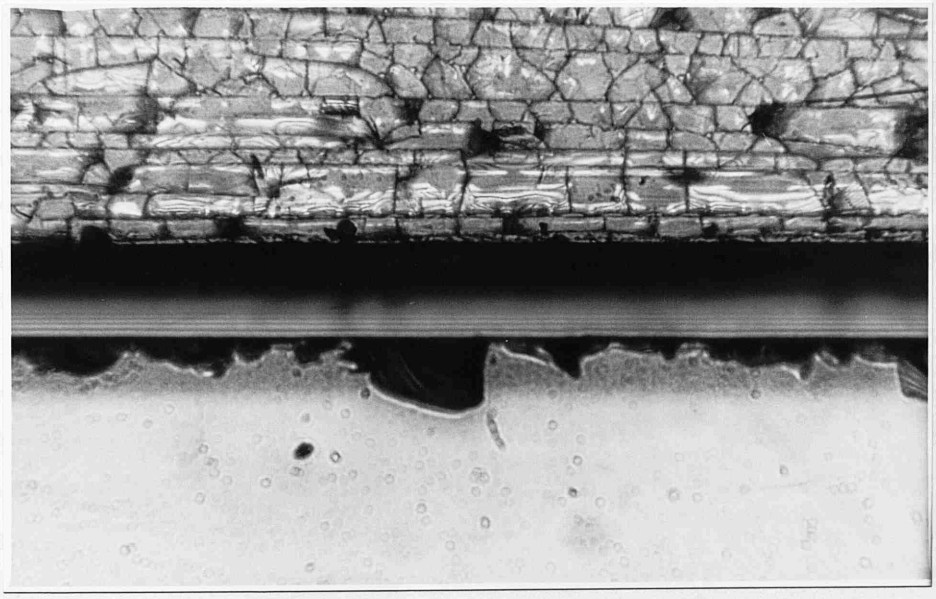

Fig.4.3.9 Microcracking and its control, upper half:
T= 520 °C and t= 1 hour for K^+ and Na^+ – exchange; lower half:
T= 490 °C and t= 30 minutes for K^+ and Na^+ – exchange.

Microcracking of the waveguide surface always occurs, if both high temperatures (>520 °C) and long ion– exchange times (>60min) are employed during the Na^+ – exchange. On the other hand, lower temperatures (<470 °C) generally result in waveguides which are not completely buried. Proper control of the ion– exchange

temperature and time can reduce the surface microcracking to a negligible amount while keeping the waveguide completely buried. For the BDH soda lime glass, the appropriate conditions are found to be a temperature range from 480 °C to 495 °C and time duration range from 25 to 30 minutes. Within this range, the waveguide can support one to two modes at the wavelength of interest.

The top half of Fig.4.3.9 shows a photograph of microcracking on a slide ion–exchanged at T= 520 °C for t = 1 hour for both steps. The bottom half of Fig.4.3.9 shows the surface of a completely buried waveguide slide ion–exchanged at T= 490 °C for 30 minutes for both steps. It can be seen that there is virtually no microcracking for the latter case. It has already been shown, in the last section, that a waveguide fabricated at T= 490 °C for 30 minutes for both steps can be completely buried. Therefore, it can be concluded that T= 490 °C and t= 30min for both steps can produce a completely buried waveguide without any microcracking.

4.3.8 Patterned waveguides

The intention of fabricating patterned waveguides is to confine evanescent penetration to etched wells and meanwhile to reduce surface scattering. In addition, it is also expected that the strength of interaction of the evanescent wave with molecules close to the etched surface can be adjusted by the proper control of the etching depth. To show that patterned waveguides do have these features, the following experiments have been conducted.

Fig.4.3.10a shows the photograph of a patterned waveguide with 5 etched wells. The substantial reduction of surface scattering is confirmed by coupling light into both patterned waveguides and surface waveguides, and observing the streak of light on the surface. While surface waveguides always give a relatively bright streak of light which is easily observable in darkness, the streak of light is hardly observable in the case of patterned waveguides. Fig.4.3.10b and Fig.4.3.10c show respectively the photograph of the streak of guided light for a patterned waveguide and a surface waveguide.

In fact, Fig.4.3.10a and Fig4.3.10b are taken of the same slide with the former one taken when the room lights are switched on. It should be pointed out that the two photographs, Fig.4.3.10b and Fig.4.3.10c, are taken under the same conditions. Although it can not be guaranteed that the input coupling efficiency of light is the same for the two waveguides, from the authors experience, the difference is usually

not large. Therefore, between the two photographs, the brightness of the streak of guided light is a direct reflection of the scattering of guided light. It is apparent that surface scattering can be greatly reduced in the case of patterned waveguides.

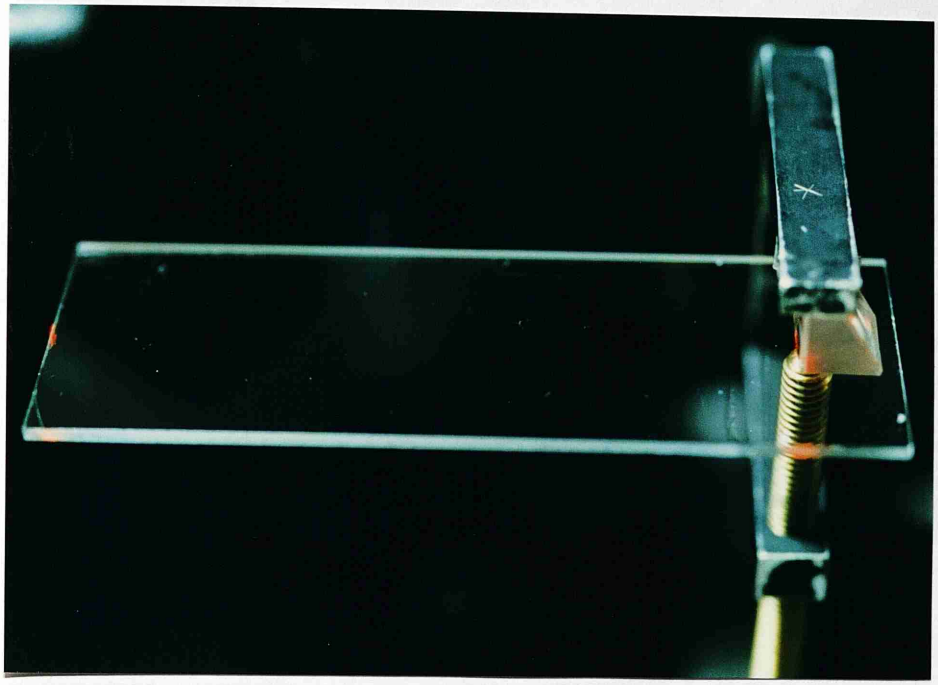

(a)

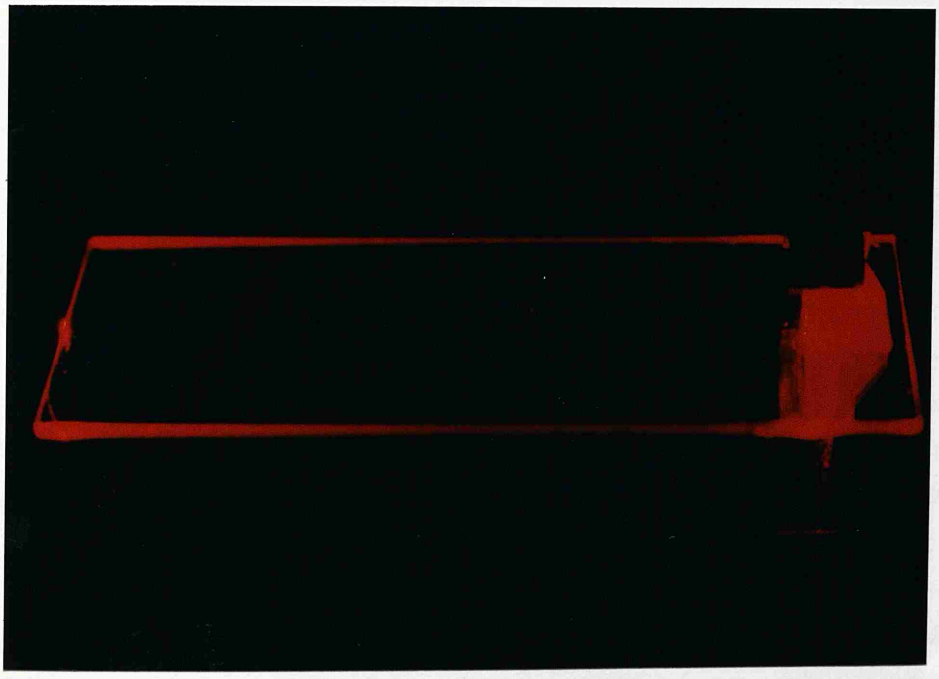

(b)

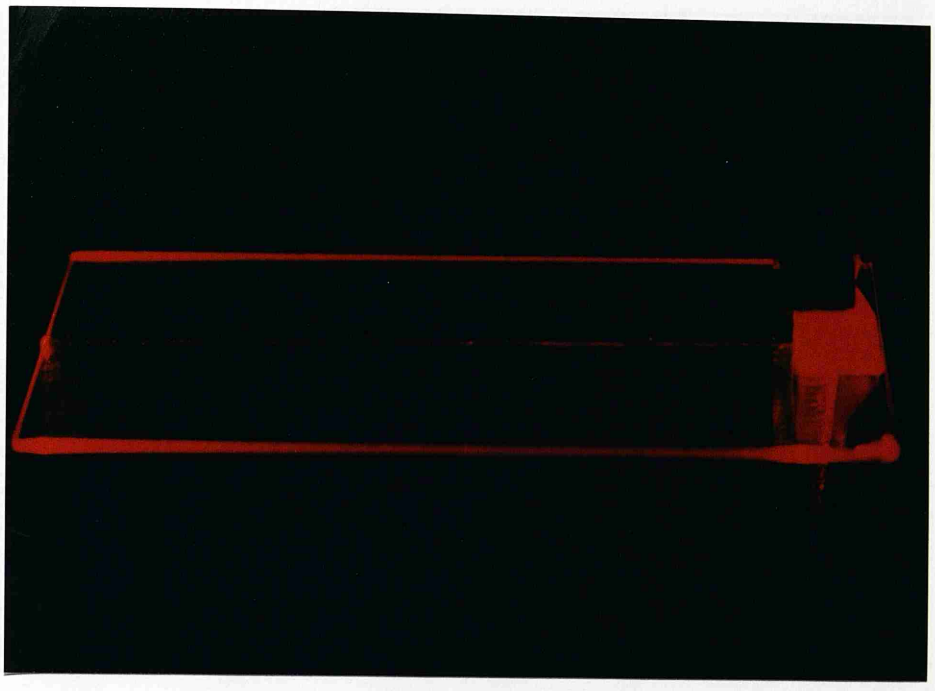

(c)

Fig.4.3.10 Photographs showing, (a) a patterned waveguide; (b) surface scattering of a patterned waveguide and (c) surface scattering of a surface waveguide

To investigate the confinement of evanescently excited fluorescence to the etched wells, an FITC (fluorescein isothiocyanate) labelled anti−rat−IgG (a fluorescently labelled antibody) solution at the conjugate concentration of 0.1mg/ml is applied to the surface of a patterned waveguide, covering both the etched wells and the unetched surface. The waveguide surface is previously treated with amino−silane and glutaraldehyde. This, as will be discussed in detail later, gives rise to the binding or immobilisation of antibody proteins to the waveguide surface.

After more than half an hour of immobilisation, the fluorescent molecules (FITCs) are excited by the 488nm laser light guided by the waveguide and it is found that evanescently excited fluorescence is indeed restricted to the etched wells as long as the wells are not etched too deeply (i.e. $< 7\mu m$). Fig.4.3.11 shows a photograph of the evanescently excited fluorescence on a patterned waveguide which has 6 identical wells. It is clear that there are 6 bright line segments and these correspond to the etched wells. The reverse side of the slide has been painted black to absorb substrate guided light. Notice the difference in colour. The excitation light is blue and the evanescently excited fluorescence is green or yellow.

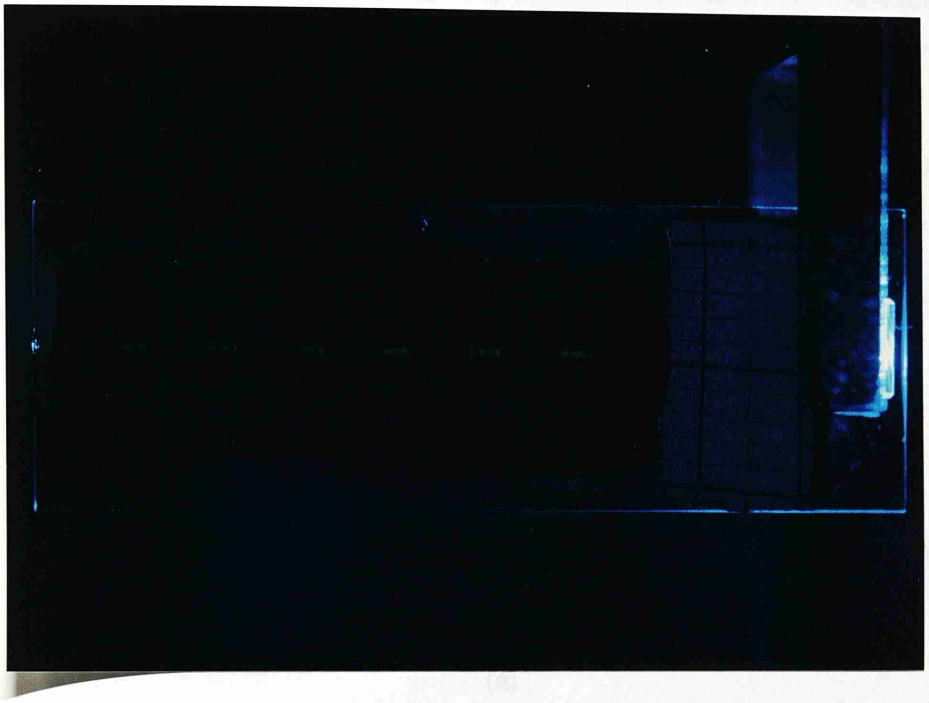

Fig.4.3.11 The confinement of evanescently excited fluorescence on a patterned waveguide

To investigate the interaction strength of an evanescent wave with fluorescence molecules attached to the etched surface, the evanescently excited fluorescence was measured as a function of the well depth. A completely buried planar waveguide is coated with photoresist. Six rectangular wells are exposed onto the photoresist and developed. Instead of immersing the whole slide into 4:1 HF as in the usual case of patterning a waveguide, the slide is held vertically and dipped into 4:1 HF step by step. As a result, each of the etched well has a different etching time and hence a different depth. The etching depth of each well is measured with a TALYSTEP machine (Rank Taylor Hopson). The waveguide slide is cleaned and treated with amino– silane and glutaraldehyde.

FITC labelled anti– rat– IgG solution at the concentration of 0.1mg/ml is again applied to the slide surface covering all the wells. After an incubation time of about one hour, the solution is washed away and dried. A thin film (about 0.5mm thick) of immersion oil which has a refractive index close to that of the substrate of the glass slide is then applied to the waveguide surface. This is for the enhancement of the evanescently excited fluorescence as will be discussed in detail in the next chapter. The evanescent fluorescence from each well, excited by the same beam of

guided light, is measured by scanning a photomultiplier below the waveguide slide (details in chapter 7). Fig.4.3.12(a) shows the results of this measurement and Fig.4.3.12(b) shows a photograph of the situation.

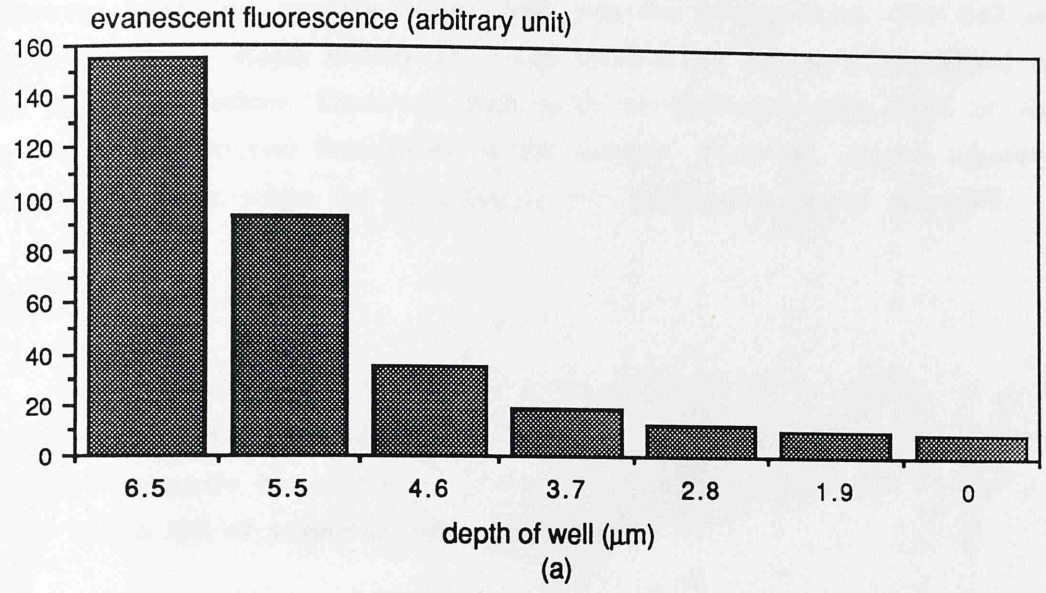

(a)

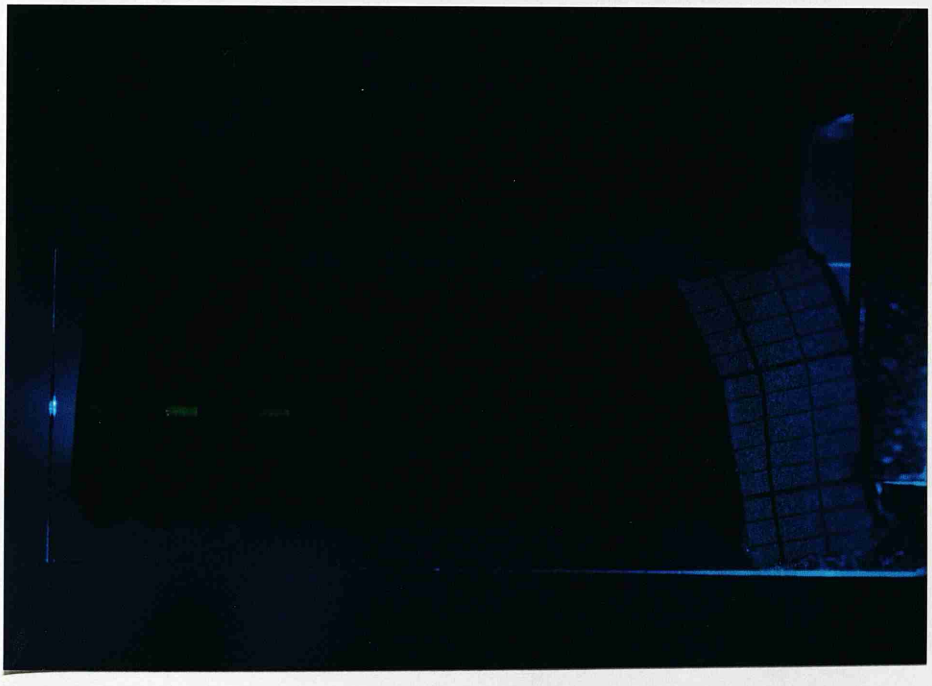

(b)

Fig.4.3.12 (a) Evanescently excited fluorescence as a function of the etching depth; (b) A photograph showing the same situation. (the ion−exchange conditions for both steps are T= 490 °C and t= 30min)

The difference in colour between the excitation light and the excited fluorescence light can again been seen from the photograph. It is clear that the evanescent interaction strength is adjustable with the etching depth. The well must not be etched too deeply because that might result in the leakage of the guided light into the cover medium. Therefore, there exists an optimum etching depth at which the evanescently excited fluorescence is the strongest. From the author's experience, this depth is about 6.0μm for the potassium ion-exchanged patterned waveguide.

4.4 Summary and conclusion

The technology for the fabrication of K^+ and Na^+-exchanged patterned waveguides has been successfully developed. The performance of the fabricated patterned waveguide has shown the properties which are desirable for the waveguide to act as the IRE of evanescent wave biosensors.

The ion-exchange conditions for fabricating completely buried planar waveguides using only thermal K^+- and Na^+-exchange processes are determined. Under such conditions, problems of microcracking of the guiding layer and partial burial of the waveguide are solved. The refractive index profiles of both K^+-exchanged surface and buried waveguides have been observed directly for the first time (to the author's knowledge) using a Mach-Zehnder interference microscope. Comparison of the observed index profile with the index profile predicted by solving the diffusion equation with the help of the inverse WKB method shows good agreement.

It has been shown that: 1) surface scattering of the ion-exchanged waveguide can be greatly reduced by burying and patterning the waveguide (consequently, when such patterned waveguides are used as the sensing element of an evanescent immunosensor, the background ground noise introduced by surface scattering of ion-exchanged surface planar waveguide can be greatly reduced); 2) the evanescent interaction strength of a patterned waveguide can be controlled by appropriate etching of the wells; and 3) the evanescently excited fluorescence of a patterned waveguide can be confined to the etched wells. The last feature implies that differential and multichannel immunoassays, as will be discussed later, can be easily conducted with patterned waveguides.

CHAPTER 5 FLUORESCENCE, ITS EXCITATION BY AN EVANESCENT WAVE AND EVANESCENT FLUORESCENCE IN SOLID PHASE IMMUNOASSAYS

5.1 Introduction

Now that the sensing element has been developed with features suitable for evanescent fluorescence immunosensing, it is necessary to investigate the phenomenon of evanescent excitation of fluorescence using the sensing element. Although a number of papers have been published concerning the evanescent excitation of fluorescence through total internal reflection (Harrick 1967, Carniglia et al. 1972 and Lee et al. 1979), these investigations have not been extended to the case where excitation of fluorescence is achieved via a planar waveguide. In addition, despite experimental investigations into antibody–antigen reactions through total internal reflection fluorescence (TIRF) (Lok et al. 1983a and 1983b, and Sutherland et al. 1984a), no theoretical description seems to have been given.

A brief introduction will be given of the basic concepts associated with fluorescence excitation and emission. The angular distribution of evanescently excited fluorescence is investigated bearing in mind that the excitation will be achieved via a planar waveguide. It is found, from the investigation, that the evanescently excited fluorescence can be substantially enhanced through index–matching of the cover medium to that of the substrate.

A key issue with immunosensors is the differentiation of specific binding from non–specific binding. Since differential measurement of evanescent fluorescence can be easily achieved with a patterned waveguide and it helps to discriminate between signals of specific binding and of non–specific binding, a mathematical model is established and the relevant expressions for the evanescently excited fluorescence for such a situation are derived.

5.2 Fluorescence

5.2.1 Fluorescence and energy levels

Generally speaking, fluorescence is the emission of light of one wavelength

during the time a substance is irradiated with light of a shorter wavelength. The phenomenon of fluorescence can be understood by viewing a molecule as a system consisting of a number of energy states and levels. The energy states are associated with the electron energy of a molecule and the energy levels within a specific energy state are related to the vibrational and rotational energies (Nairn 1976).

5.2.2 Light absorption and emission

In the explanation of fluorescence, light is considered both as an electromagnetic wave and as a stream of discrete energy units called photons. The energy of a photon is directly proportional to its frequency, i.e.

$$E = h\upsilon \qquad (5.2.1)$$

where h is Planck's constant (6.554×10^{-34} J·sec) and υ is the frequency of the light wave involved.

The absorption and emission of energy by a molecule is also governed by Planck's quantum theory, i.e.

$$E_2 - E_1 = h\upsilon \qquad (5.2.2)$$

where E_1 and E_2 are the energy levels of a molecule and $h\upsilon$ is the quantum of energy equivalent to the change from E_2 to E_1. When radiation is involved in the process, υ represents the frequency of the light absorbed or emitted.

Fig.5.2.1 shows the energy changes associated with the phenomenon of fluorescence in a diatomic molecular system. The curve G corresponds to the potential energy of the ground state and E to that of the excited state. There are generally a number of vibrational and rotational energy levels associated with each potential curve. The total energy of the system is expressed as parallel lines and the vertical lines in the diagram represent energy transitions in such a system.

Transition A in Fig.5.2.1 represents the absorption of a quantum of energy by the molecule which is transferred to one of the upper vibrational levels of the excited states. As internal conversion is much more likely than is emission from any excited state above the lowest, the excited molecule usually loses vibrational energy

and reaches the lowest vibrational level of the excited state. If this state is stable for about 10^{-8} seconds, it is possible for the molecule to lose a quantum of radiation in the transition F to one of the higher vibrational levels of the ground state (Nairn 1976).

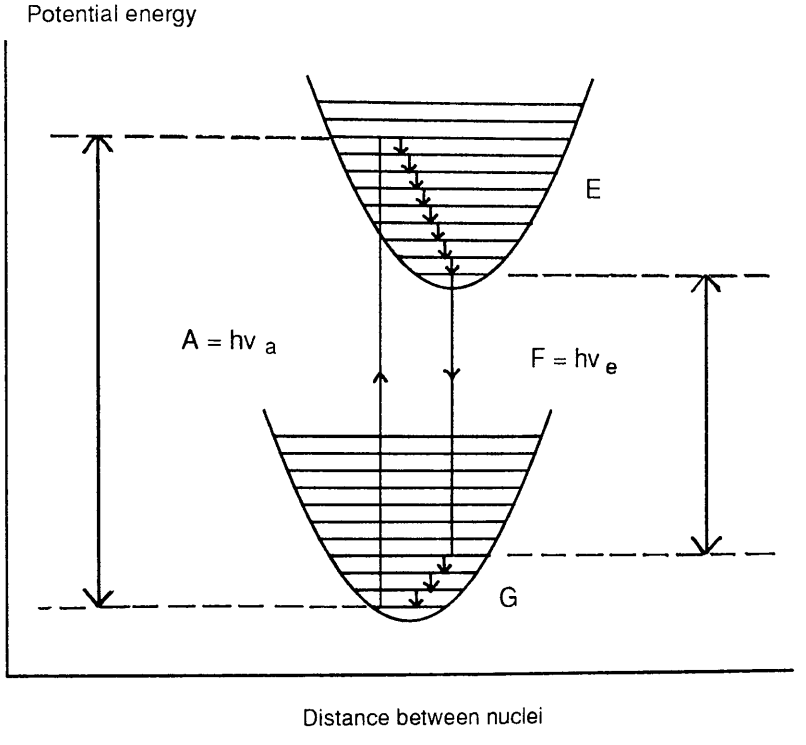

Fig.5.2.1 Energy diagram of a diatomic molecule illustrating absorption and emission transitions

5.2.3 Absorption and emission spectrum

As the energy difference A is greater than F, the emitted photons will have less energy, and therefore longer wavelength than the exciting photons. This phenomenon is known as Stoke's law.

The amplitude and profile of the absorption spectrum of a molecule is determined by the probability that a transition from the ground state to a particular vibrational or rotational level of an excited state will take place. Using Stoke's law, it is obvious that the wavelength of the peak of the fluorescence emission spectrum is longer than the wavelength of the peak in the absorption spectrum. Fig.5.2.2 shows the absorption and emission spectrum of the fluorescent dye fluorescein at pH= 7.1.

Although an excitation photon may have an energy over a range larger than

that of the fluorescence photon, the spectrum of the fluorescence light is the same regardless of the wavelength of the excitation light. This results from the fact that part of the additional energy transmitted to the absorbing molecule by the excitation light is lost by non– fluorescent transitions.

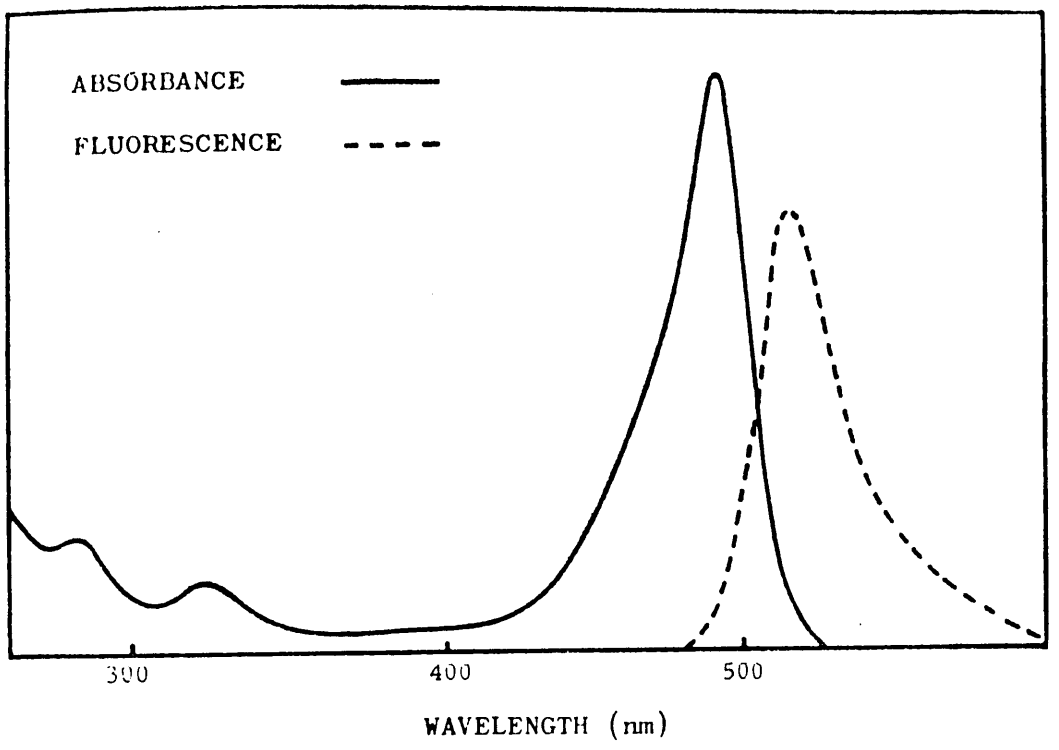

Fig.5.2.2 The absorption and emission spectrum of fluorescein at pH 7.1 (after Nairn 1976)

5.2.4 Fluorescence intensity

The intensity of fluorescence is determined mainly by three considerations. The first is the efficiency with which the substance converts absorbed radiation into fluorescent radiation; the second is the absorption of the excitation light by the fluorescent material; and the third is the intensity of exciting radiation.

Quantum yield (fluorescence efficiency)

The quantum yield or fluorescence efficiency η of a fluorescent material is defined as the ratio of the number of fluorescent photons emitted, N_f, to the number of photons of light absorbed, N_a, (Molloy 1975), i.e.

$$\eta = N_f/N_a \qquad (5.2.3)$$

The efficiency, η, of a fluorescent dye is independent of excitation wavelength as long as excitation is below the peak wavelength of the main absorption band. It is influenced by such factors as concentration of dye, temperature, pH, viscosity, and chemical nature of the solvent.

Absorption

Fluorescence is a two step process in which the excitation light is first absorbed and then the fluorescent light is emitted at a longer wavelength. Therefore the fluorescence intensity is dependent on the absorption properties of the fluorescent material. Consider the case where an electromagnetic wave is propagating perpendicularly through a cell filled with a solution of absorbing substance. The absorption of the electromagnetic wave is governed by Lambert's law and Beer's law (Molloy 1975). A combination of these two laws results in

$$\ln(I_0/I) = \alpha \cdot L = a \cdot s \cdot L \qquad (5.2.4)$$

where I_0 and I are the initial and final intensities of the electromagnetic wave, α (1/m) is a constant called the absorption coefficient, s is the molar concentration of the solute (mole/m^3), a (m^2/mole) is the molar absorption coefficient and L (m) is the length of the cell.

Alternatively, (5.2.4) can be expressed as

$$E = \log_{10}(I_0/I) = 2.303a \cdot s \cdot L = \epsilon \cdot s \cdot L \qquad (5.2.5)$$

where $\epsilon = 2.303a$ is the molar extinction coefficient, and $E = \log_{10}(I_0/I)$ is the extinction.

Fluorescence intensity

It has been mentioned that the quantum efficiency of a given fluorescent material is dependent on many factors including temperature, viscosity and presence of other molecules in the solution. For a given set of conditions, the amount of fluorescent light emitted is proportional to the amount of light absorbed. Using

equations (5.2.3)–(5.2.5), the fluorescence intensity can be expressed

$$I_f \propto \eta \cdot I_a = \eta \cdot (I_0 - I)$$

$$= \eta \cdot I_0 (1 - e^{-\alpha.L})$$

$$= \eta \cdot I_0 (1 - e^{-a.s.L}) \qquad (5.2.6)$$

$$\approx I_0 \cdot \eta \cdot \epsilon \cdot s \cdot L/2.303 \qquad (\text{when } \alpha \cdot L = \epsilon \cdot s \cdot L/2.303 \ll 1)$$

where I_a is the amount of light absorbed. In the last expression, the exponential term has been expanded and higher order terms ignored.

Thus at low concentrations, the fluorescence intensity is directly proportional to (i) the excitation intensity, (ii) the quantum yield, (iii) the molar extinction coefficient, and (iv) the concentration of the fluorophors.

5.3 Evanescent Excitation of Fluorescence

Up till now, consideration of fluorescent intensity has only been given to the case of a uniform incident wave passing through a cell. In the case of evanescent wave excitation, the situation is quite different. The excitation light intensity decays exponentially and since the evanescent energy is only a small fraction of the incident energy, the absorption of the excitation energy by the fluorescent medium is usually ignored.

5.3.1 Angular distribution of evanescent fluorescence

Consider total internal reflection at the base of a hemicylindrical prism where a beam of incident light is directed through the prism onto the base of the prism (Fig.5.3.1). An evanescent wave is generated on the interface in the optically rarer medium, if the angle of incidence θ_i is greater than the critical angle

$$\theta_c = \sin^{-1}(n_3/n_1) \qquad (5.3.1)$$

where n_3 and n_1 are the refractive indices of the optically rarer and denser media respectively.

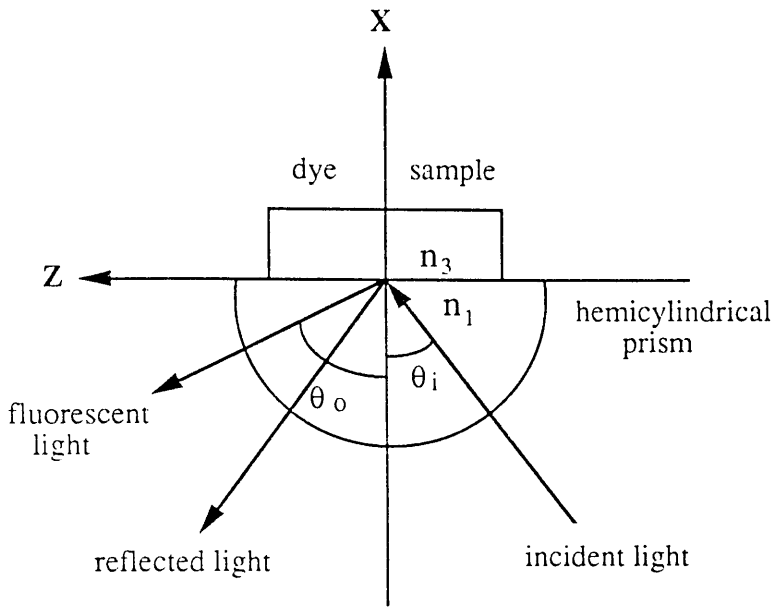

Fig.5.3.1 Configuration for excitation of fluorescence by evanescent waves

The angular distribution of evanescently excited fluorescence in this case has been investigated both theoretically and experimentally by Lee et al. (1979). Based on the principle of reciprocity and the result that evanescent photons can be emitted and absorbed like plane wave photons, Lee et al. have provided the expressions for the angular distribution of evanescent fluorescence. Although Lee's paper has been cited by a number of people (Andrade et al. 1985, Newby et al. 1984, Badley et al. 1987, Sutherland et al. 1984a, Place et al. 1985 and Glass et al. 1987), the author rederived the formula and found that there was an error in Lee's formula and only a minor modification is needed.

Referring to Fig.5.3.1, if the thickness of the covering fluorescent medium, t, is much greater than the penetration depth of the relevant evanescent wave (i.e. $t \gg d_p$ and d_p', where the penetration depth is defined as the distance at which the electric field has decayed to 1/e of its value at the optical interface), Lee's expressions for the fluorescence intensity excited by a beam incident at θ_i per unit incident intensity and observed at θ_0 are given by

$$I_f(\theta_i,\theta_0) \propto \alpha\cdot\eta\cdot|T(\theta_i)|^2\cdot|T'(\theta_0)|^2/[2(1/d_p+1/d_p')], \quad \text{for} \quad \theta_i > \theta_c,\ \theta_0 > \theta_c' \qquad (5.3.2)$$

$$I_f(\theta_i,\theta_0) \propto \alpha\cdot\eta\cdot|T(\theta_i)|^2\cdot|T'(\theta_0)|^2\cdot[d_p/2],$$
$$\text{for} \quad \theta_i > \theta_c,\ \theta_0 \leqslant \theta_c' \qquad (5.3.3)$$

$$I_f(\theta_i,\theta_0) \propto \alpha\cdot\eta\cdot|T(\theta_i)|^2\cdot|T'(\theta_0)|^2\cdot[d_p'/2],$$
$$\text{for} \quad \theta_i \leqslant \theta_c,\ \theta_0 > \theta_c' \qquad (5.3.4)$$

$$I_f(\theta_i,\theta_0) \propto \alpha\cdot\eta\cdot|T(\theta_i)|^2\cdot|T'(\theta_0)|^2\cdot t,$$
$$\text{for} \quad \theta_i \leqslant \theta_c,\ \theta_0 \leqslant \theta_c' \qquad (5.3.5)$$

where the prime ' relates to the fluorescent light. θ_c is the critical angle pertaining to the wavelength of the exciting light (λ_e) and θ_c' is the critical angle pertaining to the wavelength of the fluorescent light (λ_f),

$$d_p = (\lambda_e/2\pi)\cdot(n_1^2\cdot\sin^2\theta_i - n_3^2)^{-1/2}. \qquad (5.3.6)$$

$$d_p' = (\lambda_f/2\pi)\cdot(n_1'^2\cdot\sin^2\theta_0 - n_3'^2)^{-1/2} \qquad (5.3.7)$$

α is the absorption coefficient and η is the fluorescence efficiency. $|T(\theta_i)|^2$ and $|T'(\theta_0)|^2$ are called the transmission terms for the incident intensity on the cover medium side of the interface and for the fluorescent intensity on the prism side of the interface, respectively. In Lee's paper, it is said that the transmission terms for the incident beam polarised vertically ($\perp$) and horizontally ($\parallel$) with respect to the plane of incidence can be related to the Fresnel transmission coefficient of amplitude, $t_\perp$ and $t_\parallel$, as follows

$$|T_\perp(\theta_i)|^2 = (n_3/n_1)\cdot|t_\perp|^2/\cos\theta_i \qquad (5.3.8)$$

$$|T_\parallel(\theta_i)|^2 = (n_3/n_1)\cdot|t_\parallel|^2\cdot(\sin^2\theta_t \pm \cos^2\theta_t)/\cos\theta_i \qquad (5.3.9)$$

where

$$t_\perp = \frac{E_{ty}}{E_{iy}} = \frac{2n_1\cdot\cos\theta_i}{n_1\cdot\cos\theta_i + n_3\cdot\cos\theta_t} = \frac{2\sin\theta_t\cos\theta_i}{\sin(\theta_t+\theta_i)} \qquad (5.3.10)$$

$$t_\parallel = \frac{n_1}{n_3}\cdot\frac{H_{ty}}{H_{iy}} = \frac{2n_1\cdot\cos\theta_i}{n_3\cdot\cos\theta_i + n_1\cdot\cos\theta_t} = \frac{2\sin\theta_t\cdot\cos\theta_i}{\sin(\theta_i+\theta_t)\cdot\cos(\theta_i-\theta_t)} \qquad (5.3.11)$$

θ_t is the angle of transmission and is determined by $\sin\theta_t = (n_1/n_3)\cdot\sin\theta_i$. It is

also said that the ± sign in equation (5.3.9) results from computation of the sum of the squares of the transmitted electric intensity ($E \cdot E^*$) components when $\theta_i \leqslant \theta_c$ (+ sign) and when $\theta_i > \theta_c$ (− sign).

The transmission terms for the fluorescent beam, $|T_\perp'(\theta_0)|^2$ and $|T_{||}'(\theta_0)|^2$, are also given by (5.3.8) and (5.3.9) with θ_i and θ_t replaced by θ_0 and θ_t' (where $\sin\theta_t' = (n_1'/n_3')\sin\theta_0$) and with n_3/n_1 substituted by its value at λ_f, i.e. n_3'/n_1'.

In Lee's treatment of evanescent wave intensities, the transmitted intensity is simply taken as proportional to the square of the total electric field. But in the evanescent case, this is not in agreement with the definition that intensity is time averaged power flow (Appendix 5.1).

In fact, it is well known that when internal reflection occurs, the mean energy flow normal to the optical interface is zero and there is only energy flow along the interface. Once the definition of intensity is taken into consideration, it is found that equations (5.3.8) and (5.3.9) should be replaced by (Appendix 5.2)

$$|T_\perp(\theta_i)|^2 = (n_3/n_1)\cdot|t_\perp|^2/\cos\theta_i \qquad \text{for } \theta_i \leqslant \theta_c$$

$$= \tan\theta_i \cdot |t_\perp|^2 \qquad \text{for } \theta_i > \theta_c \qquad (5.3.12)$$

$$|T_{||}(\theta_i)|^2 = (n_3/n_1)\cdot|t_{||}|^2/\cos\theta_i \qquad \text{for } \theta_i \leqslant \theta_c$$

$$= \tan\theta_i \cdot |t_{||}|^2 \qquad \text{for } \theta_i > \theta_c \qquad (5.3.13)$$

Fig.5.3.2 shows the theoretical angular distribution of the evanescently excited fluorescence intensity. The parameters chosen are $n_1 = 1.519$, $n_3 = 1.33$, $\lambda_e = 488$nm, $\lambda_f = 525$nm and $\theta_i = 85^0$. These parameters approximately correspond to the situation where a homogeneous aqueous FITC (fluorescein isothiocyanate)− labelled antibody solution is applied to a K^+ − exchanged surface planar waveguide in which 488nm laser light is guided. In the figure, V stands for vertical (i.e. TE) polarisation and H stands for horizontal (i.e. TM) polarisation. Therefore, V− V means that the polarisation of both the excitation light and the fluorescent light are all vertical whereas H− H means that the polarisation of both the excitation light and the fluorescent light are all horizontal. In addition to the curves calculated from the (5.3.12) and (5.3.13), as a comparison, the corresponding curves resulting from Lee's formulae (5.3.8) and (5.3.9) are also given. It can be seen that the general trends of

the four curves are quite similar although there are slight differences between the curves calculated from the new formula and those from Lee's formula.

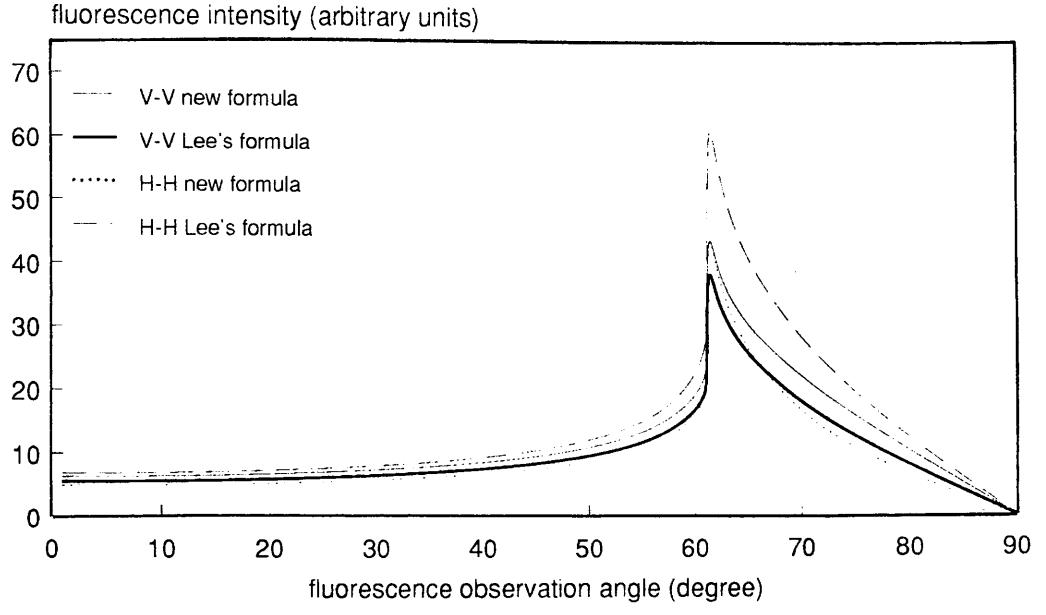

Fig.5.3.2 Theoretical angular distribution of the evanescently excited fluorescence intensity

From the angular distribution expressions it can be found that, with evanescent excitation, the overall fluorescence intensity of a thick cover film of a dye solution radiating into the optically denser medium is highest at the critical angle $\theta_i = \theta_c$, and, for a fixed $\theta_i > \theta_c$, the relative fluorescence intensity peaks at $\theta_0 = \theta_c'$ (Lee et al 1979).

5.3.2 Enhancement of evanescent fluorescence through index-matching

Theoretical consideration

A guided mode in a patterned waveguide undergoes total internal reflections at the upper surface, therefore, the incident angle θ_i of a guided mode at the upper interface of a waveguide must be greater than the corresponding critical angle θ_c. Since most optical waveguides have a substrate which has a much higher refractive index than that of an aqueous solution, the cut off condition formed by the guiding layer and the substrate causes the guided excitation light to strike the upper interface at an angle which is far beyond the critical angle of the upper interface. Considering that the overall evanescently excited fluorescence is strongest when the incident angle

approaches the critical angle, to bring the incident angle to the critical angle, one possibility is to use, instead of an aqueous solution, a cover medium whose refractive index is close to that of the substrate.

The fluorescence observation angle can be arbitrarily chosen and in general, fluorescence emitted within a certain solid angle is detected.

To theoretically investigate the effect of index–matching on the evanescently excited fluorescence, consider first a simple case in which the incident angle is fixed and the refractive index of the cover medium, n_3, is assumed. Fig.5.3.3 shows the theoretical angular distribution of evanescently excited fluorescence for V–V polarisation at a number of values of n_3. In the calculation, it is assumed that $n_1 = 1.519$, $\lambda_e = 488$nm, $\lambda_f = 525$nm, $\theta_i = 85^0$ and the absorption coefficient α and the fluorescence efficiency η are the same when the cover medium index n_3 is changed. Note that a logarithmic scale has been used for the fluorescence intensity and that unit incident excitation light intensity has been assumed.

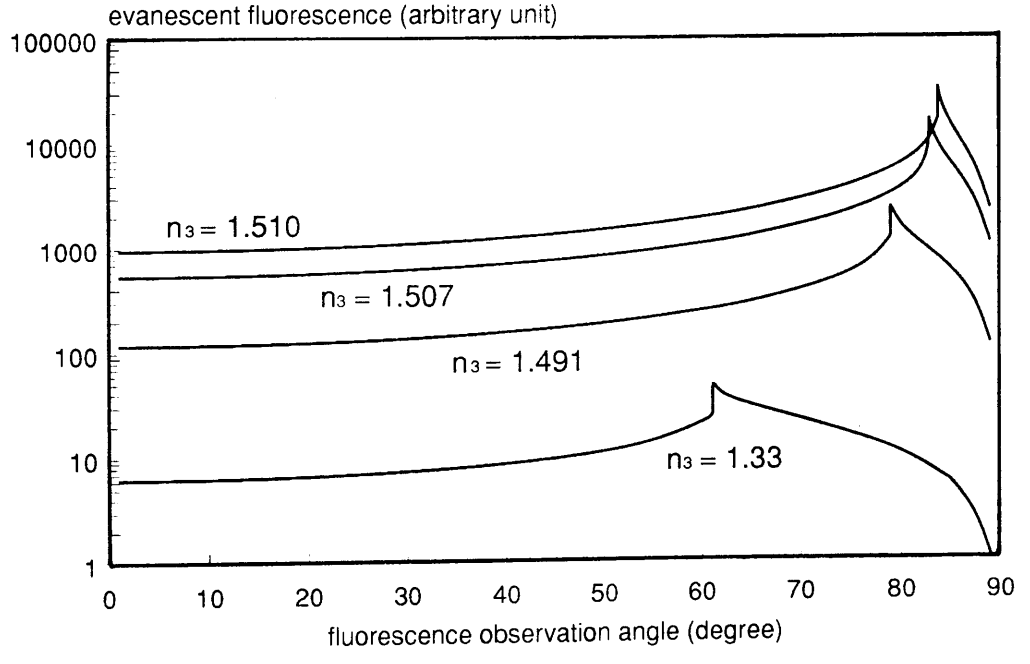

Fig.5.3.3 Angular distribution of evanescent fluorescence for V–V polarisation at a number of n_3 values with $n_1 = 1.519$, $\lambda_e = 488$nm, $\lambda_f = 525$nm, $\theta_i = 85^0$

From the above diagram, it can be seen that as n_3 increases, the evanescently excited fluorescence increases as well and this increase is very drastic as n_3 approaches n_1. It should be remembered that the expressions in the last section hold

on condition that the thickness of the cover medium t is much greater than the penetration depth d_p and d_p'. This requirement will not be met if n_3 is brought too close to n_1 which may lead to a substantial increase in d_p.

When index-matching is applied to a K^+-exchanged surface waveguide, the situation is complicated in that the change in the refractive index of the cover medium n_3 will result in a change in the incident angle θ_i which means that θ_i is no longer fixed. Since it is not easy to predict the incident angle θ_i for a graded-index planar waveguide, to roughly take the change in θ_i into consideration, a K^+-exchanged surface waveguide can be regarded as a three layer dielectric planar waveguide with $n_1=1.519$, $n_2=1.510$ (Fig.3.3.1). To ensure single mode operation of such a waveguide in the range $1.33 < n_3 < 1.510$, the thickness of the guiding layer is taken as $d=1.4\mu m$.

In a three layer dielectric waveguide, given n_1, n_2, n_3 and d, the effective refractive index n_{eff} of the waveguide can be determined using the eigenvalue equation (3.3.8) or (3.3.14) as described in chapter 3. The incident angle θ_i is related to the effective index by $\theta_i=\sin^{-1}(n_{eff}/n_1)$. The expression for the vertically polarised transmission term, $|T_\perp(\theta_i)|^2$, can therefore be expressed in terms of the n_3, n_1 and n_{eff} as

$$|T_\perp(\theta_i)|^2 = \frac{4n_{eff}(n_1^2-n_{eff}^2)^{1/2}}{(n_1^2-n_3^2)} \qquad (5.3.14)$$

If the observation of fluorescence is restricted to its peak value, i.e. $\theta_0=\theta_c'$ and no dispersion in the refractive indices n_1, n_2 and n_3 is assumed between the excitation wavelength λ_e and the fluorescence wavelength λ_f, the expression for the transmission term $|T_\perp(\theta_c')|^2$ is

$$|T_\perp(\theta_c')|^2 = 4n_3/(n_1^2-n_3^2)^{1/2} \qquad (5.3.15)$$

Therefore, using (5.3.3), the peak fluorescence intensity per unit incident light intensity can thus be expressed as

$$I_f(n_3,n_1,n_{eff}) \propto (4\alpha\eta\lambda_e/\pi)\,\frac{n_3\cdot n_{eff}\cdot(n_1^2-n_{eff}^2)^{1/2}}{(n_{eff}^2-n_3^2)^{1/2}\cdot(n_1^2-n_3^2)^{3/2}} \qquad (5.3.16)$$

Notice that (5.3.16) requires that the intensity of the light incident onto the interface is unity. Fig.5.3.4 is the calculated fluorescence enhancement as a function of n_3 for the V– V polarisation. The fluorescence enhancement, E_f, is defined as the peak fluorescence intensity at n_3 with respect to that at $n_3=1.33$, i.e.

$$E_f=I_f(n_3,n_1,n_{eff})/I_f(n_3=1.33,n_1,n_{eff}) \qquad (5.3.17)$$

In Fig.5.3.4, the starting point is 1, i.e. $E_f(1.33)=1$. There is a substantial increase in the peak evanescent fluorescence as n_3 approaches n_2. It can be seen that the evanescently excited fluorescence can be increased by at least two orders of magnitude through index– matching.

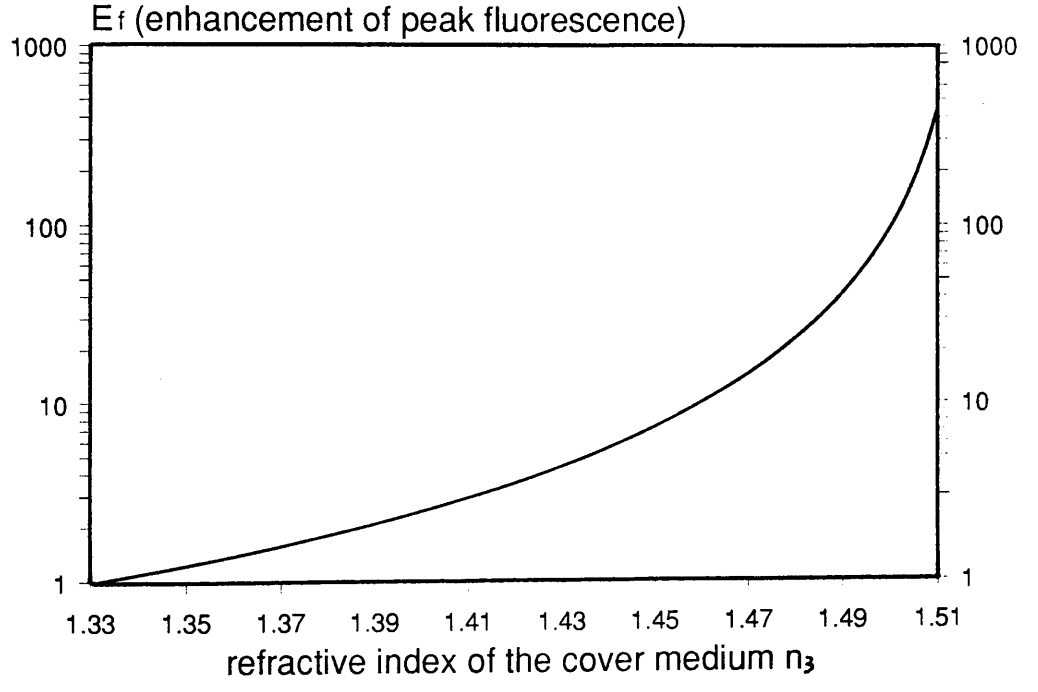

Fig.5.3.4 Enhancement of peak evanescent fluorescence through index– matching

The increase in the evanescent fluorescence intensity through index– matching is attributable to both the increase in the excitation intensity at the optical interface and the increase in the penetration depth of the excitation evanescent wave. The increase in the penetration depth of the excitation evanescent wave reduces the differentiation of fluorescence emitted by surface bound molecules from that emitted by those in the bulk. The increase in the excitation light intensity at the interface is beneficial to the excitation of surface bound fluorescent molecules. To see which factor increases faster, both the excitation light intensity at the interface I_{ts} and the penetration depth of the excitation light d_p can be plotted as a function of n_3.

It can be shown (Appendix 5.1) that for TE polarisation and $\theta_i > \theta_c$, the excitation light intensity at the interface is given by

$$I_{ts} = I_e(\theta_i)|_{x=0} = I_i \cdot \sin\theta_i \cdot |t_\perp|^2$$

$$= \frac{4 \cdot n_{eff} \cdot (n_1^2 - n_{eff}^2)}{n_1 \cdot (n_1^2 - n_3^2)} \cdot I_i \qquad (5.3.18)$$

where I_i is the incident light intensity. From (5.3.6),

$$d_p = \lambda_e / [2\pi \cdot (n_1^2 \cdot \sin^2\theta_i - n_3^2)^{1/2}]$$

$$= \lambda_e / [2\pi \cdot (n_{eff}^2 - n_3^2)^{1/2}] \qquad (5.3.19)$$

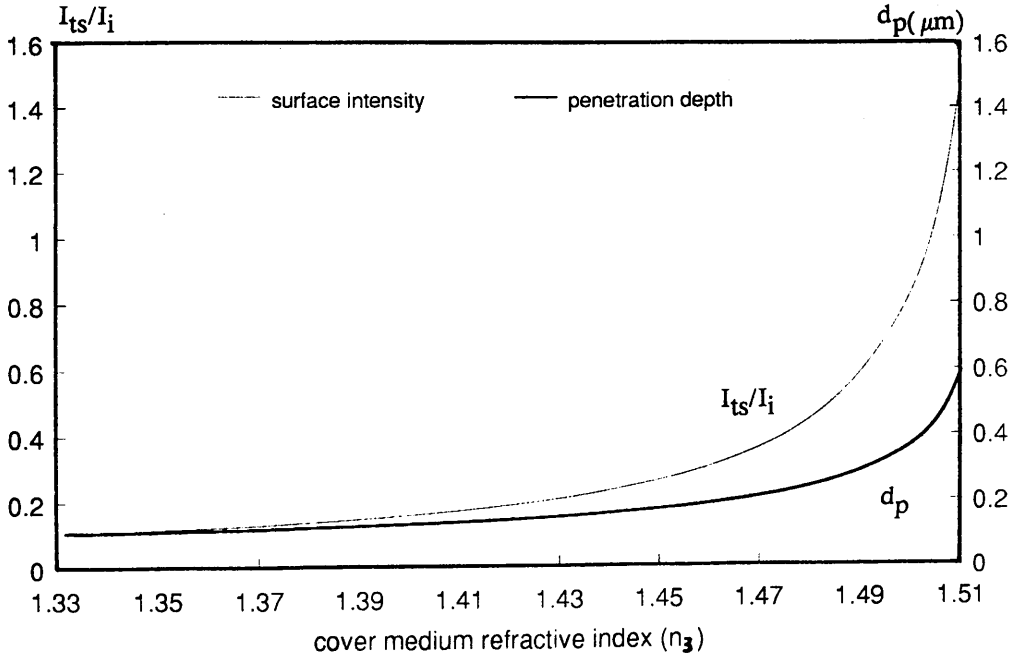

Fig.5.3.5 surface excitation light intensity (I_{ts}/I_i) and excitation penetration depth as a function of the refractive index of the cover medium (n_3)

Fig.5.3.5 shows I_{ts}/I_i and d_p as functions of n_3 over the range 1.33 to 1.510. The parameters used are the same as in Fig.5.3.4. As can been seen, with the increase in n_3, I_{ts}/I_i increases faster than d_p and the difference in their increasing rate becomes bigger at higher n_3. In fact, when n_3 is increased from 1.33 to 1.510,

the surface excitation light intensity is increased by about 15 times whereas the penetration depth is increased by about 6 times. It is therefore reasonable to conclude that the enhancement in the evanescently excited fluorescence is mainly brought about by the increase in the surface excitation light intensity rather than the increase in the penetration depth.

Experimental results

An experiment is conducted to prove that the evanescently excited fluorescence on the surface of a planar waveguide can indeed be substantially increased through index-matching. As shown in Fig.5.3.6(a), FITC labelled anti-rat-IgG proteins are first covalently immobilised into the etched wells of an ion-exchanged patterned waveguide. The concentration of the FITC-protein solution is 10μg/ml (in 0.01M PBS) and details of the covalent immobilisation procedure will be given in the next chapter. After rinsing the unimmobilised proteins off the waveguide slide and blowing the slide dry, a suitable immersion oil which has a refractive index slightly less than that of the substrate glass is applied to cover the two wells in the front. Meanwhile, RO (reverse osmosis) water is applied to cover the two wells at the back of the slide.

A beam from a 488nm laser is coupled through an prism on the etched end of the patterned slide into the waveguide and propagates along the wells to excite fluorescence evanescently. A photomultiplier with filters in front of it is placed either below the waveguide slide or in-plane with the slide and scans along the wells to record the evanescent fluorescence from each well. In the case of in-plane detection, the edge of the slide is painted with immersion oil as well to reduce diffuse reflection.

Fig.5.3.6(b) shows the measurement result. It should be noted that background noise from the non-fluorescent region has been subtracted from the signal reading and the value is the average of about 5 readings. It can be clearly seen that by using an index-matching medium rather than water solution, the evanescently excited fluorescence can indeed be substantially enhanced. It is also obvious that the enhancement in the case of in-plane detection (about 50) is greater than that in the case of right angle detection (about 13). This is because the photomultiplier in the in-plane position detects fluorescence at angles near the critical angle.

As far as the sensitivity of an evanescent fluorescence immunosensor is concerned, a high value for the evanescent fluorescence intensity is desirable. Index matching achieves enhancement at the cost of an increase in the penetration depth. A method to account for the influence of the fluorescent molecules not bound to the sensor surface is differential measurement and this will be discussed below.

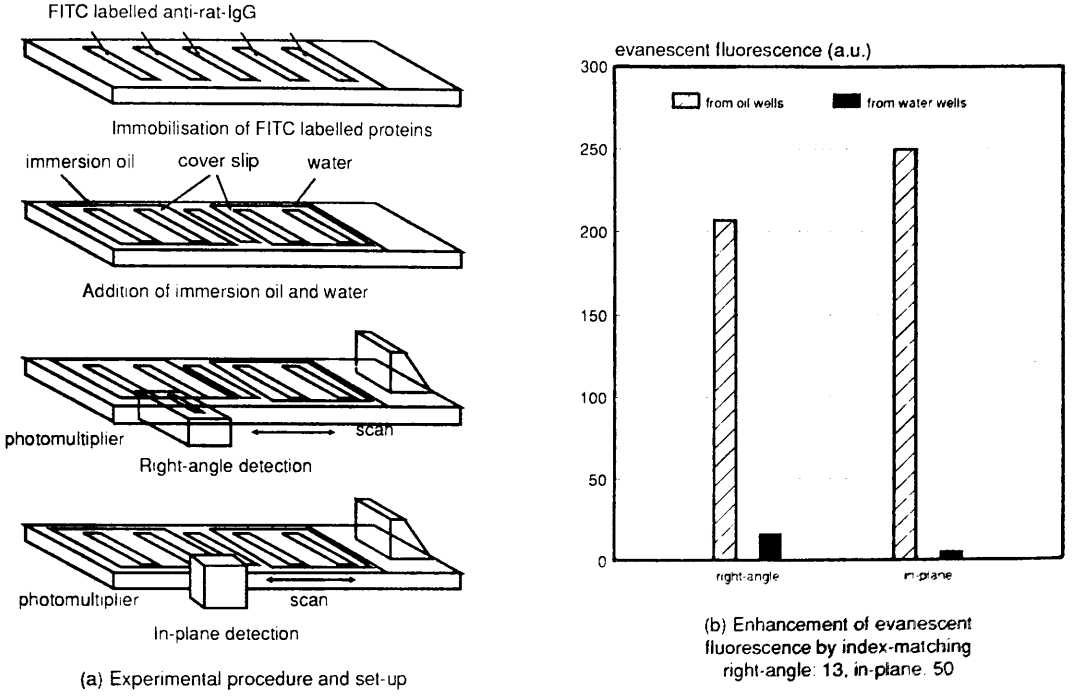

Fig.5.3.6 Experimental procedure and set– up for the demonstration of the enhancement of evanescent fluorescence through index– matching and results

5.4 Evanescently excited fluorescence in the case of solid phase fluorescence immunoassay

In the last section, it was assumed that the cover fluorescent medium is homogeneous, i.e. the absorption coefficient α and the fluorescence efficiency η are the same everywhere within the medium. However, in an evanescent fluorescence solid phase immunoassay, this is no longer the case. The binding of fluorescently labelled antibodies (or antigens) to the immobilised antigens (or antibodies) will result in the formation of a thin film on the optical interface where the concentration of the fluorescent molecules is much higher than that in the bulk medium. Therefore, (5.3.2)–(5.3.5) can no longer be directly used and new expressions taking this into consideration need to be derived.

5.4.1 Evanescently excited fluorescence in the case of both washed and wash-free immunoassays

In the derivation of the transmission term $|T(\theta_i)|^2$ (Appendix 5.2), it is shown that (5.3.2)-(5.3.5) is a direct result of the following integration under the condition that the fluorescent cover medium is homogeneous and has a thickness which is much greater than the penetration depth of the evanescent wave, i.e. $t \gg (2/d_p + 2/d_p')^{-1}$,

$$I_f(\theta_i, \theta_0) \propto \int_0^t \alpha \cdot \eta \cdot |T(\theta_i)|^2 \cdot |T'(\theta_0)|^2 \cdot \exp[-D \cdot x] \cdot dx \qquad (5.4.1)$$

where D can be regarded as the effective decay factor and is given by

$$D = \begin{cases} 2/d_p + 2/d_p' & \text{for } \theta_i > \theta_c \text{ and } \theta_0 > \theta_c' \\ 2/d_p & \text{for } \theta_i > \theta_c \text{ and } \theta_0 \leqslant \theta_c' \\ 2/d_p' & \text{for } \theta_i \leqslant \theta_c \text{ and } \theta_0 > \theta_c' \\ 0 & \text{for } \theta_i \leqslant \theta_c \text{ and } \theta_0 \leqslant \theta_c' \end{cases} \qquad (5.4.2)$$

The physical meaning of (5.4.1) is that the total evanescently excited fluorescence can be viewed as contributed by a large number of very thin layers of fluorescent medium. For a very thin layer at x from the optical interface, its evanescent fluorescence is modified by the transmission terms as well as the penetration depths of the incident and/or fluorescent waves.

Consider a patterned waveguide. If antigens and control proteins are immobilized in the etched wells and fluorescently labelled antibodies are later applied to all the wells, they will bind to one of the immobilized antigens where there is a specificity between the immobilized antigen and the applied antibody. As will be discussed in the next chapter (also Eddowes 1987/88), after the binding of antibodies to their appropriate antigens has reached its equilibrium, the equilibrium fractional surface coverage of the antibody binding sites, which is defined as the number of occupied binding sites divided by the total number of binding sites, can be expressed by

$$\Theta_{eq} = K_a[Ab]_{eq}/(1+K_a[Ab]_{eq}) \qquad (5.4.3)$$

where $[Ab]_{eq}$ is the concentration of antibody in solution at equilibrium and K_a is the association constant of the antibody-antigen pair. Assuming that the antibody

concentration is not very high so that $K_a[Ab]_{eq} \ll 1$, (5.4.3) can be approximately written as

$$\Theta_{eq} \approx K_a[Ab]_{eq} \qquad (5.4.4)$$

The specific binding of fluorescently labelled antibodies to immobilised antigens results in the formation of an antigen–antibody layer on the waveguide surface. In section 5.2, it has been mentioned that the absorption coefficient α is proportional to the concentration of the fluorescent molecule. Therefore, different absorption coefficients are assigned to the antibody–antigen layer and the bulk medium. If the thickness of the antigen–antibody layer is t_1, the absorption coefficient and the fluorescence efficiency of this layer are α_1 and η_1 respectively, the absorption coefficient and the fluorescence efficiency of the rest of the cover medium are α_2 and η_2 respectively, and the cover medium is much thicker than the penetration depth of either the excitation or the fluorescent light, the evanescent fluorescence intensity can be expressed as

$$I_f(\theta_i, \theta_0) = \int_0^{t_1} C_1 \cdot \exp(-2D \cdot x)dx + \int_{t_1}^{\infty} C_2 \cdot \exp(-2D \cdot x)dx \qquad (5.4.5)$$

where

$$C_1 = \alpha_1 \cdot \eta_1 \cdot |T(\theta_i)|^2 \cdot |T'(\theta_0)|^2 \qquad (5.4.6)$$

$$C_2 = \alpha_2 \cdot \eta_2 \cdot |T(\theta_i)|^2 \cdot |T'(\theta_0)|^2 \qquad (5.4.7)$$

and

$$D = \delta + \delta', \qquad \text{for } \theta_0 > \theta_c'$$

or

$$= \delta, \qquad \text{for } \theta_0 \leqslant \theta_c'$$

Completion of the integration in (5.4.5) results in

$$I_f(\theta_i, \theta_0) = [\zeta \cdot \alpha_1 \cdot \eta_1 + (1-\zeta) \cdot \alpha_2 \cdot \eta_2] \cdot |T(\theta_i)|^2 \cdot |T'(\theta_0)|^2/(2D) \qquad (5.4.8)$$

where the dimensionless factor ζ represents the contribution of the excitation light to the excitation of fluorescence within the antibody–antigen layer and is given by

$$\zeta = 1-\exp[-2D\cdot t_1] \qquad (5.4.9)$$

From equation (5.4.8), it can be seen that the evanescently excited fluorescence is composed of two parts. The first part

$$I_{f_1} = \alpha_1\cdot\zeta\cdot\eta_1\cdot|T(\theta_i)|^2\cdot|T'(\theta_0)|^2/(2D) \qquad (5.4.10)$$

is contributed by the binding of the applied fluorescently labelled antibody to the surface of the waveguide and the second part

$$I_{f_2} = \alpha_2\cdot(1-\zeta)\cdot\eta_2\cdot|T(\theta_i)|^2\cdot|T'(\theta_0)|^2/(2D) \qquad (5.4.11)$$

is introduced by the fact that the evanescent wave has a tail which can penetrate beyond the antigen–antibody layer into the cover medium.

Since the absorption coefficient α (1/m) is proportional to the concentration of the fluorescent molecules, if the density of binding sites on the waveguide surface is represented by Γ (mole/m^2), the corresponding concentration of antigen–antibody complex within the antigen–antibody layer can be expressed as

$$[AgAb]_{eq} = \Gamma\cdot\Theta_{eq}/t_1 \approx \Gamma\cdot K_a\cdot[Ab]_{eq}/t_1 \qquad (5.4.12)$$

Therefore, assuming that the fluorescent molecule/antibody ratio is χ, the absorption coefficient of the fluorescent material within the antibody–antigen layer can be expressed as

$$\alpha_1 = a\cdot\chi\cdot[AgAb]_{eq} \approx a\cdot\chi\cdot(\Gamma\cdot K_a/t_1)\cdot[Ab]_{eq} \qquad (5.4.13)$$

where **a** (m^2/mole) is the molar absorption coefficient characteristic of the fluorescent material.

In the case where a washing step is adopted and after the washing step, an ideal non–fluorescent cover medium is applied to the waveguide, $\alpha_2 = 0$ and/or

$\eta_2 = 0$. As a result, the evanescently excited fluorescence is given by

$$I_{f_1}(\theta_i, \theta_0) = a \cdot \chi \cdot \zeta \cdot (\Gamma \cdot K_a / t_1) \cdot [Ab]_{eq} \cdot \eta_1 \cdot |T(\theta_i)|^2 \cdot |T'(\theta_0)|^2 / (2D) \qquad (5.4.14)$$

This equation shows that with a washing step and the use of a non-fluorescent cover medium, the evanescently excited fluorescence is directly proportional to the binding site density Γ, the association constant K_a and the equilibrium antibody concentration $[Ab]_{eq}$. When multichannel immunoassays on a patterned waveguide are conducted as will be discussed, owing to the fact that the association constant of specific binding is much greater than that of non-specific binding, the evanescent fluorescence signal from the specific well will therefore be much greater than those from the non-specific wells.

However, in real situations, α_2 and η_2 cannot be taken as zero. In addition, there are background fluorescence signals introduced by a number of factors. One of the factors is non-specific binding which may contribute significantly to the background fluorescence.

Other factors which introduce background fluorescence into the system include fluorescence from the glass material, the protein molecules and scattered excitation light which cannot be completely filtered out by the optical filter system. All these can be contributed by both the guiding layer guided excitation light and substrate guided excitation light. Taking all these factors into consideration and still assuming the incident light intensity is unity, the dimensionless fluorescence intensity should be expressed as

$$I_f(\theta_i, \theta_0) = I_{f_{1S}} + I_{f_{1n}} + I_{f_2} + I_{f_3} + I_{f_4} \qquad (5.4.15)$$

where $I_{f_{1S}}$ is given by (5.4.14),
$I_{f_{1n}}$ is introduced by non-specific binding,
I_{f_2} is given by (5.4.11),
I_{f_3} is related to the guiding layer guided excitation energy,
and I_{f_4} is related to the substrate guided excitation energy.

Although only I_{f1s} is proportional to the association constant K_a and is the signal one wants to detect, I_{f1n}, I_{f2}, I_{f3} and I_{f4} are usually always present to some extent.

On the other hand, when the applied antibody solution is left on the waveguide surface rather than washed away, the medium beyond the antibody–antigen layer will be fluorescent. With a similar argument as for α_1 in (5.4.13), it is not difficult to find that the absorption coefficient of the fluorescent medium beyond the antibody–antigen layer should be given by

$$\alpha_2 = a \cdot \chi \cdot [Ab]_{eq} \qquad (5.4.16)$$

where again a (m^2/mole) is the molar absorption coefficient of the fluorescent material, χ is the fluorescent molecule/antibody ratio and $[Ab]_{eq}$ is the equilibrium antibody concentration in the sample solution.

It can be assumed that the fluorescence efficiency of surface bound fluorescent molecules is the same as that of the molecules in the sample solution. Therefore,

$$\eta_2 = \eta_1 \qquad (5.4.17)$$

Consequently, the part of the fluorescence which is introduced by the tail of the evanescent excitation wave is given by

$$I_{f2} = (1-\zeta) \cdot a \cdot \chi \cdot [Ab]_{eq} \cdot \eta_1 \cdot |T(\theta_i)|^2 \cdot |T'(\theta_0)|^2/(2D) \qquad (5.4.18)$$

As a result, I_{f2} in this case is greater than its corresponding value when the fluorescently labelled antibody solution is washed away and replaced by a non–fluorescent cover medium. Although this fluorescence signal is unwanted, it is a noise signal which is always present in wash–free evanescent wave immunoassays. Nevertheless, in general, this I_{f2} is not a factor which significantly influences the sensitivity of the method. A comparison of (5.4.14) and (5.4.18) shows that the difference between the two equations lies in the two dimensionless constants of proportion, $\zeta \cdot (\Gamma \cdot K_a/t_1)$ and $(1-\zeta)$. It can be shown (Appendix 5.3) that, in general, $\zeta \cdot (\Gamma \cdot K_a/t_1)$ is much greater than $(1-\zeta)$. Therefore, the influence from the tail of

the evanescent excitation wave can be ignored.

5.4.2 Differential evanescent fluorescence in a solid phase immunoassay

In (5.4.15), only I_{f1s} is proportional to the association constant K_a and is the signal one wants to detect. Unfortunately, the noise signals I_{f1n}, I_{f2}, I_{f3} and I_{f4} are usually present to some extent. However, these noise signals can, in theory, be eliminated by the differential method if the propagation loss of the excitation light is ignored.

Consider two identical wells on a patterned waveguide. One well is immobilised with specific antigens which have an association constant of K_a to the later applied fluorescently labelled antibody and the other well is immobilised with control proteins which is not specific to the later applied antibody. Whether a washing step is adopted or not, as long as both wells are treated equally, the fluorescence from the specific well, I_{fs}, is composed of the different contributions according to

$$I_{fs}=I_{f1s}+I_{f1n}+I_{f2}+I_{f3}+I_{f4} \qquad (5.4.19)$$

and the fluorescence from a non-specific control well, I_{fn}, is composed of the background fluorescence, i.e.

$$I_{fn}=I_{f1n}+I_{f2}+I_{f3}+I_{f4} \qquad (5.4.20)$$

With the differential measurement method, the fluorescence signal from a specific well is subtracted by that from a non-specific well. This results in

$$I_{fs} - I_{fn} = I_{f1s} \qquad (5.4.21)$$

Therefore, the influence from the background noise can, in theory, be removed.

5.4.3 Background fluorescence signals

In practice, there will always be fluctuations in the background fluorescence which will limit the sensitivity of the system. It has been shown (Appendix 5.3) that I_{f2} is generally much less than I_{f1s}. But the relationship between I_{f1s} and I_{f1n}, I_{f3} and I_{f4} is hard to predict as the magnitude of these background fluorescence terms

depends critically on a number of factors including the efficiency of non-specific blocking, the roughness of the waveguide surface, whether the substrate guided excitation light is absorbed or not, the fluorescence of the glass material and the efficiency of the optical filter system.

From the author's experience, the background noise introduced by non-specific binding (i.e. $I_{f_{1n}}$) can be greatly reduced by proper treatment of the waveguide surface. As will be shown in the next chapter, strong non-specific binding is mainly caused by the fact that the immobilisation binding sites are not fully occupied by antigens and/or blocking agent. These unoccupied immobilisation binding sites will then bind the fluorescently labelled antibodies strongly and indiscriminately. Therefore, efficient blocking of the unoccupied immobilisation binding sites is very important in reducing $I_{f_{1n}}$.

It is worth pointing out that I_{f_4}, which is related to substrate guided excitation light, may contribute significantly to the background fluorescence in the case of a wash-free immunoassay. In the case of a patterned waveguide, the substrate guided excitation light will first propagate through a region where there is air on both sides of the glass slide. Considering that the refractive index of air is 1.0 and the refractive index of the substrate is 1.510, it can be calculated that the critical angle of the air-glass interface is $\theta_{ca}=\sin^{-1}(1/1.510)\approx 41.5^0$. Therefore, those exciting light rays which are within the incident angular region $41.5^0<\theta_i<90^0$ will be guided by the substrate. However, as soon as that light ray enters the sample solution region, owing to the fact that the refractive index of the aqueous solution is $n_w=1.33$, the critical angle of the upper surface is now changed to $\theta_{cw}=\sin^{-1}(1.33/1.51)\approx 61.7^0$. As a result, in addition to the fact that the light the incident angle of which lies within $61.7^0<\theta_i<90^0$ will excite the sample solution evanescently, the remainer, i.e. with angle of incidence within $41.5^0<\theta_i<61.7^0$, will all be transmitted into the sample solution. The fluorescence excited by this light will be substantial because it is not evanescent and will excite the fluorescent molecules within the whole sample solution.

Minimizing substrate guided excitation light is therefore very important in reducing the background fluorescence. From the author's experience, it can be greatly reduced by painting the reverse side of the substrate black.

5.5 Summary

The intensity of fluorescence is determined mainly by three considerations. The first is the fluorescence efficiency, η, with which the substance converts absorbed radiation into fluorescent radiation; the second is the absorption of the excitation light by the fluorescent material and this absorption is proportional to the number of fluorescent molecules illuminated; the third is the intensity of exciting radiation.

Fluorescence can be excited by an evanescent wave generated on an optical interface by total internal reflection. The expression for the fluorescence intensity excited by an evanescent wave is different from that by a plane wave. With evanescent excitation, the evanescently excited fluorescence is modified by both the transmission terms and the penetration depths. The overall fluorescence intensity of a thick cover fluorescent medium is highest at the critical angle $\theta_i = \theta_c$, and, for a fixed $\theta_i \succ \theta_c$, the relative fluorescence intensity peaks at $\theta_0 = \theta_c'$.

The evanescently excited fluorescence can be substantially increased by increasing the refractive index of the cover medium (i.e. by index-matching) to bring the critical angle close to the incident angle. Although index-matching also leads to an increase in the penetration depth of the excitation wave, the increase in the intensity of the excitation light at the interface is more rapid and is the main reason for the enhancement in the evanescently excited fluorescence.

In an evanescent fluorescence immunoassay, the fluorescence intensity signal is composed of four parts. The first part is contributed by both specific and non-specific binding between the applied antibody and the immobilised antigen; the second part is introduced by fact that the evanescent wave has a tail which can penetrate beyond the antigen-antibody layer into the cover medium; the third and fourth parts are attributable to the background fluorescence which are related to waveguide guided excitation light and substrate guided excitation light.

The contribution from background fluorescence signals to the detected fluorescence can, in principle, be eliminated by performing a differential evanescent fluorescence immunoassay. However, even with differential immunoassays, the sensitivity of the system is limited by the fluctuation in the background fluorescence. The background fluorescence introduced by non-specific binding can be greatly reduced by efficient blocking of the immobilisation binding sites and the background

fluorescence introduced by substrate guided excitation light can be greatly reduced by painting the reverse side of the substrate black.

CHAPTER 6 ANTIBODY, ANTIGEN AND CONVENTIONAL SOLID PHASE FLUORESCENCE IMMUNOASSAYS

6.1 Introduction

The essence of an immunoassay is the specific binding of an antibody with its appropriate antigen. Since an immunosensor employs this highly specific binding, it is therefore necessary to introduce some fundamental aspects of antibody–antigen reaction. Furthermore, in most immunosensors, antibodies or antigens must be immobilised on a solid phase which acts as the sensing element. Consequently, investigations must be made on how to effectively immobilise proteins onto the sensing element. It has been pointed out previously that a problem associated with solid phase immunoassay is the non–specific binding and it influences the sensitivity of the method. Hence, ways to effectively reduce this undesirable binding need to be found.

In this chapter, the basic concepts of antibody–antigen reaction vital to the understanding of the principle of immunoassays are given. These are followed by an introduction to labelled solid phase immunoassays which constitute an important part of the working principle of an optical evanescent wave immunosensor. The results of the investigation on the immobilisation of proteins onto the solid phase are discussed and practical procedures for successful protein immobilisation and the efficient blocking of non–specific binding are described. Finally, as a comparison with evanescent fluorescence immunoassays, conventional fluorescence immunoassays are conducted and their experimental results are discussed.

6.2 Fundamentals concerning antibody–antigen reactions

6.2.1 The immune response, antibodies and antigens

Our immune system saves us from certain death by infection because when we are infected, the various responses of the immune system destroy and eliminate invading microorganisms and any toxic molecules produced by them. If a child is born with a severely defective immune system, it will soon die unless the most extraordinary measures are taken to isolate it from a host of infectious agents, including bacteria, viruses and parasites. Our immune system scans an extremely large

number of molecular units to decide which ones are foreign and initiate their destruction. Any substance capable of eliciting an immune response is referred to as an antigen (or immunogen).

There are two broad classes of immune responses, namely, 1) humoral antibody responses and 2) cell-mediated immune responses. The humoral antibody responses involve the production of special kinds of proteins called antibodies or immunoglobulins, which circulate in the bloodstream and bind specifically to the foreign antigen that induced them. The binding of an antibody to its antigen makes it easier for phagocytic cells to ingest the antigen and often activates a system of blood proteins, collectively called complement, that helps to destroy the antigen.

Cell-mediated immune responses involve the production of specialised cells that react mainly with foreign antigens on the surface of host cells, either killing the host cell if the antigen is an infecting virus or inducing other host cells, such as macrophages, to destroy the antigen.

The cells responsible for immunity are white blood cells known as lymphocytes. There are two different classes of lymphocytes. The first is T cells or lymphocytes which are responsible for cell-mediated immunity. The second is B cells or lymphocytes which produce antibodies. The immune system is composed of billions of lymphocytes (about 2×10^{12} in man, Alberts et al. 1983, pp952) and can respond to millions of different foreign antigens in a highly specific way.

6.2.2 The clonal selection theory, monoclonal and polyclonal antibodies

The clonal selection theory explains how the immune system produces such a diversity of specific antibodies. According to this well accepted theory, during development, each lymphocyte becomes committed to react with a particular antigen before ever being exposed to it. The specificity of an antibody is determined by its amino acid sequence. A cell expresses its commitment in the form of surface receptor proteins that specifically fit the antigen. The binding of an antigen to the receptors activates the cell, causing it both to multiply and mature. The immune system is composed of millions of different families, or clones, of cells, each consisting of T or B lymphocytes descended from a common ancestor. Since each ancestral cell is committed to make one particular antigen-specific receptor protein, all cells in a clone have the same antigen specificity.

A very large number of biologically interesting macromolecules, including virtually all proteins and most polysaccharides, can serve as antigens (Alberts et al. 1983, pp958). The specific affinity of an antibody is not for the entire macromolecular antigen but for particular sites on it. Those parts of an antigen's surface that combine with the antigen–binding site on an antibody molecule or on a lymphocyte receptor are called antigenic determinants (or epitopes). If two or more of the antigenic determinants are identical (as in a polymer with a repeating structure), the antigen is said to be multivalent. Most small foreign molecules do not stimulate antibody formation. However, they elicit the formation of a specific antibody if they are attached to macromolecules. In this case, the macromolecule is called the carrier of the attached chemical group and the small foreign molecules by itself is called a hapten. Antibodies elicited by attached haptens will bind unattached haptens as well.

Most antigens have a variety of different antigenic determinants on their surface that stimulate the production of antibodies or T–cell responses. A single antigenic determinant will, in general, activate many different clones, each of which produces an antigen–binding site with a different affinity for the determinant. Such responses are said to be polyclonal. When only a few clones respond, the response is said to be oligoclonal; and when the total response is made by a single B– or T–cell clone, it is said to be monoclonal. Antibodies produced in a polyclonal response are called polyclonal (or heterogeneous) antibodies because they are products of many different antibody–producing cells. On the other hand, antibodies produced in a monoclonal response are referred to as monoclonal (or homogenous) antibodies.

6.2.3 Antibody structure and classification

An antibody molecule is a Y shaped protein with two identical antigen–binding sites—one at the tip of each arm of the Y (Fig.6.2.1). As a result of their bivalence, antibodies can cross–link antigen molecules into a large lattice, as long as the antigen molecules each have three or more antigenic determinants. The basic structural unit of an antibody molecule consists of four polypeptide chains, i.e., two identical light (L) chains (each usually containing about 220 amino acids), and two identical heavy (H) chains (each usually containing about 440 amino acids). The two arms of the Y, each of which contains a light chain and half a heavy chain, are called the Fab (fragments antigen–binding) of the antibody and the tail of the Y is called Fc (fragment crystallizable). There are five different classes of antibodies (IgA,

IgD, IgE, IgG, and IgM), each with a distinctive H chain (α, δ, ϵ, γ, and μ, respectively) and thus has a different biological property. The light chain can be subdivided into κ or λ light chains and either type of L chain (κ or λ) can be associated with any class of H chain. IgG antibodies constitute the major class of immunoglobulins in the blood.

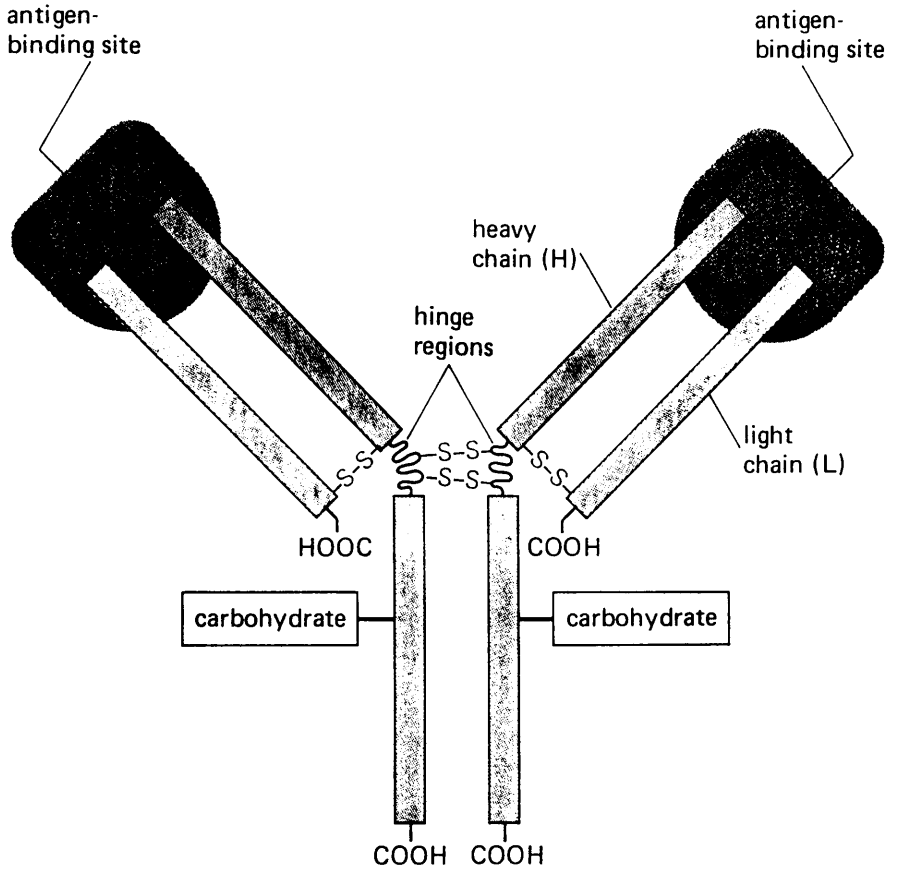

Fig.6.2.1 Schematic illustration of an antibody molecule with two identical antigen– binding sites (after Alberts et al. 1983).

6.2.4 Antibody– antigen binding

The binding of an antibody to an antigen is reversible and is mediated by the sum of many relatively weak non– covalent forces, including hydrophobic and hydrogen bonds, van der Waals forces, and ionic interactions. The strength of an antibody– antigen interaction depends on both the affinity and the number of binding sites.

The binding reaction between an antigen with a single antigenic determinant (denoted as Ag) and a single antigen– binding site (denoted as Ab) can be expressed as

$$Ag + Ab \rightleftarrows AgAb \qquad (6.2.1)$$

The equilibrium point depends both on the concentration of Ab and Ag and on the strength of their interaction. If square brackets are used to represent concentrations at equilibrium, the strength of the interaction is then expressed by the affinity (or association) constant K_a (m^3/mole) defined as

$$K_a = [AgAb]/[Ag][Ab] \qquad (6.2.2)$$

Values of K_a range from 50 to as high as 10^9 m^3/mole (Alberts et al. 1983, pp970).

The affinity of an antibody only reflects the goodness of the fit of an antigenic determinant to a single antigen– binding site, and it is independent of the number of sites. To express the total binding strength of all binding sites, the word avidity is used. A typical IgG molecule will bind at least 10,000 times more strongly to a multivalent antigen if both antigen– binding sites are engaged than if only one site is involved (Alberts et al. 1983, pp970).

The precise antigen specificity of antibodies makes them versatile and powerful tools that can be used to detect, quantify and localize a large variety of biologically interesting molecules at low concentrations in complex matrices. To measure antibody– antigen reactions, there exist a large number of methods. In high sensitivity immunoassays, labelled antigens or antibodies are employed for their detection. Such immunoassay methods include radioimmunoassay, enzyme immunoassays and fluoroimmunoassays. In principle, any chemicals for which specific binding agents exist can be measured by these methods. Most chemicals with molecular weights greater than 250 dalton can be made to elicit specific antibodies (Andrade et al. 1985) and can therefore be measured. Owing to the advent of monoclonal antibody production technology, immunosensors with extremely high selectivity and sensitivity have become a possibility.

6.3 Labelled solid phase immunoassay

6.3.1 Radioimmunoassay and enzyme immunoassay

A common way of quantifying immunoreactions is to use radioactive compounds and link them to a given antibody or antigen. For example, in direct measurement, the amount of labelled antibody or antigen that combines specifically with the material under test is measured. Radioimmunoassay is extremely versatile and sensitive, but it has certain drawbacks. Radiation from radioactive isotopes may cause health hazards, it is comparatively expensive and the useful lifetime of an assay kit is limited by the half–life of isotopes which is usually about two months.

As an alternative, enzyme immunoassays have been developed where enzyme–coupled antibodies are used to bind to specific molecules and the activity of the enzyme is measured to determine the analyte. Enzyme reactions can be quantified by various measuring techniques including potentio–, ampero– or colorimetry. The most frequently applied technique is measuring a coloured product of a reaction which is formed from a colourless substrate due to the catalytic activity of the marker enzyme. A great advantage of colorimetry is its high sensitivity which is comparable with that of radioimmunoassays.

6.3.2 Fluorescence immunoassay

Another alternative is offered by fluorescence immunoassay which is based on the labelling of samples with fluorescing compounds. Conventionally, fluorescence immunoassays are conducted with the aid of a fluorescence microscope. In such cases, the sample under examination is stained with an antibody labelled with a fluorescent molecule (also called probe).

In principle, fluoroimmunoassays should have the potential of providing high sensitivity in a non–isotopic test format. This is because the number of photons emitted from a sample of fluorescently labelled molecules can exceed the number of gamma ray photons from the same number of gamma–ray–emitting tagged molecules. Nevertheless, fluoroimmunoassays have not replaced radioimmunoassays because of the fact that conventional fluorescent probes emit photons in the same spectral region where most endogenous materials fluoresce. As a result, even though the fluorescently labelled molecules of interest may emit a very large and measurable

number of photons, the background does this as well. This makes the discrimination of signal from background difficult.

To solve this problem, a number of efforts have been made. The most promising solution is the use of time–resolved fluorescence (Soini and Hemmila 1979, Hemmila 1985). In this technique, fluorescent probes with long excited state lifetimes are used. After the molecule is excited with a short pulse of light, the emitted fluorescence is measured in a properly selected time window. Measurement starts after an initial delay time during which any short–lived fluorescence has decayed. It is thus possible to exclude practically all sources of background fluorescence and achieve very high sensitivity of specific signal detection. The only limiting background fluorescence measured, will be due to non–specific binding of the labelled reagents used.

Also efforts have been made to synthesize chemical dyes which emit at the red end region of the spectrum. Although few developments in this field have made significant improvement in solving the background problem, the realization and demonstration that phycobiliproteins could be used as fluorescent labels has opened up new opportunities for fluorescence techniques in immunoassays. The extremely high extinction coefficient and quantum yields (5.2.4), along with other chemical and physical properties, have made possible several applications that were not possible using conventional fluorescent labels (Kronick 1988).

6.3.3 Direct, competitive and sandwich immunoassays

In practice, labelled immunoassays are often conducted on a solid phase and are therefore frequently called solid phase immunoassays. In these immunoassays, the term immunoadsorbent is often used and implies an antigen or antibody which has been rendered water–insoluble. Solid phase immunoassays are generally subdivided into heterogeneous (separation required) assays and homogeneous (separation free) assays.

If the analyte to be sensed, say antibody, is labelled, the simplest way to perform the assay is to immobilise the antigen onto a solid support and apply a solution of fluorescently labelled antibodies. After a certain time of incubation, the free antibodies in the solution are removed by a washing step and the position as well as the amount of labelled antibodies can then be established. This is called direct immunoassays. Fig.6.3.1 is a schematic illustration of direct solid phase

immunoassays.

On the other hand, if the analyte to be sensed is not labelled, two basic types of heterogeneous assays, i.e. the competitive assay and the sandwich (also called two– site) assay can be employed.

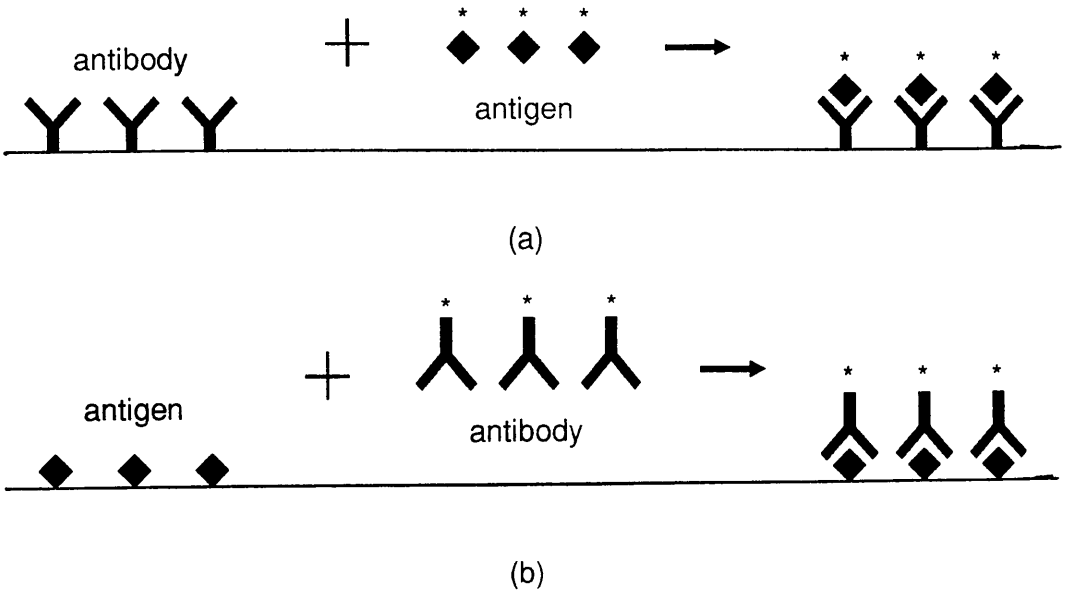

Fig.6.3.1 Direct solid phase immunoassays, (a) for antigen, (b) for antibody

Fig.6.3.2 outlines the principle of competitive immunoassays. The labelled antigen is incubated with a limiting quantity of antibody and a labelled antigen– antibody complex is formed. If an unlabelled antigen is introduced (e.g. as an unknown in a patient's body fluids), it competes with labelled antigen for the limited number of antigen– binding site of the antibody. Thus, the quantity of labelled antigen which is displaced is proportional to the quantity of antigen present in the unknown.

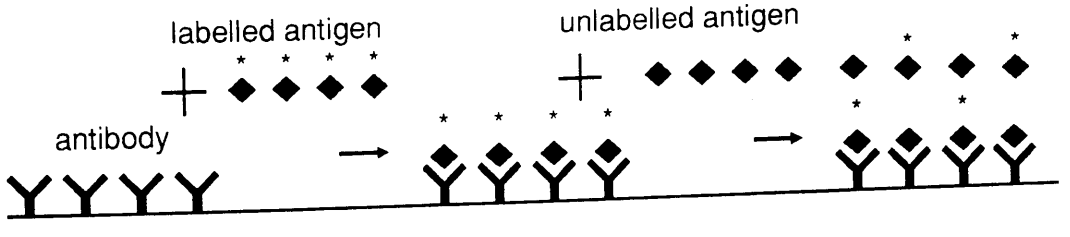

Fig.6.3.2 Illustration of the principle of a competitive solid phase immunoassay

In sandwich immunoassays, double antibody method is used in which the second antibody is labelled. It is especially applicable to systems of multivalent antigens. As

shown in Fig.6.3.3, a solid phase antibody is incubated with the antigen (generally introduced as an unknown quantity in the patient's fluids) to form a solid phase complex. Following removal of the incubation medium, the complex is incubated with labelled second antibody. The quantity of labelled antibody is thus proportional to the quantity of antigen present in the sample. As a result, the multivalent antigen is sandwiched between the immobilised antibody and the labelled antibody. Using immobilised antigen and labelled antigen (or anti–antibody), the same procedure may be employed to determine antibody.

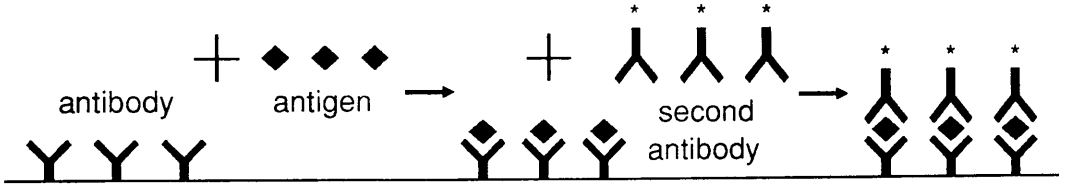

Fig.6.3.3 Illustration of the principle of a sandwich solid phase immunoassay

6.3.4 Theory of solid phase immunoassays at equilibrium

The theory of antibody–antigen reactions of a solid phase immunoassay is slightly different from that in the liquid phase case as described in 6.2.4. It has been developed by Eddowes (1987/88). Since it is important for the understanding of a solid phase immunosensor, it is necessary to repeat some of the main points here.

The forward and reverse reaction rate

Consider the reaction between an antigen, Ag, in solution and its complementary antibody immobilised on a surface. The rate, v, in units of moles per square meters per second, i.e. moles $m^{-2}\,s^{-1}$, of adsorption is given by

$$v_a = k_a \cdot [Ag] \cdot \Gamma \cdot (1-\Theta) \qquad (6.3.1)$$

and that of desorption by

$$v_d = k_d \cdot \Gamma \cdot \Theta \qquad (6.3.2)$$

where k_a ($m^3 \cdot mole^{-1} \cdot s^{-1}$) and k_d (s^{-1}) are the rate constants for adsorption and desorption respectively, [Ag] ($mole/m^3$) is the concentration of antigen in solution, Γ

(moles m^{-2}) is the density of antigen–binding sites on the surface, and Θ is the fractional surface coverage of antigen with respect to the total antigen–binding sites.

Surface coverage at equilibrium

At equilibrium, the adsorption and desorption rates balance. By equating (6.3.1) and (6.3.2), and defining the dissociation constant as

$$K_d = k_d/k_a \qquad (6.3.3)$$

an expression is obtained relating the equilibrium fractional surface coverage, Θ_{eq}, to the dissociation constant and the equilibrium antigen concentration

$$\Theta_{eq} = [Ag]_{eq}/([Ag]_{eq}+K_d) \qquad (6.3.4)$$

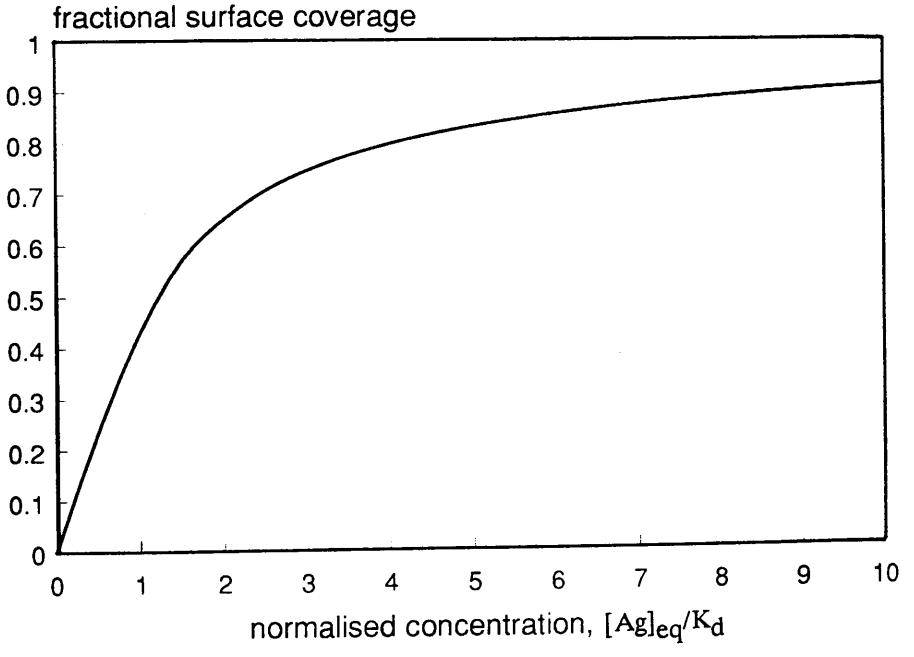

Fig.6.3.4 Equilibrium surface coverage as a function of normalised antigen concentration

Fig.6.3.4 shows the equilibrium surface coverage as a function of normalised equilibrium antigen concentration, $[Ag]_{eq}/K_d$. It can be seen from the curve that due to the limited binding sites on the solid phase, the equilibrium surface coverage is not a linear function of the equilibrium antigen concentration. The equilibrium surface coverage Θ_{eq} approaches its saturation value when $[Ag]_{eq}/K_d$ reaches 4 or 5. It is,

therefore, apparent that the upper concentration sensing limit is roughly equal to the dissociation constant. The lower detection limit will be determined by the sensitivity of the detection method and is expected to be some orders of magnitude lower than K_d. In general situations with K_d being in the range of 10^{-3} 10^{-7} (mole/m^3), an immunosensor based on equilibrium surface coverage measurement could have a sensitivity from micromolar down to picomolar range.

Initial and equilibrium antigen concentration and conditions for linear approximation

The equilibrium concentration $[Ag]_{eq}$ is different from the initial concentration $[Ag]_i$ if the depletion of the solution concentration is considerable when species bind to the surface. Assuming that an amount of antigen, $\Theta_{eq}\Gamma S$ (moles), adsorbs on an area, S (m^2) from a volume, V (m^3) to leave an equilibrium concentration, $[Ag]_{eq}$, in solution, the depletion of the solution concentration is $\Theta_{eq}\Gamma S/V$ and the initial and equilibrium concentration is related by

$$[Ag]_i = [Ag]_{eq}\left[1 + \frac{\Gamma S}{V([Ag]_{eq}+K_d)}\right] \qquad (6.3.5)$$

It is thus clear that for $[Ag]_i \approx [Ag]_{eq}$, the condition $S\Gamma/V \ll ([Ag]_{eq}+ K_d)$ must be satisfied. For immunosensor applications, to avoid saturation, it is required that $[Ag]_{eq} \leqslant K_d$. This reduces the inequality to $S\Gamma/V \ll K_d$. Combination of (6.3.5) with (6.3.4) leads to the conclusion that a linear approximation between the equilibrium surface coverage Θ_{eq} and initial antigen concentration $[Ag]_i$, i.e.

$$\Theta_{eq} \approx [Ag]_i/K_d \qquad (6.3.6)$$

is valid only if $S\Gamma/V$, $[Ag]_i \ll K_d$.

6.4 Protein immobilisation

6.4.1 Protein immobilisation in general

A very important issue for the successful development of a solid phase immunosensor is apparently the immobilisation of biocomponents onto the transducing element. This immobilisation may be achieved by many ways, both physical and chemical, including adsorption; entrapment; protein crosslinking; and covalent binding

(or coupling). However, the immobilisation procedure must meet the requirements of reproducibility, high protein loading, immunological activity, and stability. Also, the procedure should not cause chemical or physical changes to the surface which cause undesirable effects such as light scattering.

The two most commonly used methods for protein immobilisation are physical adsorption and covalent binding (or coupling). Physical adsorption is achieved by keeping the protein solution in contact with the solid surface for a comparatively long time. This is a poorly understood process (Lundström 1983). It is attractive because proteins can be readily adsorbed onto glass surfaces. In addition, the protein–glass bonds are so tight that strong acids or alkalis are required to recover the proteins. However, the reproducibility of protein loading is poor and it is difficult to predict the configuration of proteins on the surface (Sutherland et al. 1987).

Covalent binding is the formation of covalent bonds between the biocomponent and the surface of the transducing element or a matrix kept in close proximity to the transducer. It is a more attractive approach as it potentially allows control of the immobilisation reaction and a certain degree of predictability. Typically, the reaction with silane coupling agents is used. These agents are monomeric silanes which have organo–functional groups at one end and groups which react with the inorganic surface at the other end. A typical agent is γ–aminopropyltriethoxy silane (APTS) which can be used in a three–step procedure to attach proteins to silica. In an acidic environment, the ester groups on the APTS hydrolyse to form hydroxyl groups which can then condense with surface silanol groups to give a silica surface with pendant amino groups (6.4.1)

$$\text{Silica—SiOH} + C_2H_5OSi(OC_2H_5)_2(CH_2)_3\text{–}NH_2 \rightarrow$$

$$\text{Silica—SiOSi}(OC_2H_5)_2(CH_2)_3\text{–}NH_2 \qquad (6.4.1)$$

In a second step, the amino groups are used to prepare an active aldehyde intermediate by reaction with glutaraldehyde at neutral pH

$$\text{Silica—}NH_2 + OCH(CH_2)_2CHO \rightarrow$$

$$\text{Silica—N=CH}(CH_2)_2CHO \qquad (6.4.2)$$

The final step is to react the aldehyde group with a primary amine on the protein to be immobilised to form an imine coupling, i.e.

$$\text{Silica—CHO} + \text{NH}_2\text{–antibody} \rightarrow$$

$$\text{Silica—CH=N–antibody} \qquad (6.4.3)$$

6.4.2 Immobilisation procedures for physical adsorption and covalent binding.

Of the many ways concerning physical adsorption and covalent binding, the author has tested two comparatively simple ones. The first is physical adsorption which is based on a method described by Elwing and Stenberg (1981). The second is covalent binding which is based on a procedure developed and well used in the bioelectronics group of the author's department. What follows are the pratical immobilisation procedures.

Before protein immobilisation, glass slides or patterned waveguides are cleaned (as described in Section 4.2.2) in concentrated sulphuric acid for 10 to 15 minutes, rinsed thoroughly with running RO water, blown dry with filtered nitrogen gas and dried over a hot plate (90 °C).

In physical adsorption, the slides are immersed for 2 minutes in a 1% (v/v) solution of dichlorodimethylsilane (also called repel coat) in trichloroethylene, rinsed in trichloroethylene, rinsed under running RO water, and blown dry with compressed nitrogen gas. This treatment generates a hydrophobic surface which would spontaneously adsorb many proteins. Physical adsorption is then achieved by dropping with a pipette a small amount (25 μl to 100 μl) of a protein solution (usually at 0.1mg/ml in 0.01M PBS (pH 7.2)) on the slide surface or in the etched wells and incubating overnight (10 to 12 hours) at 37 °C. In order to maintain a high humidity to prevent the evaporation of protein solutions, an airtight wet plastic box is used to contain the slides.

In covalent binding, as an initial step, a mixture of 95% absolute alcohol, 1% amino–silane [$\text{H}_2\text{N}-(\text{CH}_2)_2-\text{NH}-(\text{CH}_2)_3-\text{Si}(\text{OCH}_3)_3$] and 4% RO water is made. Acetic acid is then added to adjust the pH of the mixture to pH= 5.0. Cleaned slides are immersed in the mixture for 2 minutes, rinsed in absolute alcohol and blown dry. The silane is cured in an oven at T= 115 °C for 15 minutes. In the

second step, the silanated slides are immersed in 1%(v/v) glutaraldehyde [$COH-(CH_2)_2-COH$] solution in 0.01M PBS (pH 7.2) for 1 hour, rinsed with RO water and blown dry with compressed air. Finally, protein solutions (usually at 0.1mg/ml in 0.01M PBS (pH 7.2)) are applied to the surface of the slides for 1 hour and the slides are again rinsed under running RO water and blown dry with compressed air.

6.4.3 Protein loading with the two immobilisation methods

In comparing the loading of proteins onto plain slide surface with the two immobilisation methods, FITC labelled anti-rat-IgG is used. Owing to the fact that the fluorescence microscope available does not have a light intensity detection system, a simple experimental set-up as shown in Fig.6.4.1 is employed for the quantification of FITC labelled proteins on a plain glass slide. Since fluorescence intensity is proportional to the number of fluorescence molecules as discussed in the last chapter, the density of FITC labelled anti-rat-IgG immobilised on the surface (i.e. protein loading) is therefore proportional to the fluorescence intensity from the surface. During all these measurements, the distance between the laser illuminated area on the slide and the photomultiplier is fixed and a reference laser light intensity is recorded to compensate for the fluctuation of the laser light intensity.

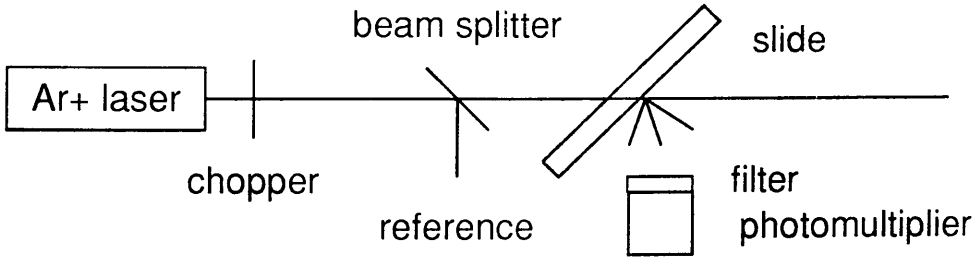

Fig.6.4.1 Experimental set-up for the measurement of protein loading

In Fig.6.4.2, protein loading is plotted as a function of the concentration of the protein solution. Fig.6.4.2a is for the case of covalent binding. The incubation time is 1 hour which has been established as sufficient for the immobilisation reaction to reach its equilibrium. Fig.6.4.2b is for the case of physical adsorption where the incubation time is about 24 hours. A comparison of the fluorescence intensities in (a) and (b) shows that the loading of proteins is more in the case of covalent binding than in the case of physical adsorption. The higher the original protein solution

concentration, the higher the protein loading. It appears that in the case of covalent binding, saturation of the loading of protein may almost be reached at the concentration of 100μg/ml or 0.1mg/ml. Although a monolayer of closely packed proteins on the slide is ideal for solid phase immunoassays, owing to the relatively high cost of purified immunoglobulins, it is perhaps not economic to use highly concentrated pure antibody solutions. It is thus estimated that 100μg/ml or 0.1mg/ml is a reasonable concentration for the immobilisation of IgG molecules as has been adopted by Jonsson et al. (1985).

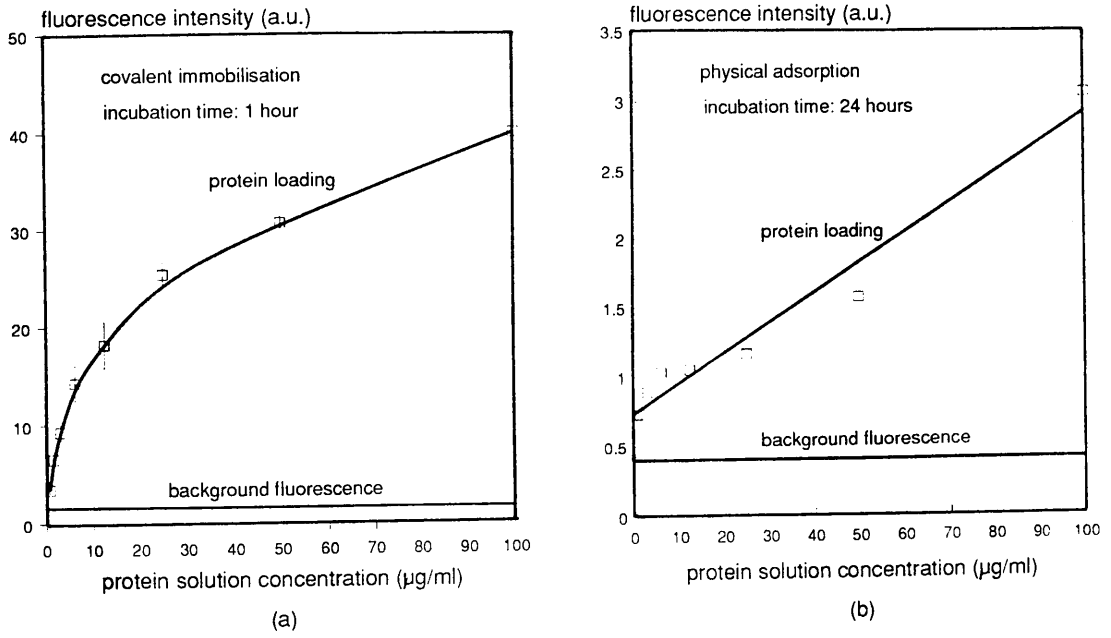

Fig.6.4.2 Protein loading as a function of the initial protein solution concentration, a) covalent binding, b) physical adsorption

As an alternative, the slides immobilised with FITC labelled proteins are examined under a fluorescence microscope. Fig.6.4.3 shows the typical microscopic photographs of the two situations. In order to show the contrast of fluorescence between the protein immobilised area and the blank area, the border of the two areas is put at the centre of the photograph. It can be seen that covalent binding produces a more uniform molecular layer on the slide with much higher loading than physical adsorption. Note that in the case of physical adsorption (Fig.6.4.3(b)), there are clumps of FITC labelled IgG molecules formed near the bordering areas. In fact, this phenomenon has been frequently observed and it sometimes happens in the central area as well. This confirms that the loading of protein in the case of physical adsorption is less predictable than in the case of covalent binding.

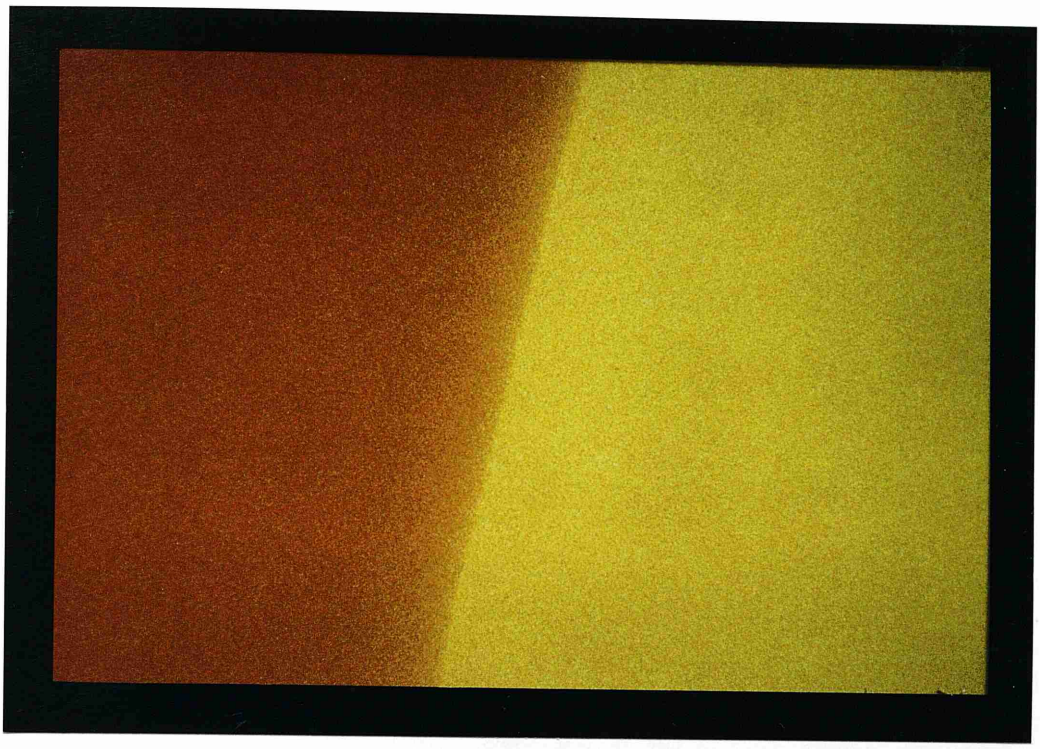

(a)

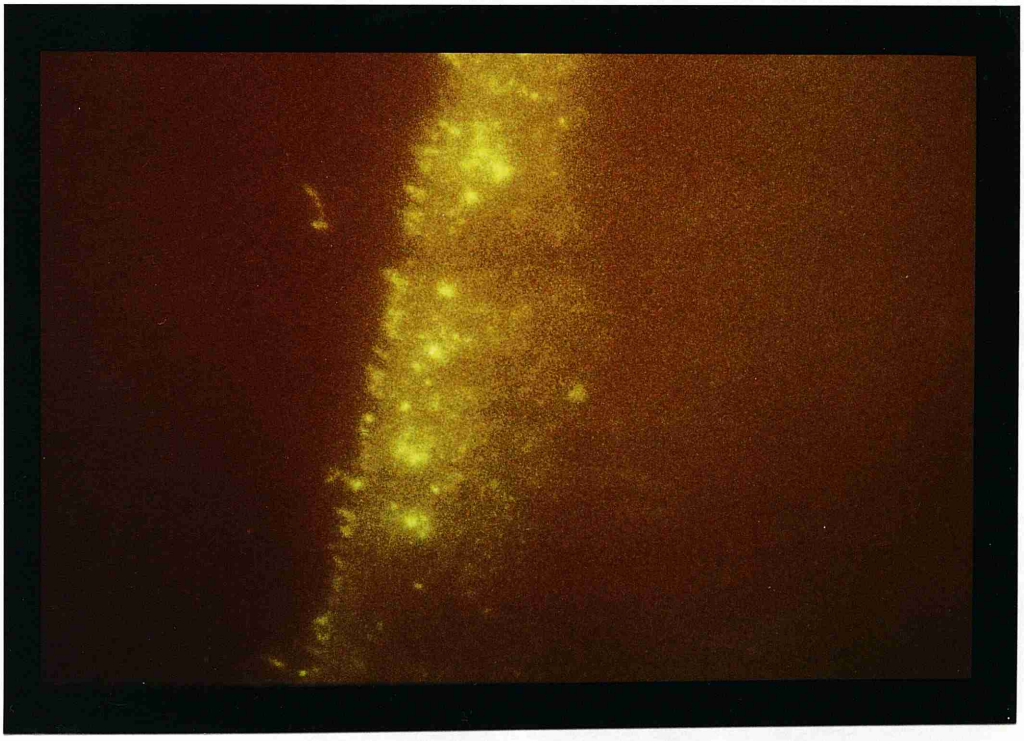

(b)

Fig.6.4.3 Microscopic photographs of the immobilisation of FITC labelled proteins (magnification X100), a) covalent binding; b) physical adsorption

From both the measurements and the photographs, it seems that covalent binding is much better than physical adsorption in term of the loading and distribution of proteins on the glass slide. However, as will be discussed in the next section, covalent binding also introduces more non-specific binding. Therefore, it is yet to be decided which is better, covalent binding or physical adsorption.

6.5 Non-specific binding, its efficient blocking and conventional fluorescence immunoassays

6.5.1 The problem of non-specific binding

As pointed out earlier, in solid phase immunosensing, the recognition of an antibody (or antigen) is achieved by the specific binding of the immobilised antigen (or antibody) on the transducing element to the applied antibody (or antigen). Non-specific binding happens when the applied analyte binds to the transducing element covered with an antigen (or antibody) which is not specific to the applied analyte. Since non-specific binding increases the background noise and thus reduces the sensitivity in solid phase immunoassays, this undesirable effect should be either greatly reduced or completely eliminated.

To investigate the problem of non-specific binding associated with both physical adsorption and covalent binding, conventional fluorescence immunoassays using the experiment set-up of Fig.6.4.1 are conducted. Rat-IgG is used as the antigen and BSA (bovine serum albumin) as the control protein. At the same concentration of 0.1mg/ml, rat-IgG and BSA are immobilised respectively onto two separated parts of a plain glass slide treated with either repel coat (dichlorodimethylsilane) or amino-silane + glutaraldehyde. Upon leaving FITC labelled anti-rat-IgG solution (excess amount at the concentration of 10μg/ml in 0.01M PBS, pH= 7.2) on these surfaces for about 30 minutes, the unbound FITC-anti-rat-IgG molecules are washed off the slides under running RO water and fluorescence intensities from a clear area where no FITC labelled anti-rat-IgG is applied, from the specific area and from the non-specific areas are measured.

Fig.6.5.1 (a) and (b) give respectively the typical values of the measured fluorescence intensities for amino-silane and repel coat treated slides. It can obviously be seen that although the overall specific fluorescence intensity of the

covalent binding slide is stronger than that of the physical adsorption slide, covalent binding also results in more non-specific binding. In fact, the ratio of specific binding to non-specific binding in the case of covalent binding is only about 4 whereas the ratio for the physical adsorption slide is about 39. The fact that the non-specific binding fluorescence in the case of covalent binding is much stronger than the background noise suggests that the strong non-specific binding is most probably introduced by the fact that there are still a considerable number of covalent binding sites which are not occupied by the applied first layer proteins. In addition, a comparison of the background noise in the two cases indicates that treating a slide with amino-silane and glutaraldehyde inherently introduces a significant amount of background fluorescence. Therefore, in terms of the sensitivity of solid phase fluorescence immunoassays, covalent binding is not necessarily better than physical adsorption.

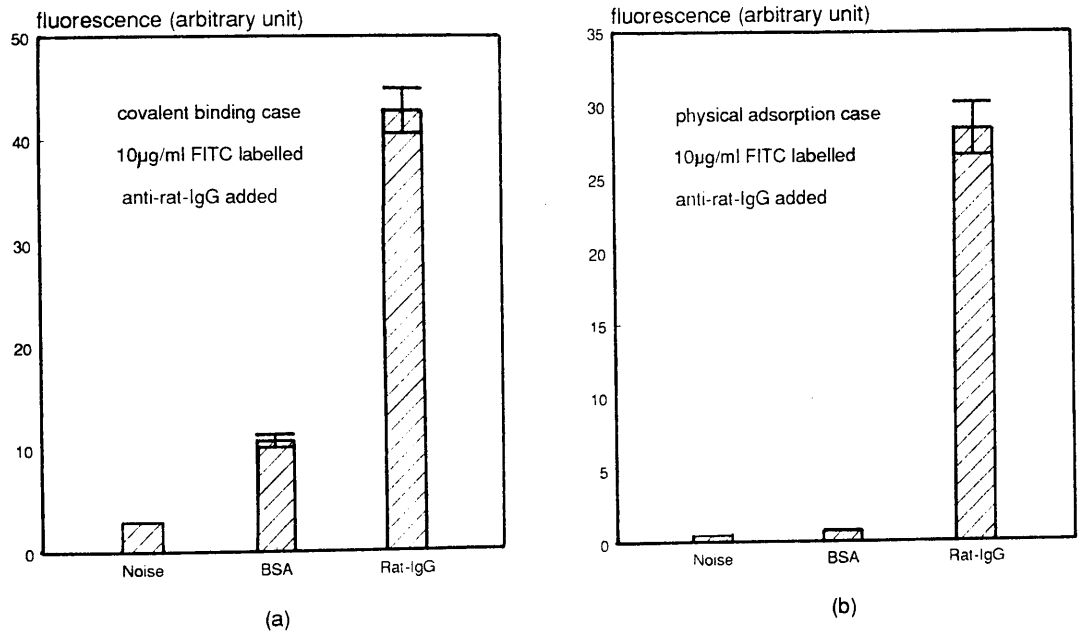

Fig.6.5.1 Fluorescence immunoassay without the blocking of non-specific binding, (a) covalent binding case; (b) physical adsorption case

Unless the cause of this relatively strong non-specific binding can be identified and the effect of this non-specific binding can be eliminated or greatly reduced, incorporating covalent binding into the system to sacrifice for the high sensitivity of the immunoassay is not necessarily beneficial. Since FITC-anti-rat-IgG can either bind directly to the covalent binding sites not occupied by the control protein or can attach itself to the control protein due to the cross-reactivity of the antibody, a test is carried out to identify which is the main cause. Solutions of the control protein

BSA at four orders of concentrations, i.e. 10.0mg/ml 1.0mg/ml, 0.1mg/ml and 0.01mg/ml are covalently immobilised onto four areas of a plain glass slide respectively. The FITC–anti–rat–IgG solution (10μg/ml) is then applied to these areas on the slide, incubated at 37°C for 30 minutes and washed under running RO water. Fig.6.5.2 shows the results of the measured fluorescence intensities from each of these areas. It clearly indicates that the non–specific fluorescence signal increases with decreasing concentration of the control protein. Since the decrease in the control protein concentration means a decrease in the number of control protein molecules covalently immobilised onto the surface and therefore more unfilled aldehyde or amino groups on the surface, the experimental results prove that the strong non–specific binding is attributable to these unfilled covalent binding sites.

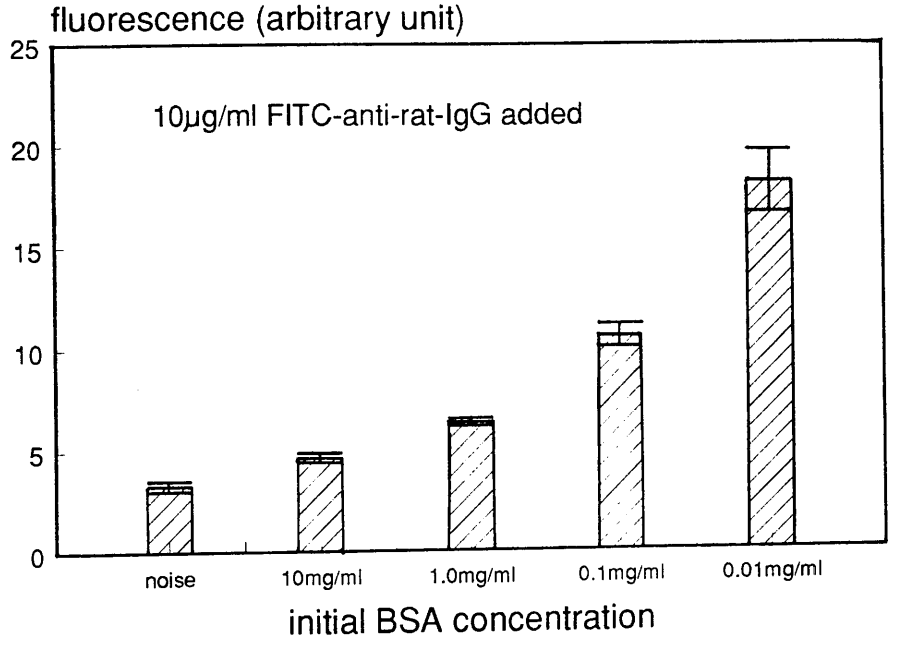

Fig.6.5.2 Non–specific binding at four orders of initial control protein concentration

Hence, the reduction of non–specific binding depends on how efficiently the covalent immobilisation binding sites can be filled by either a control protein or a blocking agent which prevents the later applied analyte from reaching the covalent binding site. From the above test, it can also be implied that in the specific area, if the covalent binding sites are not efficiently blocked, they would also give rise to fluorescence signals which would be interpreted as specific binding signal. Therefore, after the covalent immobilisation of antigens and control proteins, saturation of the unfilled covalent binding site must be rendered on both the specific area and the control area. Meanwhile, it must be checked that the blocking process does not significantly interfere with the antibody–antigen reaction.

6.5.2 Blocking of non-specific binding

In the attempt to block non-specific binding, a number of blocking agents are tested. These include ethanolamine, glycine, lysine, BSA and skimmed milk powder which mainly contains casein and albumin. Experiments reveal that ethanolamine, glycine and lysine are not as good as BSA or skimmed milk powder in terms of the blocking efficiency. On the other hand, both BSA and dried skimmed milk powder can efficiently block the non-specific binding without obvious interference with the antibody-antigen reaction, if high concentrations (≈10mg/ml) of their solution are used. Since BSA is much more expensive than skimmed milk powder, the latter is obviously more economical.

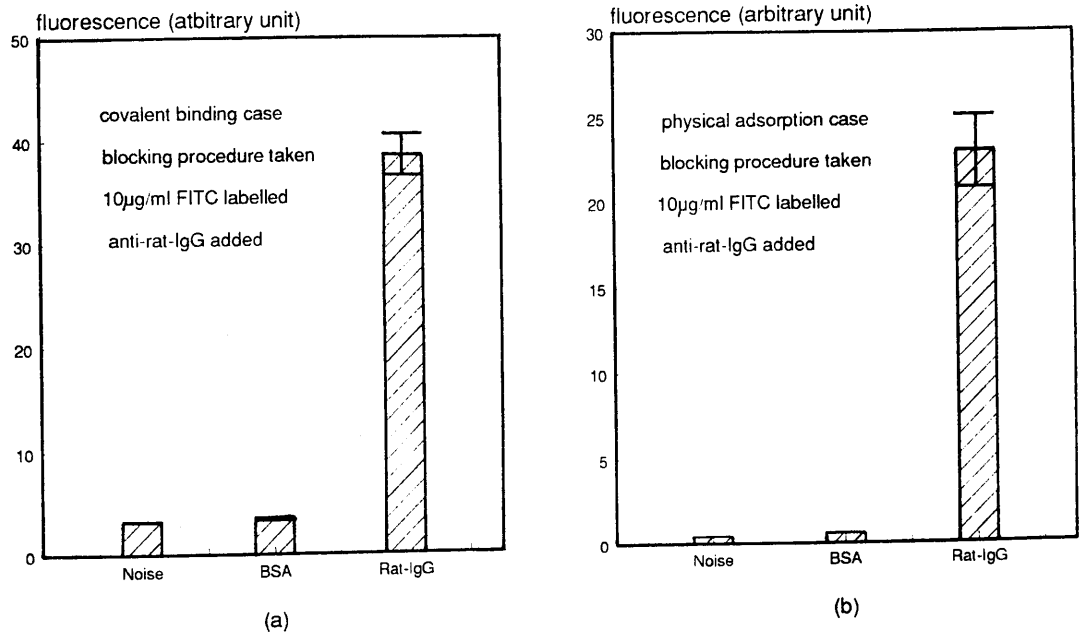

Fig.6.5.3 Blocking of non-specific binding in the case of,
(a) covalent immobilisation and (b) physical adsorption

Fig.6.5.3(a) shows the results of a conventional fluorescence immunoassay conducted on a covalent binding slide when skimmed milk powder is used as the blocking agent. For the purpose of comparison, the same results for the case of a physical adsorption slide is also included (Fig.6.5.3(b)). In the experiment, rat-IgG (0.1mg/ml) is first immobilised onto one half of the slide surface. After rinsing the slide under running RO water, a milk powder solution at the concentration of 10mg/ml in 0.01M PBS (pH 7.2), which has been filtered through a filter paper, is applied to the whole slide surface for 20 minutes. The slide is then rinsed with RO

water and blown dry. Subsequently, FITC– anti– rat– IgG (10μg/ml) is applied to both halves of the slide surface for 30 minutes. After a washing step, the amount of FITC– anti– rat– IgG bound to both halves of the slide surface as well as noise from a clean area of the slide are measured using the experimental set– up as shown in Fig.6.4.1.

From the results, it can be concluded that non– specific binding has indeed be efficiently blocked because the non– specific binding signal is only slightly stronger than the background noise. In addition, the blocking procedure has not significantly interfered with the antibody– antigen reaction since the specific binding signal is only slightly reduced with respect to the case where no blocking is performed (Fig.6.5.1). In fact, the ratio of specific binding to non– specific binding signal in the case of covalent binding has been increased from about 4 to about 11. For the case of physical adsorption, this ratio is increased from about 39 to about 43. Taking into consideration that the non– specific binding in the case of the covalent binding slide is almost the same as the background noise, it can be concluded that the relatively low ratio of specific binding to non– specific binding is attributable to the inherent background noise introduced by treating the slide with amino– silane and glutaraldehyde.

Therefore, although covalent binding results in a higher loading of protein with a more uniform distribution of the protein on the glass slide surface than physical adsorption, unless the inherent background noise can be eliminated in some way, it is not necessary better than physical adsorption if a high sensitivity of the immunoassay is required.

6.5.3 Conventional fluorescence immunoassays

The experimental results discussed in the above section show that conventional fluorescence immunoassays can be successfully performed for both a covalent binding slide and a physical adsorption slide, and that blocking of non– specific binding does increase the ratio of specific binding to non– specific binding. Since the success of an evanescent fluorescence immunoassay depends, to a great extent, on the success of its corresponding conventional fluorescence immunoassays, as a guide, it is helpful to find out the response curve of immunofluorescence as a function of the antibody concentration in conventional fluorescence immunoassays. In addition, it is also helpful to investigate the sensitivity of these immunoassays so that the sensitivity range of the

appropriate evanescent fluorescence immunoassays can be predicted.

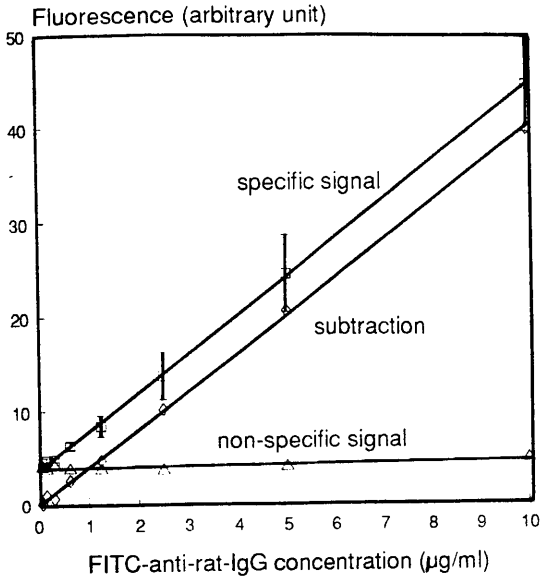

(a), conventional immunoassay
on a covalent binding slide

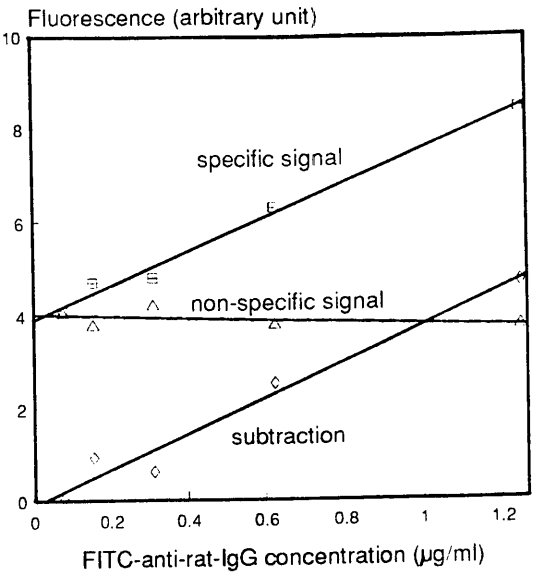

(b), enlargement of (a) at
low antibody concentrations

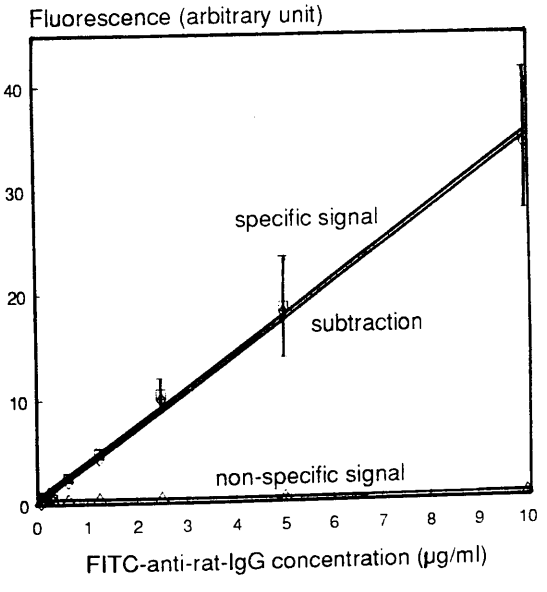

(c), conventional immunoassay
on a physical adsorption slide

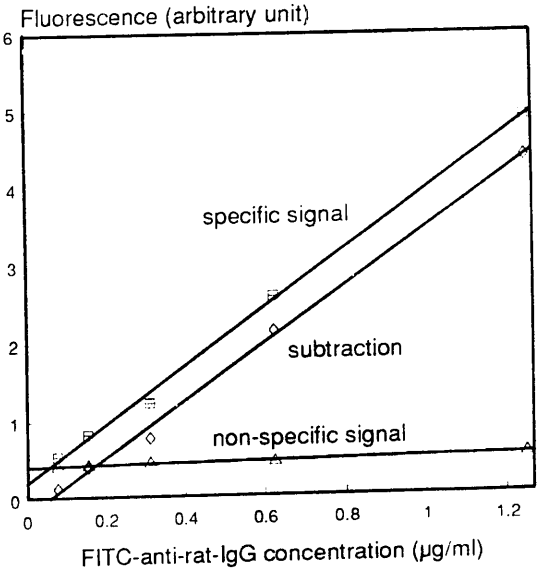

(d), enlargement of (c) at
low antibody concentrations

Fig.6.5.4 Response curves of conventional fluorescence immunoassays conducted on (a and b) the covalent binding slide and (c and d) the physical adsorption slide

Fig.6.5.4 shows the response curves of conventional fluorescence immunoassays conducted on both a covalent binding slide and a physical adsorption slide. The

experiments carried out are identical to those described in section 6.5.2 for Fig.6.5.3, with the exception that the concentration of the added FITC– anti– rat– IgG solution is now varied and the measured fluorescence intensities are drawn as a function of the antibody concentration. Since non– specific binding can be accounted for by means of the differential method as discussed in chapter 5, the response curve of non– specific binding from the control area and the differential response curve which is obtained by subtracting the non– specific fluorescence from the specific fluorescence are all included. In order to show the response curves more clearly at low antibody concentrations, enlarged diagrams (b) and (d) are also given.

It can be seen that the linearity of the measured specific fluorescence intensities with respect to the added FITC– antibody concentration is quite good in both the covalent binding case and the physical adsorption case. Therefore, the linear approximation of equation (6.3.6) is valid in this case. However, in spite of the fact that at any fixed antibody concentration, the measured specific fluorescence is always stronger in the case of covalent binding than in the case of physical adsorption, due to the relatively high intrinsic background fluorescence of the covalent binding slide, the sensitivity of the physical adsorption slide is higher than that of the covalent binding slide. In fact, if the point at which the signal to noise ratio is 1.5 is taken as the detection limit of the system, for covalent binding slides, the detection limit is at 0.6μg/ml whereas for physical adsorption slides, the limit is at 0.1μg/ml.

6.6 Summary and discussion

The fact that an antibody can bind to its appropriate antigen in a highly specific way and that a large number of biologically interesting macromolecules can serve as antigens makes antibody– antigen binding a very useful tool for the determination of low concentrations of a species of molecules in a complex matrix.

An optical evanescent wave immunosensor operates on the same principle as that of a solid phase fluoroimmunoassay. Two key issues which must be dealt with in solid phase fluoroimmunoassays are 1) efficient immobilisation of antibodies (or antigens) on the solid phase and 2) efficient blocking of non– specific binding sites on the solid phase. Physical adsorption and covalent binding are two relatively simple immobilisation techniques and are proved successful for the immobilisation of proteins onto glass surface. A comparison of the two immobilisation methods reveal that covalent binding produces a layer of protein which is more uniform and has a higher

packing density than physical adsorption.

However, covalent binding also induces more non-specific binding than physical adsorption. It is found that this non-specific binding is mainly caused by free covalent immobilisation binding sites and can be greatly reduced by treating the glass surface, after the immobilisation procedure, with a blocking agent such as skimmed milk powder at relatively high concentrations. Experiments show that this treatment hardly influences the antibody-antigen binding. During the investigation, it is also found that treating a glass slide with amino-silane and glutaraldehyde introduces an intrinsic background noise which is about 10 times the background noise of the slide treated with repel coat (dichlorodimethylsilane). Although adding a blocking procedure can greatly reduce non-specific binding, the intrinsic background noise introduced by either amino-silane or glutaraldehyde prevents covalent binding slides from reaching a higher sensitivity than physical adsorption slides.

The experimental proof that proteins can be successfully immobilised onto glass surfaces, that non-specific binding can be greatly reduced with a blocking procedure and that conventional fluorescence immunoassays can be successfully performed paves the way for a successful evanescent wave immunoassay to be conducted. The experimental design and results of several such assays become the main subject of the next chapter.

CHAPTER 7 EVANESCENT FLUORESCENCE IMMUNOASSAYS, DISCUSSION OF THE RESULTS AND FUTURE WORK

7.1 Introduction

Now that patterned waveguides have been successfully fabricated with characteristics desirable for evanescent fluorescent immunoassays, and that conventional immunoassays have been successfully conducted, the next important step is obviously to investigate the performance of the sensing element when it is applied to evanescent fluorescence immunoassays.

As pointed out in the first chapter, a problem many optical immunosensing devices have is the poor discrimination between specific and non-specific binding. The problem, however, can be overcome by means of the differential method which can be easily achieved with a patterned waveguide (chapter 5). To achieve this, one only needs to immobilise control proteins in one of the etched wells and the evanescently excited fluorescence from that well will act as the control signal. The differential signal is then obtained by subtracting the control signal from the specific signal. Although this principle is simple and has been frequently used in many areas, to the author's knowledge, it was not applied to evanescent wave immunoassays until the idea of patterned waveguides was put forward (Zhou et al. 1990, 1991a/b/c/d/ and 1992).

An interesting and attractive aspect in the development of a versatile immunosensor is the simultaneous detection of different antibodies (or antigens) using the same sensing element. As pointed out by Hlady et al. (1990), this can be achieved by immobilising different antibodies (or antigens) on spatially separated areas of a transducing element and detecting the responses from each area. Although Hlady et al. (1990) demonstrated the principle of operation of multichannel evanescent wave immunosensing, in their system, a prism was used for the generation of an evanescent wave and a beam from a xenon-mercury lamp, which was first expanded, was used to illuminate the base of the prism to excite a relatively large area which included three protein immobilised spots. A patterned waveguide is almost ideal for multichannel (or multi-analyte) immunosensing because the different antigens (or antibodies) need only be immobilised respectively in individual wells. Since every well has been made identical and has been well separated spatially, when a beam of

guided excitation light propagates along the patterned waveguide, each well will be almost equally evanescently illuminated, assuming that the propagation loss of the excitation light is negligible. Specific binding of the applied fluorescently– labelled analytes to one of the immobilised biocomponents will obviously cause the gathering of fluorescent molecules near the surface of that well. As a result, the evanescently excited fluorescence from that well will be the strongest.

In this chapter, the design of the differential and multichannel immunoassays is described and the experimental results and the sensitivity of the system are discussed.

7.2 Experimental procedures for the multichannel and differential immunoassays

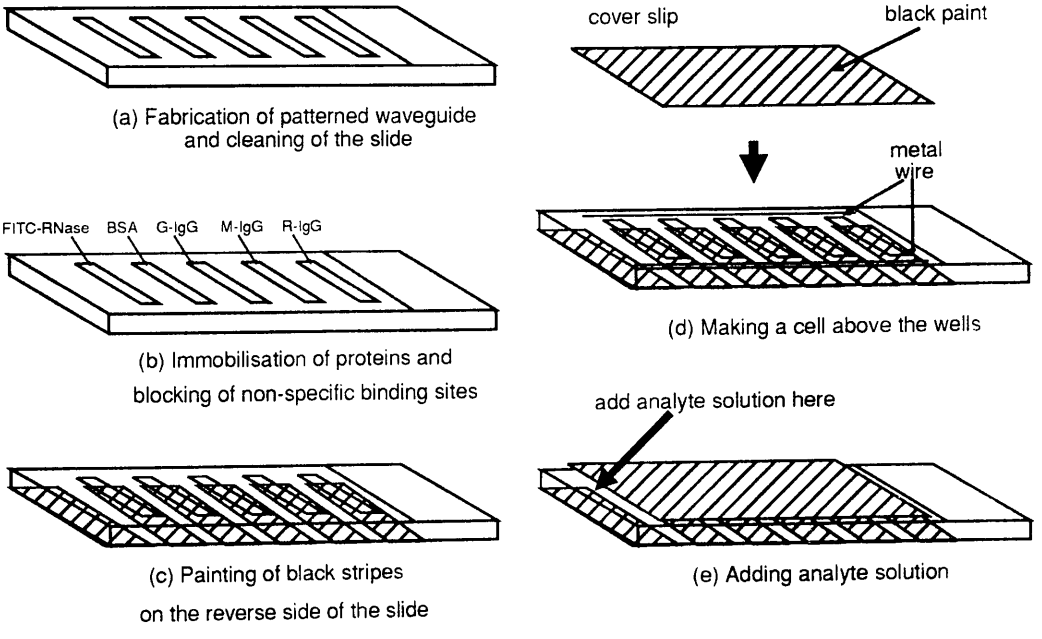

Fig.7.2.1 Experimental procedures for preparing the sensing element and adding the analyte solution

Referring to Fig.7.2.1, the differential and multichannel immunoassay is conducted as follows. As a first step, patterned waveguides with a number of etched wells (typically 6) are fabricated as described in chapter 4. The ion–exchange time and temperature for both processes are 30 min. and 490 °C respectively. An etching time of 165 sec. in 4:1 HF is chosen for the wells. After cleaning the waveguide slide with sulphuric acid (chapter 4), three different antigens, i.e. goat IgG, mouse IgG and rat IgG, the control protein BSA, and FITC labelled RNases are each covalently immobilised in one of the etched wells (chapter 6). The concentration of

all these protein solutions are at 0.1mg/ml (in 0.01M PBS). Covalent immobilisation is used here because it gives a more predictable loading of proteins onto the surface of each well than physical adsorption. The reason for immobilising FITC labelled RNases in one of the wells is to monitor the strength of the evanescent field so that the variation in the evanescent field for each measurement can be taken into account or alternatively, the strength of the evanescent field can be kept roughly the same by adjusting the laser output power. FITC–RNases are used simply because of their availability and their irrelevance to antibody–antigen binding. It ought to be pointed out that in immobilising different antigens into different individual wells, care should be taken not to let any two antigen solutions mix. In addition, in rinsing each solution off the slide, a small stream of RO water should be used and each well should be rinsed in turn to prevent one solution from getting into the adjacent wells.

Blocking of the unoccupied immobilisation binding sites is achieved using concentrated skimmed milk powder solution (chapter 6).

In order to absorb substrate guided excitation light and meanwhile leave windows for the well regions so that the evanescently excited fluorescent light can be detected from below, stripes of light–absorbing black paint are drawn on the reverse side of the waveguide slides (Fig.7.2.1(c)). A cell is then formed above the etched wells. Two spacers of metal wire (about 50mm in length and 0.18mm in diameter) are placed along the well side of the slide and a cover slip (22×50mm) with its upper surface also painted black is placed on the two wire spacers. The black paint on the upper surface of the coverslip also acts as a light–absorbing layer so that most of the light (of either fluorescent or excitation nature) trapped within the cell region is absorbed and meanwhile any ambient light is prevented by this black paint layer from getting into the photomultiplier. From the author's experience, this also plays a significant role in reducing the background noise.

The waveguide slide prepared to this stage is now ready for a direct wash–free immunoassay. A solution of either FITC labelled anti–rat–IgG or FITC labelled anti–goat–IgG at various concentrations is applied to the front inlet of the cell. Due to the capillary effect, the solution will be drawn automatically into the cell and fill the cell space if the amount applied is sufficient.

Fig.7.2.2 shows the ideal case where FITC–anti–rat–IgG solution is added. Owing to the specificity of antibody–antigen reaction, only in the rat–IgG

immobilised well are a relatively large amount of FITC–anti–rat–IgG molecules bound close to the well surface. As a result, the evanescently excited fluorescence from this well will be stronger than those from the other antigen immobilised wells although the unbound FITC labelled antibodies are not washed away.

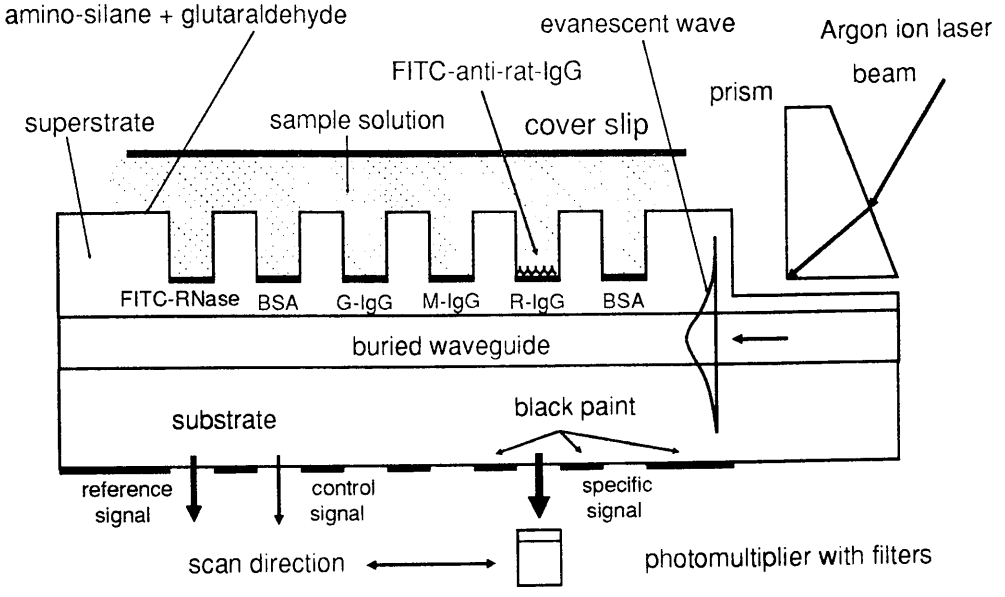

Fig.7.2.2 Schematic illustration of the sensor when FITC–anti–rat–IgG solution is added

Fig.7.2.3 shows the experimental set–up for the measurement of the evanescently excited fluorescence. After some incubation time (usually chosen to be more than 30 minutes so that the antibody–antigen reaction has almost reached its equilibrium), the patterned waveguide is mounted under an input coupling prism fixed on a rotation table as shown in Fig.4.3.1. The 488nm light beam from a small Ar^+ laser (Cathodeon Model C870, Cathodeon Limited) is passed through a chopper, reflected by a mirror and directed to the input coupling prism. As the waveguide is completely buried, the prism is placed on the etched end of the slide so that tunnelling of the evanescent wave generated at the prism base into the waveguide can take place. The rotation table is turned until strong input coupling of the excitation light is reached. This, as pointed out in chapter 4, is judged by the light field patterned emitted from the front end of the waveguide.

A photomultiplier is placed below the waveguide slide and scans along the slide so that the evanescently excited fluorescence from each of the wells can be measured. In order to reduce interference between wells, in front of the

photomultiplier are placed a vertical slit (2mm wide), an interference longpass filter (λ_{cut-on}= 520nm), a colour glass long-pass filter (OG-515) and another vertical slit (2mm wide). The laser beam is chopped at a frequency of about 250Hz. To minimise the effect of fluorescence fading (Kaufman et al. 1971; Schauenstein et al. 1982), the chopper is made in such a way that the opened slit is only a fraction of the width of the blocked region (see Fig.7.2.3). The detected signal is sent to a lock-in amplifier and analysed.

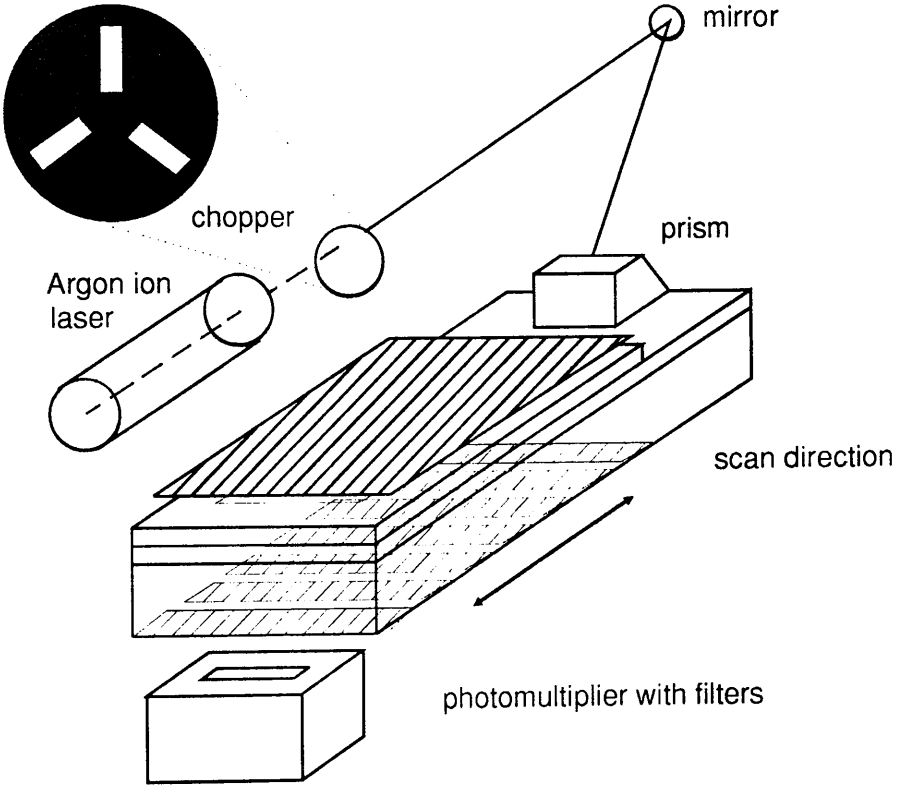

Fig.7.2.3 Experimental set-up for the evanescent fluorescence immunoassay

7.3 The wash-free immunoassay results and discussions

Fig.7.3.1 shows the measured relative evanescent fluorescence when FITC-anti-rat-IgG and FITC-anti-goat-IgG at various concentrations are added respectively into the cell. Before a full discussion of the results, it should be pointed out that the fluorescence intensity is dependent on a number of factors including the excitation light intensity, the excitation time duration (i.e. fluorescence fading), the freshness of antibodies and antigens and the incubation conditions for both the immobilisation of the first layer antigens and the later antibody-antigen reactions. In order to reduce variations among each measurement, attempts have been made to

perform the experiments in a batch mode by treating a number of slides (typically 7) simultaneously whenever possible (e.g. at the ion– exchange and incubation stages). In addition, by adjusting the laser output power, the reference signal which comes from the FITC– RNase immobilised well is kept as constant as possible so that the excitation light intensity at the well surface is roughly the same for each measurement. Effects introduced by the attenuation of the guided excitation light have been ignored.

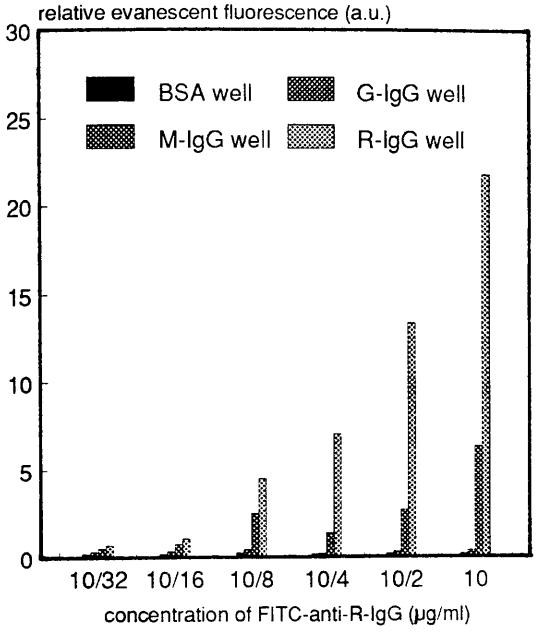

Fig.7.3.1(a) Response when FITC-anti-R IgG at various concentrations is added

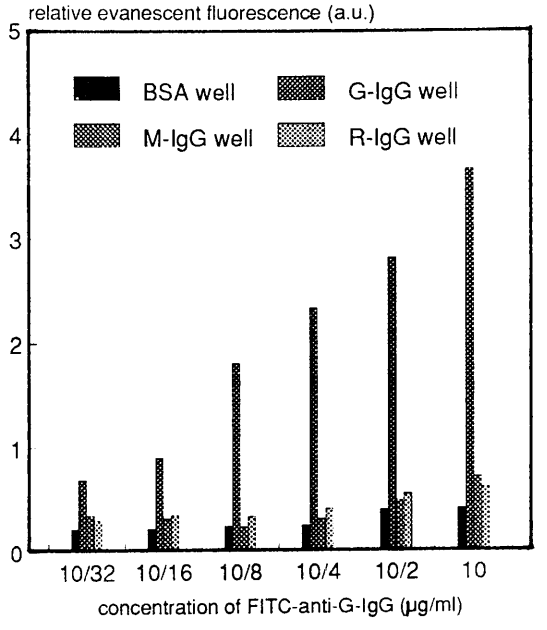

Fig.7.3.1(b) Response when FITC-anti-G IgG at various concentrations is added

Fig.7.3.1 Wash– free multichannel immunoassay results

In the figures, the vertical axis is the relative evanescent fluorescence defined as the evanescently excited fluorescence intensity, I_f, divided by the reference fluorescence intensity, I_r, which comes from the FITC– RNase immobilised well. Only averaged values are given. The horizontal axis lists the immobilised antigens and the control protein BSA. The responses at different concentrations are represented by different groups of the response bars.

As can be seen from Fig.7.3.1(a), when FITC– anti– rat– IgG solution within the indicated concentration range is added, the binding of the applied FITC– anti– rat– IgG with the immobilised rat– IgG is always the strongest compared to its binding with the other immobilised antigens and the control protein BSA. This experimental fact proves that wash– free differential immunoassays can indeed be

performed using the ion–exchanged patterned waveguide. From Fig.7.3.1(b), it can be seen that when FITC–anti–goat–IgG solution is added, the evanescently excited fluorescence from the goat–IgG immobilised well is the strongest. Taking into account that every waveguide slide has been treated in the the same way, this shows that a single waveguide slide can be used to sense different antibodies simultaneously. In other words, a wash–free multichannel or multi–analyte immunoassay has been successfully demonstrated.

In chapter 6, it has been pointed out that monoclonal antibodies are more specific than polyclonal antibodies. Note that the FITC–anti–rat–IgG is polyclonal and the FITC–anti–goat–IgG is monoclonal. Although there is a clear difference between specific binding and non–specific binding, a slightly closer examination of Fig.7.3.1(a) reveals that there is always a relatively strong binding of the FITC–anti–rat–IgG to the immobilised mouse–IgG. This, in fact, proves that the performance of the sensor is quite good because the primary structures of rat and mouse IgG molecules are highly homologous. It is therefore unsurprising that some degree of cross–reactivity (i.e. binding of anti–rat–IgG to mouse–IgG) should be observed when a heterologous polyclonal antiserum which has not been affinity–purified is used as a detecting reagent as in the case here.

On the other hand, when monoclonal FITC–anti–goat–IgG is added (Fig.7.3.1(b), while the strongest binding always occurs between the specific antibody–antigen combination, the binding of anti–goat–IgG to the other non–specific antigens is always relatively weak compared with the polyclonal antibody case. This confirms that monoclonal antibodies are indeed more selective than polyclonal antibodies.

The differential responses of the sensor at various concentrations of the added antibody solution can be more clearly shown by drawing a differential response curve as shown in Fig.7.3.2. The vertical axis is the differential evanescent fluorescence defined as $F_d = (I_x - I_B)/I_r$, where I_x is the evanescently excited fluorescence from an antigen immobilised well and the antigen x can be R–IgG, M–IgG or G–IgG; I_B is the evanescently excited fluorescence from the BSA immobilised (i.e. control) well and I_r is the evanescent fluorescence from the FITC–RNase immobilised well. The horizontal axis shows the concentration of the added FITC–antibody solution. The error bars are derived from the root mean square error of a number of measurements (typically five) for the same slide. It is clear that at low concentrations

(<5μg/ml), the specific differential evanescent fluorescence is roughly proportional to the analyte concentration. With further increase in the analyte concentration, a saturation trend (especially in case (b)) is observed. Both the linear proportionality and the saturation trend are in agreement with the theory on solid phase immunoassays as discussed in chapter 6.

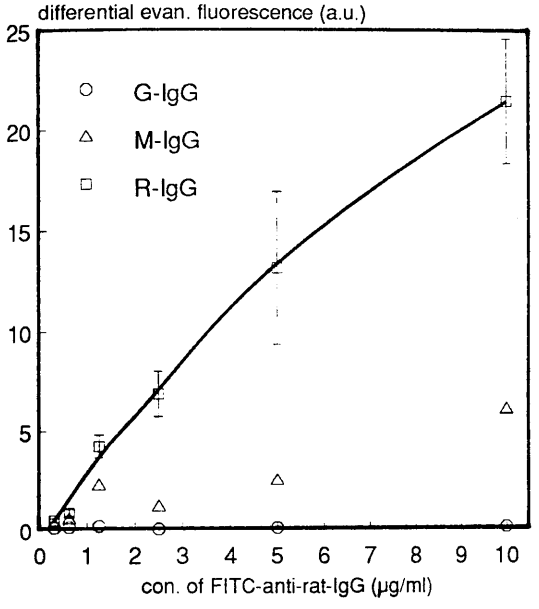

Fig.7.3.2(a) Differential response curve when FITC-anti-rat-IgG at various concentrations is added

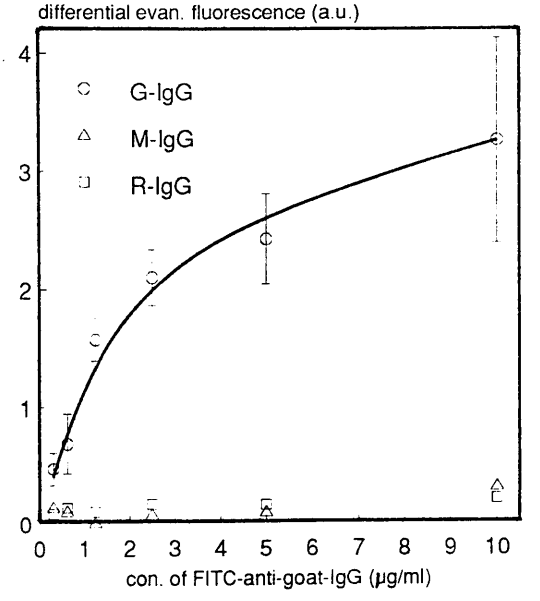

Fig.7.3.2(b) Differential response curve when FITC-anti-goat-IgG at various concentrations is added

Fig.7.3.2 Differential response curves of the multichannel immunoassay

When evanescent fluorescence intensity is considered, it is experimentally obvious that polyclonal antibodies give higher fluorescence signals than monoclonal antibodies. Polyclonal antisera contain many antibodies directed against multiple different epitopes (or antigenic determinants) on the target, while a monoclonal antibody recognises a single epitope on a given antigen. Therefore, use of polyclonal reagents allows multiple antibodies to bind to the target antigen, giving an amplification of the signal, while a monoclonal antibody can bind to a given antigen only at one site; that is, at the epitope for which it is specific.

When the resolution limit of the immunoassays is considered, it can be seen from the results that for both the polyclonal FITC–anti–rat–IgG solution and the monoclonal FITC–anti–goat–IgG solution, at the concentration of about 0.3μg/ml, the specific signal is still at least twice as strong as the control signal. This indicates that the resolution limit is around 0.3μg/ml. It should be noted that the sensitivity of

a wash–free evanescent fluorescence immunoassay will be limited by that of a corresponding conventional fluorescence immunoassay (chapter 5). Considering that covalent immobilisation is adopted here which means a relatively high background noise level and that the corresponding conventional fluorescence immunoassay for FITC–anti–rat–IgG in the case of covalent immobilisation has a sensitivity at the concentration level of 0.5μg/ml (chapter 6), the wash–free immunoassay result, in term of its sensitivity, is most encouraging.

7.4 Further work

From the immunoassay results, it can be seen the major problem for the sensor is that the sensitivity is still not high enough for real practical use. This, as has been pointed out, is caused by the high background noise which is associated with conventional fluorescence immunoassays. The author strongly believes that the sensitivity can be substantially increased by the method of time–resolved fluorescence immunoassay. As has already been described in chapter 6, this immunoassay method involves the use of long–lived (10 to 1000μs) fluorescent probes. The autofluorescence of most organic molecules has short decay lifetimes (of the order of 10ns). By exciting fluorescence with a short pulse of laser light and detecting the excited fluorescence after the autofluorescence has completely decayed, the noise from such autofluorescence can be completely eliminated. The only limiting background fluorescence measured will be due to non–specific binding of the labelled reagents used. It has been shown that time–resolved fluorescence immunoassay can have a sensitivity which is of the same order as or even higher than that of radio and enzyme immunoassays (Soini and Lövgren 1988).

It should be noted that all the assays conducted here are direct fluorescence immunoassays in which the antibodies sensed are fluorescently labelled. However, this does not at all mean that wash–free indirect immunoassays cannot be conducted. To perform a real immunoassay in which the analyte is not labelled, the method of sandwich immunoassay can be employed. Fluorescently labelled second antibodies which are specific to the analyte can be loosely attached to the lower side of the cover slip (see Fig.7.2.2). Upon addition of the sample solution, these fluorescently labelled antibodies detach from the cover slip, diffuse in the solution within the cell and bind to the analyte. As a result, the analyte molecule will be sandwiched between the immobilised antibody or antigen and a number of fluorescently labelled second antibodies. In fact, the sandwich method should result in a higher sensitivity

than the direct immunoassay method as more fluorescent probes can be linked to a single immobilised antibody or antigen.

It is obvious that the coupling of light into the waveguide using an input coupling prism is not convenient. To simplify the procedure, gratings can be fabricated on the waveguide slide. In this case, the excitation laser beam is illuminated onto the grating and if the angle of incidence is right, it will be coupled into the waveguide.

Another area which is worth investigation is the dynamic behaviour of the sensor as all the experiments done so far are for the equilibrium case. It has been mentioned that rapidity is one of the essential requirements for a disposable wash–free immunosensor. Although the response time for an antibody–antigen reaction to reach its equilibrium will most likely be determined by the reaction itself and will usually be from a few minutes to 30 minutes, there is the possibility that the information on the concentration of an antibody solution can be obtained within a much shorter time if the rate of change measurement method is employed (Eddowes 1987/88).

7.5 Conclusion

The author has demonstrated the principle of operation of a novel optical evanescent wave immunosensor. The sensing element is a K^+ and Na^+–exchanged patterned waveguide. To the author's knowledge, this is the first time that such a patterned waveguide has been successfully fabricated and applied to wash–free multi–analyte immunoassays. Because of the evanescent nature, the low cost of waveguide fabrication and the pattern feature, the device greatly favours the concept of a disposable, wash–free immunosensor.

Ion–exchange conditions for fabricating completely buried waveguides in glass using purely thermal K^+ and Na^+–exchange processes have been experimentally determined. Within such an appropriate range of the ion–exchange temperature and time, the two problems frequently encountered in burying K^+–exchanged surface waveguide, i.e., partial burial of the surface waveguide and microcracking of the guide layer, have been solved. The refractive index profiles of both surface and buried planar waveguides have been determined by solving the one–dimensional diffusion equation with of aid of the inverse WKB method. Furthermore, the refractive index profiles have been obtained directly by observing the interference

fringes of a sliced piece of planar waveguide with the aid of a Mach–Zehnder transmitted–light interference microscope. It should be noted that due to the very small refractive index change associated with K^+–exchanged waveguides, to the author's knowledge, no report of direct observation of such index profiles has been made before. In addition to the application of the patterned waveguide to evanescent wave immunosensing, the success in burying K^+–exchanged surface waveugide completely implies that surface scattering can be greatly reduced. Therefore, the propagation loss of such a buried waveguide is much lower than that of a surface waveguide.

A mathematical model has been established to explain the working principle of an evanescent fluorescence immunosensor. It has been shown that the evanescently excited fluorescence intensity can be substantially increased by matching the refractive index of the cover medium with that of the substrate. The sources of noise associated with an evanescent fluorescence immunoassay have been analysed. The author has found that substrate guided excitation light contributes a significant amount of background noise and that by adding a light absorption layer, the background noise can be greatly reduced. It is shown that by employing the method of differential measurement, the influence on the signal by noise can, in principle, be reduced. The author therefore suggests that an evanescent fluorescence immunosensor should always have an internal reference channel.

In the investigation of protein immobilisation, a comparison has been made between covalent immobilisation and physical adsorption. Covalent immobilisation is found to produce a more uniform layer of protein on the glass surface with higher loading of protein than physical adsorption. However, covalent immobilisation also introduces more non–specific binding and more background fluorescence. While the relatively strong non–specific binding can be greatly reduced by blocking the covalent immobilisation binding sites with concentrated BSA or milk powder solution, the relatively high background fluorescence is found to be related to the covalent coupling (or linking) agent (amino–silane and/or glutaraldehyde). Therefore, this background fluorescence can not be removed in a simple way unless a time–resolved fluorescence immunoassay method is adopted.

Using a number of channels which can be easily provided on a patterned waveguide, wash–free multi–analyte immunoassays with internal reference and internal monitoring of the excitation light intensity have been successfully performed.

Preliminary experimental results show that the selectivity, the sensitivity and the response curves of the device are all encouraging. In spite of the fact that the sensitivity is still not high enough for practical diagnostical testing, the time-resolved fluorescence immunoassay method holds a bright prospect for the solution of the problem. Considering that direct immunoassay for analytes not labelled with fluorescent probes can be performed by the method of sandwich immunoassay and that light coupling into the waveguide can be much simplified by grating coupling instead of prism coupling, the future of the device looks very promising.

REFERENCES

Adams, M.J. (1981) *An Introduction to Optical Waveguides*, John Wiley & Sons, New York, pp. 90–134

Albert, J. and Yip, G.L. (1985) "Refractive–index profiles of planar waveguides made by ion–exchange in glass" *Appl. Opt.* 24 3692–3693

Albert, J. and Yip, G.L. (1987) "Stress–induced index change for $K^+ - Na^+$ ion exchange in glass" *Electron. Lett.* 23 737–738

Alberts, B., Bray, D., Lewis J., Raff, M., Roberts, K. and Watson, J.D. (1983) *Molecular Biology Of The Cell*, Garland Publishing Inc., London, pp. 951–1012

Andrade, J.D. and Van Wagenen, R.A. (1983). US Patent 4,368,047

Andrade, J.D., Van Wagenen, R.A., Gregonis, D.E., Newby, K. and Lin, J.–N. (1985) "Remote Fiber–Optic Biosensors Based on Evanescent–Excited Fluoro–Immunoassay: Concept and Progress" *IEEE Trans. on Electron Devices* ED–32 1175–1179

Attridge, J.W., Daniels, P.B., Deacon, J.K., Robinson, G.A. and Davidson, G.J. (1990) "Sensitivity enhancement of optical immunosensors by the use of surface plasmon resonance and fluorescence" *Biosensors '90, The first world congress on biosensors, 2–4 May 1990, Singapore,* Elsevier Science Publishers Ltd., England, pp. 55–56

Azzam, R.M.A., Rigby, P.G. and Krueger, J.A. (1977) "Kinetics of protein adsorption and immunological reaction at a liquid/solid interface by ellipsometry" *Phys. Med. Biol.* 22 422–430

Badley, R.A., Drake, R.A.L., Shanks, I.A., Smith, A.M. and Stephenson, P.R. (1987) "Optical biosensors for immunoassay– The Fluorescence Capillary Fill Device" *Phil. Trans. Roy. Soc. Lond.* 316 143–160

Benner, R.E., Dornhaus, R. and Chang, R.K. (1979) "Angular emission profiles of dye molecules excited by surface plasmon waves at a metal surface" *Opt. Commun.* 30 145–149

Bluestein, B.I., Walczak, I.M. and Chen, S.Y. (1990) "Fiber optic evanescent wave immunosensors for medical diagnostics" *Trends in Biotechnology* 8 161–168

Brandenburg, A. (1986) "Stresses in ion–exchanged glass waveguides" *J. Lightwave Technol.* LT–4 1580–1593

Burghardt, T.P. and Axelrod, D. (1981) "Total internal reflection/fluorescence photobleaching recovery study of serum albumin adsorption dynamics" *Biophys. J.* 33 455–468

Carniglia, C.K., Mandel, L. and K.H. Drexhage (1972) "Absorption and Emission of Evanescent Photons" *J. Opt. Soc. Am.* **62** 479–486

Carr, R.J.G., Brown, R.G.W., Rarity, J.G. and Clarke, D.J. (1987) "Laser light scattering and related techniques" *Biosensors*, Oxford Science Publications, New York, pp. 679–701

Carter, T., Dahne, C. and Place, J.F. (1982) European Patent Application EP 81–801255.0

Chiang, K.S. (1985) "Construction of refractive–index profiles of planar dielectric waveguides from the distribution of effective indexes" *J. Lightwave Technol.* LT–3 385–391

Cohen, R.J. and Benedek, G.B. (1975) "Immunoassay by light scattering spectroscopy" *Immunochem.* **12** 349–351

Cullen, T.J., Ironside, C.N., Seaton C.T. and Stegeman, G.I. (1986) "Semiconductor Doped Glass Ion–exchanged Waveguide" *Appl. Phys. Lett.* **49** 1403–1405

Cullen, D.C., Brown, R.G.W. and Lowe, C.R. (1988) "Detection of immuno–complex formation via surface plasmon resonance on gold–coated diffraction gratings" *Biosensors* 3 211–225

Cuypers, P.A., Hermans, W.T. and Hemker, H.C. (1978) "Ellipsometry as a tool to study protein films at liquid–solid interfaces" *Anal. Biochem.* **84** 56–57

Dahne, C., Sutherland, R.M., Place, J.F. and Ringrose, A.R. (1984) "Detection of antibody–antigen reactions at a glass–liquid interface: a novel fibre–optic sensor concept" *OFS'84, Proceedings of the second international conference on optical fibre sensors* (Ed. R.T. Kersten and R. Kist), VDE–Verlag, Berlin, pp. 75–79

Daniels, P.B., Deacon, J.K., Eddowes, M.J. and Pedley, D.G. (1988) "Surface plasmon resonance applied to immunosensing" *Sensors and Actuators* **15** 11–18

Deacon, J.K., Stops, J.E., Thomson. A.M., Roberts, P.R., Whiteley, S.C., Attridge, J.W., Love, C.A., Robinson, G.A. and Davidson, G.P. (1990) "An assay for human chorionic gonadotrophin using the fluorescence capillary fill immunosensor" *Biosensors '90, The first world congress on biosensors, 2–4 May 1990, Singapore,* Elsevier Science Publishers Ltd., England, pp. 57–58

Drake, R.A.L., Sawyers C.G. and Robinson G.A. (1988) European Patent Application 88300458.2

Eagen, C.F. and Weber, W.H. (1979) "Modulated surface–plasmon resonance for adsorption studies" *Phys. Rev.* **19** 5068–5082

Eddowes, M.J. (1987/88) "Direct Immunochemical Sensing: Basic Chemical Principles and Fundamental Limitations" *Biosensors* 3 1–15

Elwing, H. and Stenberg, M. (1981) "Biospecific bimolecular binding reactions–A new

ellipsometric method for their detection, quantification and characterization" *J. Immunol. Methods* **44** 343–349

Fahrenfort, J. (1961) "Attenuated total reflection. A new principle for the production of useful infra–red reflection spectra of organic compounds" *Spectrochim. Acta.* **17** 698–709

Findakly, T. (1985) "Glass waveguides by ion–exchange: a review" *Optical Engineering* **24** 244–250

Flanagan, M.T. and Pantell, R.M. (1984) "Surface plasmon resonance and immunosensors" *Electr. Lett.* **20** 968–970

Flanagan, M.T., Sloper, A.N. and Ashworth, R.H. (1988) "From electronic to opto–electronic biosensors" *Anal. Chim. Acta.* **213** 353–355

Gedeon, A (1974) "Comparison between rigorous theory and WKB–analysis of modes in graded–index waveguides" *Opt. Commun.* **12** 329–332

Gendreau, R.M., Winters, S., Leininger, R.I., Fink, D., Hassler, C.R. and Jakobsen, R.J. (1981) "Fourier–transform infrared spectroscopy of protein adsorption from whole blood: *ex–vivo* dog studies" *App. Spectr.* **35** 355–357

Gendreau, R.M., Leilinger, R.I., Winters, S. and Jakobsen, R.J. (1982) "Fourier transform infrared spectroscopy for protein–surface studies" *Biomaterials Interfacial Phenomena and Applications*, (Ed. S. L. Cooper and N. A. Peppas) Adv. Chem. Ser. **199** 371–395

Giaever, I. (1973) "The antibody–antigen reaction: A visual observation" *J. Immunol.* **110** 1424–1426

Giaever, I. (1974) "Surface physics applied to immunology" *Bull. Am. Phys. Soc.* **19** 564–564

Giaever, I. (1976a) US Patent 3,979,184

Giaever, I. (1976b) "Visual detection of carcinoembryonic antigen on surfaces" *J. Immunol.* **116** 766–771

Giaever, I., Keese, C.R. and Ryves, R.I. (1984) "A new assay for rheumatoid factor" *Clin. Chem.* **30** 880–883

Goldman M. (1968) *Fluorescent antibody methods*, Academic Press Inc., London

Gortych, J.E. and Hall, D.G. (1986) "Fabrication of planar optical waveguides by K^+–ion exchange in glass" *IEEE J. Quan. Elec.* **QE–22** 892–895

Harrick, N.J. (1965) "Electric Field Strengths at Totally Reflecting Interfaces" *J. Opt. Soc. Am.* **55** 851–857

Harrick, N.J. (1967) *Internal Reflection Spectroscopy*, Interscience, New York

Harrick, N.J. and Loeb, G.I. (1973) "Multiple internal reflection spectroscopy" *Anal. Chem.* **45** 687–691

Hemmila, I (1985) "Fluoroimmunoassays and immunofluorometric assays" *Clin. Chem.* **31** 359–370

Hirschfeld, T. (1965) "Total Reflection Fluorescence" *Can. Spectrosc.*, **10** 128–128

Hirschfeld, T. (1971). US Patent 3,604,937

Hlady, V., Lin, J.N. and Andrade, J.D. (1990) "Spatially Resolved Detection of Antibody–Antigen Reaction on Solid/Liquid Interface using Total Internal Reflection Excited Antigen Fluorescence and Charged–Coupled Device Detection" *Biosensors & Bioelectronics* **5** 291–301

Izawa, T. and Nakogome, H. (1972) "Optical waveguides by electrically induced migration of ions in glass plates" *Appl. Phys. Lett.* **21** 584–586

Jonsson, U., Malmqvist, M. and Ronnberg, I. (1985) "Immobilization of immunoglobulins on silica surfaces" *Biochem. J.*, **227** 373–378

Kaufman, G.I., Nester, J.F. and Wasserman, D.E. (1971) "An experimental study of lasers as excitation sources for automated fluorescent antibody instrumentation" *J. of Histochemistry and Cytochemistry* **19** 469–476

Kronick, M.N. and Little, W.A. (1973) "A new fluorescent Immunoassay" *Bull. Am. Phys. Soc.* **18** 782–782

Kronick, M.N. and Little, W.A. (1975) "A new immunoassay based on fluorescence excitation by internal reflection spectroscopy" *J. Immunol. Methods* **8** 235–242

Kronick, M.N. (1988) "Phycobiliproteins as labels in immunoassay" *Nonisotopic Immunoassay* (Ed. T.T. Ngo), Plenum Press, London, pp. 163–185

Lee, El–H., Benner, R.E., Fenn, J.B. and Chang, R.K. (1979) "Angular distribution of fluorescence from liquids and monodispersed spheres by evanescent wave excitation" *Appl. Opt.* **18** 862–868

Liedberg, B., Nylander, C. and Lundström, I. (1983) "Surface plasmon resonance for gas detection and biosensing" *Senosrs & Actuators* **4** 299–304

Lok, B.K., Cheng, Y.–L. and Robertson, C.R. (1983a) "Total internal reflection fluorescence: A technique for examining interaction of macromolecules with solid surfaces" *J. Coll. Interf. Sci.* **91** 87–103

Lok, B.K., Cheng, Y.–L. and Robertson, C.R. (1983b) "Protein adsorption on cross–linked polydimethylsiloxine using total reflection fluorescence" *J. Coll. Interf. Sci.* **91** 104–106

Lukosz, W and Tiefenthaler, K. (1983) "Embossing technique for fabricating integrated optical components in hard inorganic waveguiding materials" *Opt. Lett.* **8** 537–539

Lukosz, W. and Tiefenthaler, K. (1988) "Sensitivity of integrated optical grating and prism couplers as (bio)–chemical sensors, *Sensors and Actuators* **15** 273–284

Lukosz, W., Nellen, Ph.M., Stamm, C.H. and Weiss, P. (1990a) "Output Grating Couplers on Planar Waveguides as Integrated Optical Chemical Sensors" *Sensors and Actuators,* B1 585–588

Lukosz, W., Clerc, D., Nellen, Ph.M., Stamm, Ch. and Weiss, P. (1990b) "Output–Grating–Couplers on Planar Optical Waveguides as Direct ImmunoSensors and –Assays" *Biosensors '90, The first world congress on biosensors, 2–4 May 1990, Singapore,* Elsevier Science Publishers Ltd., England, pp. 245–246

Lundström, I. (1983) "Surface physics and biological phenomena" *Phys. Scrip.* T4 5–13

Mandenius, C. F. and Mosbach, K. (1988) "Detection of biospecific interactions using amplified ellipsometry" *Anal. Biochem.* 170 68–72

Marcuse D. (1974) *Theory of dielectric optical waveguides*, Academic Press, London

Mathot, C. and Rothen, A. (1965) "Immunological electro adsorption method as applied in the case of mice leukaemia" *Nature* 207 1263–1264

Mathot, C., D'Alessandro, P.A., Scher, S. and Rothen, A. (1967) "The immune response of golden hamsters to *leishmania donovani* as tested by immunoelectroadsorption" *Am. J. Trop. Med. Hyg.* 16 443–446

McCourt, M., Rimet, R. and Nissim, C. (1987) "Multiplexing characteristics of K^+ and Ag^+ ion–exchanged directional couplers" *EFOC/LAN 87, The Fifth Annual European Fibre Optic Communications & Local Area Networks Exposition, Proceedings, 3–5 June 1987, Basel, Switzerland,* pp. 111–114

Miller, J.N. (1990) "Immunoassay: the ideal trace organic analysis method" *Phil. Trans. R. Soc. Lond.* A333 71–83

Milliou, A., Zhenguang, H., Cheng, H.C., Srivastava, R. and Ramaswamy, R.V. (1989) "Fiber–Compatible $K^+ - Na^+$ Ion–exchanged Channel Waveguides: Fabrication and Characterization" *IEEE J. Quan. Elec.* 25 1889–1897

Molloy, J.O. (1975) *Practical Experiments In Life Sciences*, MSE Scientific Instruments, United Kingdom.

Nairn, R.C. (1976) *Fluorescent protein tracing* (fourth edition), Longman group limited, Edinburgh

Nellen, Ph. M., Tiefenthaler, K. and Lukosz, W. (1988) "Integrated optical input grating couplers as biochemical sensors" *Sensors and Actuators* 15 285–295

Nellen, Ph.M. and Lukosz, W. (1990) "Integrated Optical Input Grating Couplers as Chemo– and Immunosensors" *Sensors and Actuators,* B1 592–596

Newby, K., Reichert, W.M., Andrade, J.D. and Benner, R.E. (1984) "Remote spectroscopic sensing of chemical adsorption using a single multimode optical

fiber" *Appl. Opt.* 23 1812–1815

Nylander, C., Leidberg, B. and Lind, T. (1982/83) "Gas detection by means of surface plasmon resonance" *Sensors and Actuators* 3 79–88

Ockman, N. (1978) "The antibody–antigen interaction at an aqueous–solid interface: a study by means of polarized infrared ATR spectroscopy" *Biopolymers* 17 1273–1284

Parry, R.P., Love, C.A. and Robinson, G.A. (1990) "Detection of Rubella antibody using an optical immunosensor" *J. Virol. Methods* 27 39–48

Place, J. F., Sutherland, R. M. and Dähne, C.; (1985) "Opto–Electronic Immunosensors: A Review of Optical Immunoassay at Continuous Surfaces" *Biosensors* 1 321–353

Pockrand, I., Swalen, J.D., Gordon, I. and Philpott, M.R. (1977) "Surface plasmon spectroscopy of organic monolayer assemblies" *Surf. Sci.* 74 237–244

Poste, G. and Moss, C. (1972) "Antigen–antibody reactions in thin films" *The Study of Surface Reactions in Biological Systems by Ellipsometry*, Pergamon Press, New York, 206–231

Price, C. P., Spencer, K. and Whicher, J. (1983) "Light scattering immunoassay of specific proteins: a review" *Ann. Clin. Biochem.* 20 1–14

Ramaswamy, R.V. and Iraj Najafi, S. (1986) "Planar, buried, ion–exchanged glass waveguides: diffusion characteristics" *IEEE J. Quan. Elec.* QE–22 883–891

Ramaswamy, R.V. and Srivastava, R. (1988) "Ion–exchanged glass waveguides: A review" *J. Lightwave Technol.* 6 984–1001

Robinson, G.A. (1990) "Optical Immunosensing Systems–Meeting the Market Needs" *Biosensors '90, The first world congress on biosensors, 2–4 May 1990, Singapore,* Elsevier Science Publishers Ltd., England, *pp.* 35–37

Rockhold, S.A., Quinn, R.D., Van Wagenen, R.A., Andrade, J.D. and Reichert, M. (1983) "Total internal reflection fluorescence (TIRF) as a quantitative probe of protein adsorption" *J. Electroanal. Chem.* 150 261–275

Rothen, A. (1947a) "On the mechanism of enzymatic activity: II" *J. Biol. Chem.* 167 299–300

Rothen, A. (1947b) "Immunological reactions between films of antigen and antibody molecules" *J. Biol. Chem.* 168 75–97

Rothen, A., Mathot, C. and Thiele, E.H. (1969) "Determination of human and bovine growth hormones in the physiological range by the immunoelectroadsorption method" *Experentia* 25 420–421

Rothen, A. (1974) "Ellipsometric studies of thin films" *Progress in Surface and Membrane Science* (Ed. J.F. Danielli and M.D. Rosenberg), Academic Press,

New York, pp. 81–118

Sarid, D., Deck, R.T., Craig, A.E., Hickernell, R.K., Jameson, R.S. and Fasano, J.J. (1982) "Optical field enhancement by long–range surface plasma waves" *Appl. Opt.* 21 3993–3995

Schauenstein, K., Böck, G. and Wick, G. (1982) "The use of lasers to determine the fluorescence characteristics of fluorescein derivatives in immunofluorescence assays" *Immunofluorescence Technology. Selected Theoretical and Clinical Aspects* (Ed. Wick et al.) Elsevier Biomedical Press, Amsterdam

Seifert, M., Tiefanthelar, K., Heuberger, K., Lukosz, W. and Mosbach, K. (1986) "An integrated optical biosensor (IOBS)" *Anal. Lett.* 19 205–216

Sloper, A.N. and Flanagan, M.T. (1988) "Novel iron phosphate optical waveguides fabricated by a low temperature process" *Electron. Lett.*, 24 353–355

Sloper, A.N. Deacon, J.K. and Flanagan, M.T. (1990) "A Planar Indium Phosphate Monomode Waveguide Evanescent Field Immunosensor" *Sensors and Actuators*, B1 589–591

Soini, E. and Hemmila, I. (1979) "Fluoroimmunoassay: Present Status and Key Problems" *Clin. Chem.* 25 353–361

Soini, E and Lövgren, T, (1988) "Time–resolved Fluoroimmunoassay", *Non–isotopic Immunoassay*, (Ed. Ngo, T.T.), Plenum Press, London, *pp.* 231–241

Steward, M.W. (1977) "Affinity of the Antibody–Antigen Interaction and its Biological Significance" *Immunochemistry; An Advanced Textbook* (Eds. Glynn, L.E. & Steward, M.W.) Wiley Interscience, Chichester. Chapter 7 pp. 233–262

Stewart, G., Millar, C.A., Laybourn, P.J.R., Wilkinson, C.D.W. and De La Rue, R.M. (1977) "Planar Optical Waveguides Formed by Silver–Ion Migration in Glass" *IEEE J. Quan. Elec.* QE–13 192–200

Stewart, G. (1979) "Refractive Index Modification by Ion Exchange" *Ph.D thesis*, University of Glasgow.

Sutherland, R., Dahne, C., Place, J.F. and Ringrose, A.R. (1984a) "Optical detection of antibody–antigen reactions at a glass–liquid interface" *Clin. Chem.* 30 1533–1538

Sutherland, R., Dahne, C. and Place, J.F. (1984b) "Preliminary results obtained with a no–label homogeneous, optical immunoassay for human immunoglobulin G" *Anal. Lett.* 17 43–53

Sutherland, R., Dahne, C., Place, J.F. and Ringrose, A.R. (1984c) " Immunoassays at a quartz–liquid interface: theory, instrumentation and preliminary application to the fluorescent immunoassay of human immunoglobulin G" *J. Immunol. Methods* 74 253–265

Sutherland, R. and Dahne, C. (1987) "IRS Devices for Optical Immunoassays" *Biosensors*, Oxford Science Publications, New York, pp. 655–678

Thompson, N.L., Burghardt, T.P. and Axelrod, D. (1981) "Measuring surface dynamics of biomolecules by total internal reflection fluorescence with photobleaching recovery at correlation spectroscopy" *Biophys. J.* 33 435–454

Thompson, N.L. and Axelrod, D. (1983) "Immunoglobulin surface binding kinetics studied by total internal reflection with fluorescence correlation spectroscopy" *Biophys. J.* 43 103–114

Tiefenthaler, K and Lukosz, W (1984a) "Integrated optical humidity and gas sensors" *Proc. SPIE, Int. Soc. Opt. Eng. (USA), 2nd Int. Conf. on Optical Fiber Sensors, 5–7 Sept. 1984, Stuttgart, Germany,* 514 pp. 215–218

Tiefenthaler, K and Lukosz, W (1984b) "Integrated optical switches and gas sensors" *Opt. Lett.* 9 137–139

Tiefenthaler, K and Lukosz, W (1985) "Grating couplers as integrated optical humidity and gas sensors" *Thin Solid Films* 126 205–211

Tiefenthaler, K. and Lukosz, W. (1989) "Sensitivity of grating couplers as integrated–optical chemical sensors" *J. Opt. Soc. Am.* B6 209–220

Trurnit, H.J. (1953) "Studies on enzyme systems at a solid–liquid interface. II. The kinetics of adsorption and reaction" *Arch. Biochem. Biophys.* 48 176–199

Van Wagenen, R.A., Zdasiuk, B.J. and Andrade, J.D. (1980) "Total internal reflection fluorescence studies of albumin adsorption onto quartz" *Org. Coat. Plast. Chem.,* 42 749–753

Van Wagenen, R.A., Rockhold, S. and Andrade, J.D. (1982) "Probing protein adsorption: Total internal reflection intrinsic fluorescence" *Biomaterials. Interfacial phenomena and Applications* (Ed. S.L. Cooper and N.A. Peppas), Adv. Chem. Ser. 199 351–370

von Schulthess, G.K., Cohen, R.J. and Benedek, G.B. (1976a) "Laser light scattering spectroscopic immunoassay in the agglutination–inhibition mode for human chorionic gonadotropin (hCG) and human luteinizing hormone (hLH)" *Immunochem.* 13 963–966

von Schulthess, Sakato, N. and Benedek, G.B. (1976b) "Laser light scattering spectroscopic immunoassay for mouse IgG" *Immunochem.* 13 955–962

Walker, R.G. and Wilkinson, C.D.W. (1983) "Integrated optical ring resonantors made by silver ion–exchange in glass" *Appl. Opt.* 22 1029–1035

Watkins, R.W. and Robertson, C.R. (1977) "A total internal reflection technique for the examination of protein adsorption" *J. Biomed. Mater. Res.* 11 915–938

Weber, W.H. and Ford, G.W. (1981) "Optical electric field enhancement at a metal

surface arising from surface plasmon excitation" *Opt. Lett.* 6 3122–3124

White, J.M. and Heidrich, P.F. (1976) "Optical waveguide refractive index profiles determined from the measurement of mode indices: a simple analysis" *Appl. Opt.* 15 151–155

Williams, J.S., Stechschulz, D.J. and Sadum, E.H. (1969) "Lack of specificity of the immunoelectroadsorption test w*schistosoma mansoni* antigens and a conjugated hapten" *Am. J. Trop. Med. Hyg.* 17 568–575

Yan, A.Y. (1978) "Frequency Selective Grating Filters for Integrated Optics", *PhD thesis*, University of Glasgow

Yip, G.L. and Finak, J. (1984) "Directional–coupler power divider by two–step K^+ – ion exchange" *Opt. Lett.*, 9 423–425

Zhou, Y., Magill, J.V., Laybourn, P.J.R. and De La Rue, R.M. (1990) "The Use of Ion–exchanged Waveguides in Integrated Optical Molecular Biosensors", *Biosensors '90, The first world congress on biosensors, 2–4 May 1990, Singapore,* Elsevier Science Publishers Ltd., England, pp. 164–165

Zhou, Y., Laybourn, P.J.R., Magill, J.V. and De La Rue, R.M. (1991a) "An Evanescent Fluorescence Biosensor Using Ion–exchanged Buried Waveguides and The Enhancement of Peak Fluorescence" *Biosensors & Bioelectronics* 6 595–607

Zhou, Y., Magill, J.V., Cushley, W., De La Rue, R.M. and Laybourn, P.J.R. (1991b) "An Evanescent Fluorescence Immunosensor Based On K^+ and Na^+ – exchanged Patterned Optical Waveguides In Glass", *IEE Colloquium On "Optical Techniques and Biomedical Applications", 14 June 1991, Savoy Place, London, U.K.*, pp. 16/1–16/4

Zhou, Y., Magill, J.V., Laybourn, P.J.R., Cushley, W. and De La Rue, R.M. (1991c) "Multichannel Evanescent Fluorescence Immunosensing Using Potassium and Sodium Ion–exchanged Patterned Waveguides" *J. Molecular Electronics* 7 135–149

Zhou, Y., McNamee, K., Magill, J.V., De La Rue, R.M. and Laybourn, P.J.R. (1991d) "Potassium and Sodium Ion–exchanged Patterned Waveguides Applied to Evanescent Fluorescence Immunosensing" *Sensors, Technology, Systems and Applications V, 22–25 Sept. 1991, Edinburgh, U.K.*, (Ed. K.T.V. Grattan) Adam Hilger, Bristol, 9–13

Zhou, Y., Laybourn, P.J.R., Magill, J.V. and De La Rue, R.M. (1992) "Completely Buried Planar Waveguides Fabricated In Glass Using Thermal K^+ and Na^+ Ion–exchange" *IEE Proceedings J, Optoelectronics* (in press)

APPENDICES

Appendix 5.1

Reflection and transmission at an optical interface

Consider the interface of a prism (n_1) covered by a medium (n_3) as shown in Fig.5.3.1. When a plane electromagnetic wave impinges onto the interface from the prism side, the electric field vectors of the incident, reflected and transmitted wave can be expressed, respectively, as

$$\begin{aligned} E_i(r,t) &= E_{i0}\cdot\exp[i(k_i\cdot r-\omega t)] \\ &= E_{i0}\cdot e^{-i\omega t}\cdot\exp[ikn_1(x\cdot\cos\theta_i+z\cdot\sin\theta_i)] \end{aligned} \tag{1}$$

$$\begin{aligned} E_r(r,t) &= E_{r0}\cdot\exp[i(k_r\cdot r-\omega t)] \\ &= E_{r0}\cdot e^{-i\omega t}\cdot\exp[ikn_1(-x\cdot\cos\theta_r+z\cdot\sin\theta_r)] \end{aligned} \tag{2}$$

$$\begin{aligned} E_t(r,t) &= E_{t0}\cdot\exp[i(k_t\cdot r-\omega t)] \\ &= E_{t0}\cdot e^{-i\omega t}\cdot\exp[ikn_3(x\cdot\cos\theta_t+z\cdot\sin\theta_t)] \end{aligned} \tag{3}$$

where $k=2\pi/\lambda$, λ is the wavelength of the electromagnetic wave, θ_i, θ_r and θ_t are the angles of incidence, reflection and refraction respectively.

The boundary conditions at the interface lead to Snell's law, i.e.

$$\theta_i = \theta_r \tag{4}$$

$$n_1\cdot\sin\theta_i = n_3\cdot\sin\theta_t \tag{5}$$

and the following Fresnel's relationships

$$r_\perp = \frac{E_{ry}}{E_{iy}} = \frac{n_1\cdot\cos\theta_i - n_3\cdot\cos\theta_t}{n_1\cdot\cos\theta_i + n_3\cdot\cos\theta_t} = \frac{\sin(\theta_t-\theta_i)}{\sin(\theta_t+\theta_i)} \tag{6}$$

$$t_\perp = \frac{E_{ty}}{E_{iy}} = \frac{2n_1\cdot\cos\theta_i}{n_1\cdot\cos\theta_i + n_3\cdot\cos\theta_t} = \frac{2\sin\theta_t\cos\theta_i}{\sin(\theta_t+\theta_i)} \tag{7}$$

$$r_{\parallel} = \frac{H_{ry}}{H_{iy}} = \frac{n_3\cdot\cos\theta_i - n_1\cdot\cos\theta_t}{n_3\cdot\cos\theta_i + n_1\cdot\cos\theta_t} = \frac{\tan(\theta_i-\theta_t)}{\tan(\theta_i+\theta_t)} \tag{8}$$

$$t_{\parallel} = \frac{n_1}{n_3}\cdot\frac{H_{ty}}{H_{iy}} = \frac{2n_3\cdot\cos\theta_i}{n_3\cdot\cos\theta_i + n_1\cdot\cos\theta_t} = \frac{2\sin\theta_t\cdot\cos\theta_i}{\sin(\theta_i+\theta_t)\cdot\cos(\theta_i-\theta_t)} \qquad (9)$$

where E_y and H_y represent the amplitudes of the y component of the electric and magnetic field respectively. $\perp$ means that the electric field is perpendicular to the plane of incidence (i.e. TE mode) and $\parallel$ means that the electric field lies in the plane of incidence (i.e. TM mode); i stands for incidence, r for reflection and t for transmission.

Light intensity is defined as the time-averaged power flow. In the case of TE polarisation, if the angle of incidence is less than the critical angle, the light intensities of the incident, reflected and transmitted waves are respectively (Adams 1981)

$$I_i = (1/2)|E_{iy}(r,t)|^2\cdot n_1\cdot\sqrt{(\varepsilon_0/\mu_0)} \qquad (10)$$

$$I_r = (1/2)|E_{ry}(r,t)|^2\cdot n_1\cdot\sqrt{(\varepsilon_0/\mu_0)} \qquad (11)$$

$$I_t = (1/2)|E_{ty}(r,t)|^2\cdot n_3\cdot\sqrt{(\varepsilon_0/\mu_0)} \qquad (12)$$

where ε_0 is the permittivity of free space and μ_0 is the magnetic permeability of free space.

Similarly, for TM polarisation the light intensities can be expressed as

$$I_i = (1/2n_1)|H_{iy}(r,t)|^2\cdot\sqrt{(\mu_0/\varepsilon_0)} \qquad (13)$$

$$I_r = (1/2n_1)|H_{ry}(r,t)|^2\cdot\sqrt{(\mu_0/\varepsilon_0)} \qquad (14)$$

$$I_t = (1/2n_3)|H_{ty}(r,t)|^2\cdot\sqrt{(\mu_0/\varepsilon_0)} \qquad (15)$$

Total internal reflection and the transmitted light intensity

Equation (12) and (15) are valid only when there is a real transmitted light wave, i.e. $\theta_i < \theta_c$. In the case of total internal reflection, $\theta_i > \theta_c$ (i.e. $n_1\cdot\sin\theta_i > n_3$) and it immediately follows that the angle of transmission, θ_t, is imaginary, as

$$n_3 \cdot \cos\theta_t = (n_3^2 - n_3^2 \cdot \sin^2\theta_t)^{1/2}$$
$$= (n_3^2 - n_1^2 \cdot \sin^2\theta_i)^{1/2}$$
$$= i \cdot (n_1^2 \cdot \sin^2\theta_i - n_3^2)^{1/2} \qquad (16)$$

As a result,

$$E_t(r,t) = E_{t0} \cdot e^{-i(\omega t - \beta z)} \cdot \exp[-\delta \cdot x] \qquad (17)$$

where

$$\beta = k n_1 \cdot \sin\theta_i, \qquad (18)$$

and

$$\delta = k \cdot (n_1^2 \cdot \sin^2\theta_i - n_3^2)^{1/2}. \qquad (19)$$

Equation (17) describes an evanescent wave propagating in the z direction and decaying exponentially in the x direction.

Consider the Poynting vector $S = E \times H$ in the evanescent region for TE polarisation. Since $E = (0, E_y, 0)$, we have

$$S = E_y H_z e_x - E_y H_x e_z \qquad (20)$$

where e_x and e_z are unit vectors in the x and z directions respectively.

Therefore,

$$S_x = E_y H_z \qquad (21)$$

$$S_z = -E_y H_x \qquad (22)$$

From (17), using the real part, we have

$$E_{ty}(r,t) = E_{ty} \cdot \exp(-\delta \cdot x) \cdot \exp[-i(\omega t - \beta z)]$$
$$= E_{ty} \cdot \exp(-\delta \cdot x) \cdot \cos(\omega t - \beta z) \qquad (23)$$

Using Maxwell's equations it can be shown (Adams 1981, pp28–31) that

$$H_{tx} = -(\beta/\omega\mu_0)E_{ty} = -(\beta/\omega\mu_0)E_{ty}\cdot\exp(-\delta\cdot x)\cdot\cos(\omega t-\beta z) \quad (24)$$

$$H_{tz} = -(i/\omega\mu_0)\partial E_{ty}/\partial x = (\delta/\omega\mu_0)E_{ty}\cdot\exp(-\delta\cdot x)\cdot\sin(\omega t-\beta z) \quad (25)$$

Substitution of the two above equations into equations (21) and (22) results in

$$S_{tx} = (\delta/2\omega\mu_0)E_{ty}^2\cdot\exp(-2\delta\cdot x)\cdot\sin[2(\omega t-\beta z)] \quad (26)$$

$$S_{tz} = (\beta/2\omega\mu_0)E_{ty}^2\cdot\exp(-2\delta\cdot x)\cdot\{1+\cos[2(\omega t-\beta z)]\} \quad (27)$$

It can be seen from the two expressions that the time averaged power flow in the x direction $<S_{tx}>$ is zero, while that in the z direction $<S_{tz}>$ is not. Therefore,

$$I_t = I_{tz} = (\beta/2\omega\mu_0)|E_{ty}|^2\cdot\exp(-2\delta\cdot x)$$

$$= [kn_1\sin\theta_i/2\omega\mu_0]|E_{ty}|^2\cdot\exp(-2\delta\cdot x)$$

$$\text{for } \theta_i > \theta_c \quad (28)$$

In terms of I_i, I_t can thus be expressed as

$$I_t(\theta_i,x) = I_i(n_3/n_1)|t_\perp|^2 \qquad \text{for } \theta_i < \theta_c \quad (29)$$

$$= I_i\cdot\sin\theta_i\cdot|t_\perp|^2\exp(-2\delta\cdot x) \quad \text{for } \theta_i > \theta_c \quad (30)$$

Similarly, in the case of TM polarisation, $H = (0, H_y, 0)$ and we have

$$S = -H_yE_ze_x + H_yE_xe_z \quad (31)$$

Therefore,

$$S_x = -H_yE_z \quad (32)$$

$$S_z = H_yE_x \quad (33)$$

In the case of total internal reflection

$$H_{ty}(r,t) = H_{ty}\cdot\exp(-\delta\cdot x)\cdot\exp[-i(\omega t-\beta z)]$$

$$= H_{ty}\cdot\exp(-\delta\cdot x)\cdot\cos(\omega t-\beta z) \qquad (34)$$

$$E_{tx} = (\beta/n_3{}^2\omega\varepsilon_0)H_{ty} = (\beta/n_3{}^2\omega\varepsilon_0)H_{ty}\cdot\exp(-\delta\cdot x)\cdot\cos(\omega t-\beta z) \qquad (35)$$

$$E_{tz} = -(i/n_3{}^2\omega\varepsilon_0)\partial H_{ty}/\partial x = (\delta/n_3{}^2\omega\varepsilon_0)H_{ty}\cdot\exp(-\delta\cdot x)\cdot\sin(\omega t-\beta z) \qquad (36)$$

therefore,

$$S_{tx} = (\delta/2n_3{}^2\omega\varepsilon_0)H_{ty}{}^2\cdot\exp(-2\delta\cdot x)\cdot\sin[2(\omega t-\beta z)] \qquad (37)$$

$$S_{tz} = (\beta/2n_3{}^2\omega\varepsilon_0)H_{ty}{}^2\cdot\exp(-2\delta\cdot x)\cdot\{1+\cos[2(\omega t-\beta z)]\} \qquad (38)$$

The two expressions tell us that the time averaged power flow in the x direction $<S_{tx}>$ is zero, while that in the z direction $<S_{tz}>$ is not. In fact,

$$I_t = I_{tz} = (\beta/2n_3{}^2\omega\varepsilon_0)|H_{ty}|^2\cdot\exp(-2\delta\cdot x)$$

$$= [kn_1\sin\theta_i/2n_3{}^2\omega\varepsilon_0](n_3/n_1)^2|t_{||}|^2|H_{iy}|^2\cdot\exp(-2\delta\cdot x)$$

$$\text{for } \theta_i > \theta_c \qquad (39)$$

In terms of I_i, I_t can thus be expressed as

$$I_t(\theta_i,x) = I_i(n_3/n_1)|t_{||}|^2 \qquad \text{for } \theta_i < \theta_c \qquad (40)$$

$$= I_i\cdot\sin\theta_i\cdot|t_{||}|^2\exp(-2\delta\cdot x) \qquad \text{for } \theta_i > \theta_c \qquad (41)$$

Agreement with waveguide theory

The same expressions for the transmitted intensity can be derived using waveguide theory for a three layer dielectric waveguide. Consider just the TE mode and refer to Fig.3.3.1. The electric field distribution was expressed as (Section 3.3.1)

$$E_y = A\cdot\exp(-\delta\cdot x), \qquad x \geq 0 \tag{3.3.1}$$

$$= A\cdot[\cos(\kappa x) - (\delta/\kappa)\cdot\sin(\kappa x)], \qquad 0 \geq x \geq -d \tag{3.3.2}$$

$$= A\cdot[\cos(\kappa d) + (\delta/\kappa)\cdot\sin(\kappa d)]\cdot\exp(\gamma(x+d)), \qquad x \leq -d \tag{3.3.3}$$

where A is the amplitude of the electric field at the interface x= 0,

$$\kappa = (n_1^2k^2 - \beta^2)^{\frac{1}{2}} \tag{3.3.4}$$

$$\gamma = (\beta^2 - n_2^2k^2)^{\frac{1}{2}} \tag{3.3.5}$$

$$\delta = (\beta^2 - n_3^2k^2)^{\frac{1}{2}} \tag{3.3.6}$$

and the longitudinal propagation constant β is given by

$$\beta = k\cdot n_{eff} = k\cdot n_1\cdot\sin\theta_i \tag{3.3.7}$$

with n_{eff} being the effective refractive index of the waveguide.

However, the electric field can also be expressed as

$$E_y = A\cdot\exp(-\delta\cdot x), \qquad x \geq 0 \tag{42}$$

$$= B\cdot\exp[i\kappa x] + C\cdot\exp[-i\kappa x], \qquad 0 \geq x \geq -d \tag{43}$$

$$= D\cdot\exp(\gamma(x+d)), \qquad x \leq -d \tag{44}$$

in which the first term in (43), i.e. $B\cdot\exp[i\kappa x]$, represents an incident wave at the upper interface, whereas the second term $C\cdot\exp[-i\kappa x]$ represents a reflected wave from the upper interface. The boundary condition at the upper interface x= 0 requires that E_y and $\partial E_y/\partial x$ are continuous. This results in

$$B = [(i\delta+\kappa)/2\kappa]\cdot A \tag{45}$$

Since B is the electric amplitude of the incident light wave, using (10), the incident light intensity can be expressed as

$$\left.\begin{aligned} I_i &= (1/2)|B|^2\cdot n_1\cdot\sqrt{(\varepsilon_0/\mu_0)} \\ &= (1/2)\cdot[(\kappa^2+\delta^2)/4\kappa^2]\cdot|A|^2\cdot n_1\cdot\sqrt{(\varepsilon_0/\mu_0)} \\ &= (1/2)\cdot[(n_1^2-n_3^2)/4\cdot(n_1^2-n_{eff}^2)]\cdot|A|^2\cdot n_1\cdot\sqrt{(\varepsilon_0/\mu_0)} \end{aligned}\right\} \tag{46}$$

In the evanescent region x>0, the transmitted light intensity can be obtained by taking the time average of the Poynting vector $\mathbf{S} = \mathbf{E} \times \mathbf{H}$. It has been shown that

the net power flow is in the z direction. Therefore, the transmitted light intensity is given by

$$I_t = \langle S_z \rangle = (1/2)\cdot[-E_y H_x] = (1/2)\cdot[(-E_y)\cdot(-\beta/\omega\mu_0)E_y]$$
$$= (1/2)\cdot|A|^2\cdot\exp[-2\delta\cdot x]\cdot n_{eff}\cdot\sqrt{(\varepsilon_0/\mu_0)} \qquad (47)$$

where $< >$ means the time average.

It immediately follows that the transmitted light intensity is related to the incident light intensity by

$$I_t = \frac{4\cdot n_{eff}\cdot(n_1^2-n_{eff}^2)}{n_1\cdot(n_1^2-n_3^2)}\cdot I_i\cdot\exp[-2\delta\cdot x] \qquad (48)$$

It can be shown that in the evanescent case,

$$|t_\perp|^2 = \frac{4\cdot(n_1^2-n_{eff}^2)}{(n_1^2-n_3^2)} \qquad (49)$$

whereas from (3.3.7),

$$\sin\theta_i = n_{eff}/n_1 \qquad (50)$$

Therefore, (48) is in complete agreement with (30). The expressions for TM mode can be similarly derived and will not be given here.

<u>The incident light intensity and the optical power guided by the waveguide per unit width</u>

Marcuse (1974) has shown that for a TE mode in a three layer planar waveguide, the optical power guided by the waveguide per unit width is given by

$$P = \frac{|\beta|\cdot(d+1/\gamma+1/\delta)\cdot(\kappa^2+\delta^2)}{4\kappa^2\omega\mu_0}\cdot|A|^2 \qquad (51)$$

where d is the thickness of the guiding layer and the other parameters are as defined as in chapter 3 or in this Appendix.

Using (46), (51) can be re-expressed in terms of I_i as

$$P = 2 \cdot I_i \cdot (d+1/\gamma+1/\delta) \qquad (52)$$

It can be seen from this equation that the optical power guided per unit width is proportional to the incident light intensity.

Appendix 5.2 The transmission terms

When the transmitted electromagnetic field beyond an optical interface is to act on an atom or molecule, it has been shown that the photo-excitation is proportional to $I_t(\theta_i,x)$, regardless of whether the wave is homogeneous or evanescent (Carniglia et al. 1972). It thus follows that a fluorescent molecule located in an evanescent field at a distance x from the interface should fluoresce at a rate given by equations (30) and/or (41) (Carniglia et al. 1972).

Consider the absorption of the transmitted or evanescent light by not just one molecule but a very thin layer of molecules (thickness= $\triangle x$) located at x ($x \geq 0$) from the interface. If the incident light beam from the optically denser medium has a cross-sectional area of A, the illuminated area on the interface will be

$$A' = A/\cos\theta_i \qquad (53)$$

where θ_i is the angle of incidence. As a result, only those molecules within the area of $A' = A/\cos\theta_i$ will be illuminated (Harrick 1965). Consequently, the part of the incident light intensity (I_i) absorbed by the thin layer is

$$\triangle I_a = \alpha \cdot \triangle x \cdot I_t/\cos\theta_i \qquad (54)$$

where I_t is given by equations (30) or (41) and α is the absorption coefficient.

The fluorescent light intensity is proportional to the amount of absorbed excitation light and the fluorescence efficiency η. Consider the case of TE polarisation. For a thin layer of fluorescent molecules of thickness $\triangle x$ at x, the fluorescence intensity is therefore given by

$$\triangle I_f \propto \eta \cdot \triangle I_a = \eta \cdot \alpha \cdot \triangle x \cdot I_t/\cos\theta_i$$

$$= I_i(n_3/n_1)|t_\perp|^2(\eta \cdot \alpha \cdot \triangle x/\cos\theta_i), \qquad \text{for } \theta_i < \theta_c \qquad (55)$$

$$= I_i \cdot \sin\theta_i \cdot |t_\perp|^2(\eta \cdot \alpha \cdot \triangle x/\cos\theta_i)\exp(-2\delta \cdot x), \qquad \text{for } \theta_i > \theta_c, \qquad (56)$$

The question of how this fluorescent light is emitted to the optically denser medium is answered by applying the principle of optical reciprocity (Carniglia et al.

1972 and Lee et al. 1979). In simple words, as the exciting wave is evanescent, the excited fluorescent wave is also evanescent. Consequently, it can tunnell back in the same way as an evanescent wave is generated. Mathematically, the fluorescent light intensity in the optically denser medium propagating at an angle of θ_0 with respect to the normal of the interface is given by

$$\Delta I_f'(\theta_0,x) = (n_3'/n_1')|t'_\perp|^2 \cdot \Delta I_f/\cos\theta_0, \qquad \text{for } \theta_0 < \theta_c \quad (57)$$

$$= [\sin\theta_0 |t'_\perp|^2 \cdot \Delta I_f/\cos\theta_0] \cdot \exp(-2\delta' \cdot x), \quad \text{for } \theta_0 > \theta_c' \quad (58)$$

where TE polarisation for the fluorescent light is assumed. θ_c' is the critical angle at the fluorescence wavelength λ_f, the refractive indices n_1' and n_3' are the values at the fluorescence wavelength and

$$\delta' = k' \cdot (n_1'^2 \cdot \sin^2\theta_0 - n_3'^2)^{1/2} \quad (59)$$

$$k' = 2\pi/\lambda_f \quad (60)$$

These expressions mean that each time the light passes through the optical interface, its intensity is modified by a transmission term. Once in the optically rarer medium, depending on whether the process is evanescent or not, the light intensity will be either attenuated by an exponential decay or unaltered. If both excitation and observation are evanescent, the attenuation will be $\exp[-2(\delta+\delta')x]$. If only excitation (or observation) is evanescent, the attenuation will only be $\exp[-2\delta \cdot x]$ (or $\exp[-2\delta' \cdot x]$). If neither is evanescent, the intensity will only be modified by the optical interface. Discrimination of these four situations leads to

$$\Delta I_f'(\theta_i,\theta_0,x) \propto I_i \cdot C \cdot \Delta x \cdot \exp[-2(\delta+\delta')x], \quad \text{for } \theta_i > \theta_c,\ \theta_0 > \theta_c' \quad (61)$$

$$\Delta I_f'(\theta_i,\theta_0,x) \propto I_i \cdot C \cdot \Delta x \cdot \exp[-2\delta \cdot x], \quad \text{for } \theta_i > \theta_c,\ \theta_0 < \theta_c' \quad (62)$$

$$\Delta I_f'(\theta_i,\theta_0,x) \propto I_i \cdot C \cdot \Delta x \cdot \exp[-2\delta' \cdot x], \quad \text{for } \theta_i < \theta_c,\ \theta_0 > \theta_c' \quad (63)$$

$$\Delta I_f'(\theta_i,\theta_0,x) \propto I_i \cdot C \cdot \Delta x, \quad \text{for } \theta_i < \theta_c,\ \theta_0 < \theta_c' \quad (64)$$

where

$$C = \alpha \cdot \eta \cdot |T_\perp(\theta_i)|^2 \cdot |T_\perp'(\theta_0)|^2 \quad (65)$$

and the transmission terms, $|T_{\perp}(\theta_i)|^2$ and $|T_{\perp}'(\theta_0)|^2$, for the incident intensity on the lower index side and for the fluorescent intensity on the higher index side are respectively

$$|T_{\perp}(\theta_i)|^2 = (n_3/n_1)\cdot|t_{\perp}|^2/\cos\theta_i \qquad \text{for } \theta_i \leqslant \theta_c$$

$$= \tan\theta_i \cdot |t_{\perp}|^2 \qquad \text{for } \theta_i > \theta_c \qquad (66)$$

$$|T_{\perp}'(\theta_0)|^2 = (n_3'/n_1')\cdot|t_{\perp}'|^2/\cos\theta_0 \qquad \text{for } \theta_0 \leqslant \theta_c'$$

$$= \tan\theta_0 \cdot |t_{\perp}'|^2 \qquad \text{for } \theta_0 > \theta_c' \qquad (67)$$

Similarly, it can be shown that for TM polarisation of both excitation and fluorescence observation, the expressions for the transmission terms are also given by (66) and (67) with the subscript $\perp$ being replaced by $\parallel$, i.e.

$$|T_{\parallel}(\theta_i)|^2 = (n_3/n_1)\cdot|t_{\parallel}|^2/\cos\theta_i \qquad \text{for } \theta_i \leqslant \theta_c$$

$$= \tan\theta_i \cdot |t_{\parallel}|^2 \qquad \text{for } \theta_i > \theta_c \qquad (68)$$

$$|T_{\parallel}'(\theta_0)|^2 = (n_3'/n_1')\cdot|t_{\parallel}'|^2/\cos\theta_0 \qquad \text{for } \theta_0 \leqslant \theta_c'$$

$$= \tan\theta_0 \cdot |t_{\parallel}'|^2 \qquad \text{for } \theta_0 > \theta_c' \qquad (69)$$

The cases for TE excitation but TM observation and for TM excitation and TE observation can be included by using appropriate transmission terms.

For a dye medium (thickness t) placed on top the interface, the fluorescence intensity is obtained by integrating $\triangle I_f'(\theta_i, \theta_0, x)$ from x= 0 to x= t, i.e.

$$I_f(\theta_i, \theta_0) \propto \int_0^t C\cdot\exp(-2D\cdot x)\,dx \qquad (70)$$

where D= $\delta+\delta'$, δ, δ' and 0 respectively for the four situations represented by equations (61)−(64). Equation (70) is equation (5.4.1) in the main body of the chapter.

Appendix 5.3 A numerical example of the evanescent fluorescence constant $\zeta\cdot(\Gamma\cdot K_a/t_1)$ and $(1-\zeta)$

To show that $\zeta\cdot(\Gamma\cdot K_a/t_1)$ is much greater than $(1-\zeta)$, consider the situation where antigens are immunoglobulins and they are closely packed on the waveguide surface. According to Eddowes (1987/88), the radius of a globular IgG is about 3×10^{-9}m. If it is assumed that one antigen has only one antigenic determinant (i.e. one binding site), this close packing will result in a packing density of $\Gamma \approx 5 \times 10^{-8}$ (mole/m^2). It is reasonable to assume that the thickness of the antigen–antibody layer is about twice the diameter of an IgG molecule, i.e. $t_1 = 12 \times 10^{-9}$m. When the observation angle of fluorescence is restricted to $\theta_0 < \theta_c'$, the effective decay factor is $D = 1/d_p$. In the case of a K^+–exchanged patterned waveguide, the refractive index of the guiding core is about $n_1 = 1.512$. When the surface is covered with an aqueous FITC–antibody solution, the refractive index of the sample solution is approximately $n_3 = 1.33$. Taking into consideration that the refractive index of the glass substrate is about $n_s = 1.510$, a reasonable incident angle of the guided excitation light would be $\theta_i \approx 88^0$. When the excitation wavelength is $\lambda_e = 488$nm, it can be calculated from (5.3.6) that $d_p \approx 100$nm. Therefore, the effective decay factor is $D = 1/d_p = 10^{-7}$ (m^{-1}). Using (5.4.9), it can be calculated that $\zeta \approx 0.213$. The values for the association constant of an antibody for its antigen range from 50 to 10^9 (m^3/mole) (Alberts et al. 1983 pp970). If a commonly accepted value of 10^7 (m^3/mole) is taken (Steward 1977), the constant of proportion for the antibody–antigen layer will be $\zeta\cdot(\Gamma\cdot K_a/t_1) \approx 8.9 \times 10^6$ which is 10^7 times greater than the other constant of proportion $(1-\zeta) \approx 0.79$.

If the angle of fluorescence observation $\theta_0 > \theta_c'$, then the effective decay factor will be $D = 1/d_p + 1/d_p'$, which is greater than $1/d_p$. From (5.4.9), it can be seen that the parameter ζ in this case will be greater than the ζ in the previous case and this will lead to an even higher contrast between the constant of proportion $\zeta\cdot(\Gamma\cdot K_a/t_1)$ and $(1-\zeta)$.